**Miroslav Morháč 1,2, Vladislav Matoušek 1, Ivan Turzo 1, Ján Kliman 1,2**

- **1 - Institute of Physics, Slovak Academy of Sciences, Bratislava, Slovakia**
- **2 - Flerov Laboratory of Nuclear Reactions, JINR Dubna, Russia**

DaqProVis, a toolkit for acquisition, interactive analysis, processing and visualization of multidimensional data

Data flow chart of data acquisition, processing and visualization system DaqProVis.
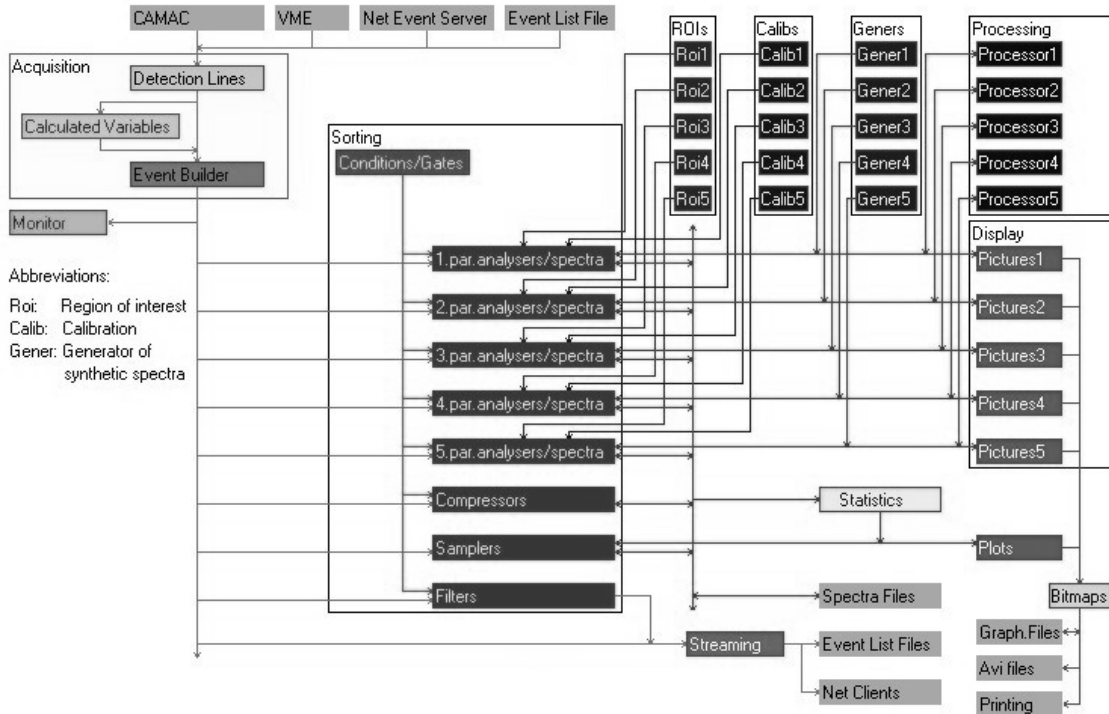
Basic features

- DaqProVis is well suited for interactive analysis of multiparameter data from small and medium sized experiments in nuclear physics.
- data acquisition part of the system allows one to acquire multiparameter events either directly from the experiment or from a list file, i.e., the system can work either in on-line or off-line acquisition mode.
- in on-line acquisition mode, events can be taken directly from CAMAC crates or from VME system that cooperates with DaqProVis in the client-server working mode.
- in off-line acquisition mode the system can analyze event data even from big experiments, e.g. from Gammasphere.
- the event data can be read also from another DaqProVis system. The capability of DaqProVis to work simultaneously in both the client and the server working mode enables us to realize remote as well as distributed nuclear data acquisition, processing and visualization systems and thus to create multilevel configurations as shown in Figure 1.
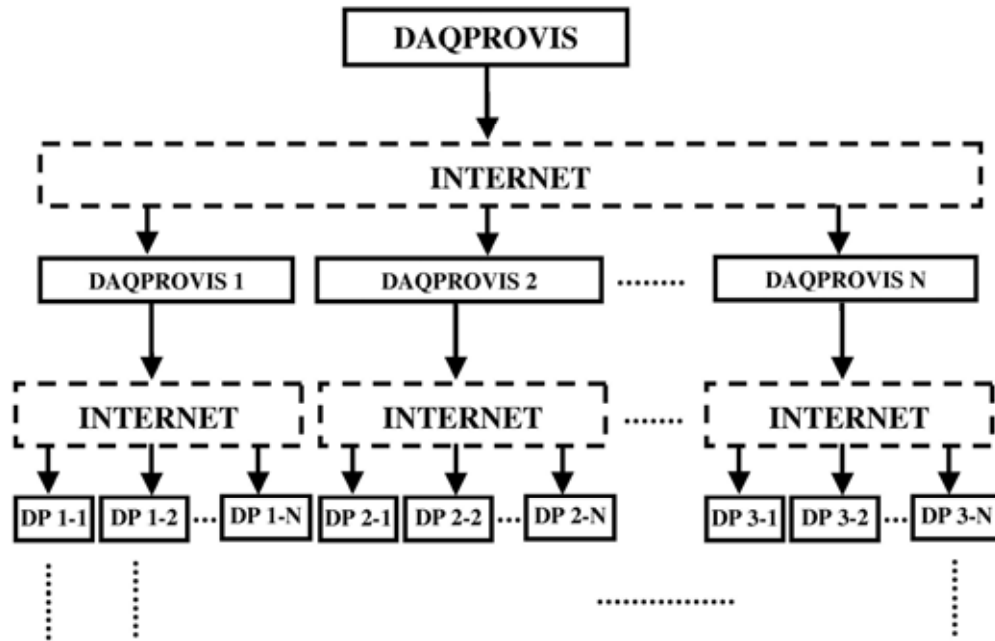
Figure 1. Multilevel configuration of DaqProVis systems

- the raw events coming from one of the above mentioned data sources can be written unchanged to a list file, or/and to other DaqProVis systems.
- they can be sorted according to predefined criteria (gates) and written to sorted streams as well.
- the event variables can be analyzed to create one-, two-, three-, four-, five-parameter histograms – spectra, analyzed and compressed using on-line compression procedure, sampled using various sampler modes (sampling, multiscaling, or stability measurement of a chosen event variable).
- once collected the analyzed data can be further processed using the algorithms
- from acquired multidimensional spectra, one can make slices of lower dimensionality.
- continuous scanning aimed at looking for and localizing interesting parts of multidimensional spectra, with automatic stop when the attached condition is fulfilled, is also possible.
- in spite of unceasing growth of today's computer memory capacities, the requirements to store multidimensional spectra very frequently go beyond the storage media volumes available.
- the amplitude analysis is carried out simultaneously with the compression, event by event, in on-line acquisition mode. After the experiment, one can extract and decompress any desired slice from the compressed multidimensional array.
- the system allows one to display one-, two-, three-, four-, five-parameter spectra using a great variety of conventional as well as sophisticated (shaded isosurface, volume rendering etc) visualization techniques.

- if desired all changes of individual pictures or entire screen connected with the change of display parameters or contents of intermediate results can be recorded in an avi file.
- it proved to be very efficient tool in the analysis of iterative processing methods, e.g. deconvolution.
- DaqProVis can be run either in the interactive manual mode or in the batch mode. In the batch mode, the commands are read from a batch file.
- its modular structure lends itself to set up the configuration of employed procedures according to specific needs of an experiment.

Event sorting

Goal: Selection of interesting events

- after taking events from any of the above-mentioned sources the first step of event processing is their selection or separation.

- the experimenter is interested only in the events satisfying predetermined conditions or gates. Consequently, the multidimensional space of event variables can be divided into two subspaces
    - subspace of event acceptance – events are taken for subsequent processing
    - subspace of rejection – events belonging to this subspace are ignored.
- based on gates events can be broken up into different output streams written in list mode either to files or sent to other clients. The gates can be used also for decision about the acceptance of an event for subsequent analysis in an analyzer or compressor.
- the basic element for data sorting is gate (condition). To satisfy typical experimental needs in DaqProVis we have implemented the following types of gates/conditions:
    - rectangular window
    - bit pattern
    - polygon
    - arithmetic function
    - spherical gates
    - ellipsoids
    - composed gate.

a. Rectangular window

- in general for n-fold rectangular window gate one can write

$$g_{l1} \leq x_1 \leq g_{u1} \quad \text{AND}$$

$$g_{l2} \leq x_2 \leq g_{u2}$$

.

.

$$g_{ln} \leq x_n \leq g_{un},$$

where x_1, x_2,..., x_n are event variables. An example of two-fold window gate in two-parameter spectrum is shown in Figure 2. The spectrum in the gate region is shown in contour display mode.
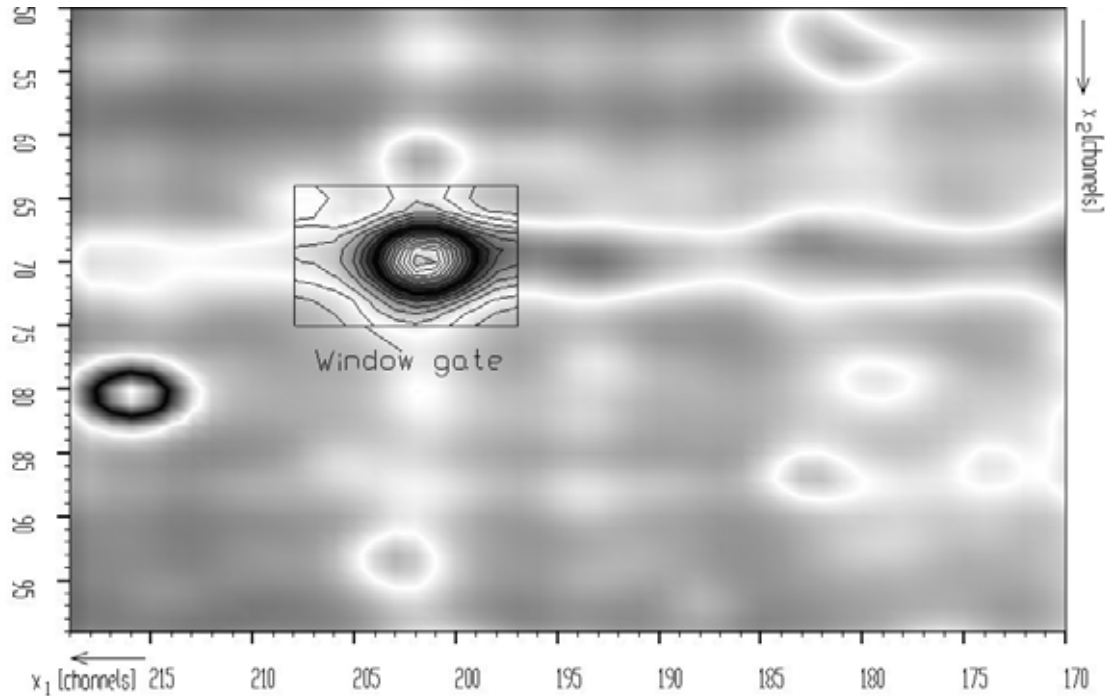

Figure 2 Example of rectangular gate applied to two-parameter spectrum

b. Bit pattern

- during the sorting the given bit pattern is applied to the tested event variable using the chosen logical function.

c. Polygon

- the proper choice of gates can lead to an improvement in spectral quality, in particular the peak – to – background ratio, and to decrease the number of uncorrelated events in the projected spectrum.
- an efficient and simple way to choose the region of event acceptance in two-dimensional space of event variables is interactive setting of appropriate closed polygon. The polygon gate consists of sequence coordinates of two event variables. It allows one to separate various parts of the spectrum (Figure 3)
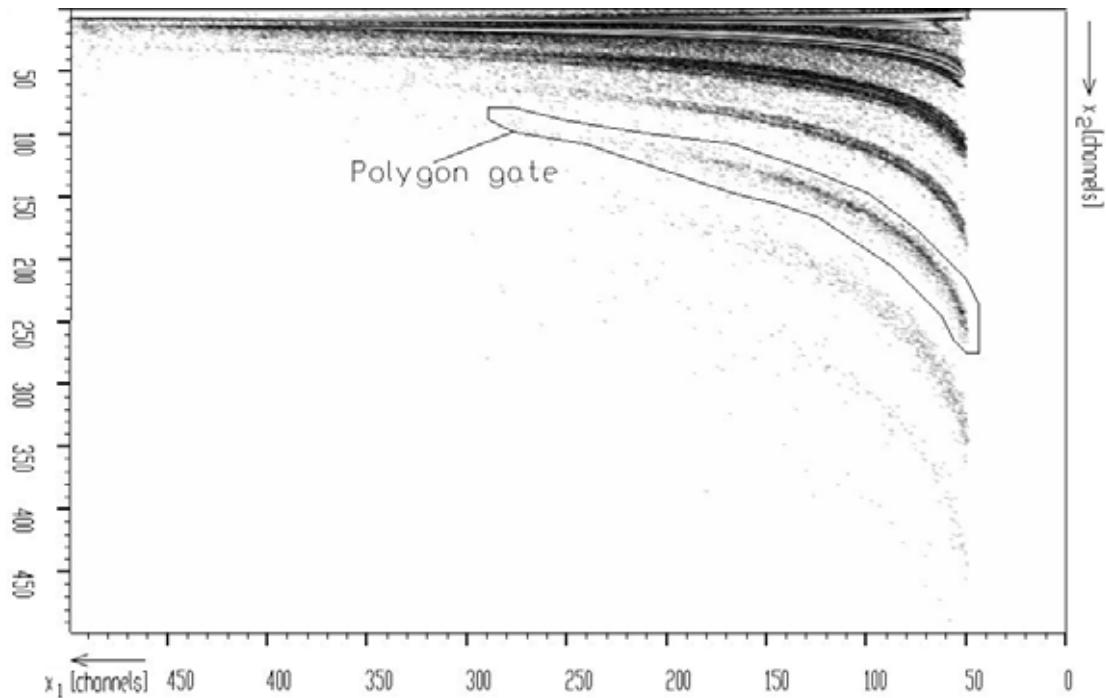
Figure 3 Example of polygon gate applied to two-parameter spectrum

- the advantage of this kind of gate is that one can design easily irregular shape. Its disadvantage is that it cannot be extended to higher dimensions and that it must be designed manually.

d. Arithmetic function

- this type of gate is represented by mathematical function of event variables (detection lines) x_1, x_2,..., x_n

$$f(x_1, x_2, ..., x_n) \leq 0.$$

- the allowed operators are +, -, *, /, ^, sqr, log, exp, cos, sin. The built-in syntax analyzer is able to recognize the expressions written in Fortran-like style using names of event variables for operands, above given operators and parentheses.
- by employing a suitable analytical function, one can specify more exactly the region of interesting parts in the spectrum.
- for instance, photopeak events are distributed approximately with Gaussian distribution. It means that in the hyperspace they have a spherical symmetry. When using gate of window type the high-fold coincidence events are unfolded into lower histogram dimension, the statistics become artificially high so that peak positions and other peak parameters may be wrong. When choosing the function with elliptic base for two variables

6

$$\left(\frac{x_1 - c_1}{r_1}\right)^2 + \left(\frac{x_2 - c_2}{r_2}\right)^2 - 1 \le 0,$$

where c_1, c_2 determine the position of the photopeak and r_1, r_2 are proportional to σ_1, σ_2, one can reduce the uncorrelated background.
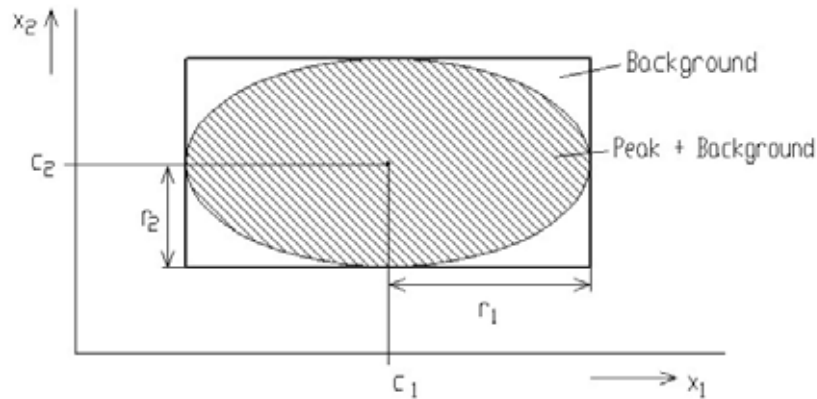
Figure 4 Arithmetic function (elliptical) gate

- the extension of this function to n-dimensional case is straightforward. However, this is just only one example of the application of this type of gate. In general one can define free any arithmetic function using the above given set of operators.

e. Spherical gates

- when sorting events with Gaussian or quasi Gaussian distribution the gates with elliptic base are of special interest. The radii of ellipses are proportional to standard deviations σ_i or to the $FWHM_i = \sqrt{2\log 2}\,\sigma_i$ (full width at half maximum) of the photopeak distribution

$$r_i = \frac{1}{2} R \cdot FWHM_i.$$

- for symmetrical n-dimensional spherical gates one can write

$$\sum_{i=1}^{n} \left(\frac{x_i - c_i}{0.5 FWHM_i}\right)^2 - R^2 \le 0.$$

- however due to various effects in detectors the peaks exhibit left-hand tailing. The problem is to extend the gate shape in the tail direction, e.g. in the variable x_2

$$\left(\frac{x_1 - c_1}{0.5 \cdot FWHM_1}\right)^2 + \left(\frac{x_2 - c_2}{0.5 \cdot FWHM_2 \cdot T}\right)^2 - R^2 \leq 0,$$

where $T \geq 1$. To introduce tailings to both directions it turns out that we have to employ logical OR function so that the gate is intersection between two-tailed spherical gates

$$\left(\frac{x_1 - c_1}{0.5 \cdot FWHM_1}\right)^2 + \left(\frac{x_2 - c_2}{0.5 \cdot FWHM_2 \cdot T}\right)^2 - R^2 \leq 0 \text{ OR}$$

$$\left(\frac{x_1 - c_1}{0.5 \cdot FWHM_1 \cdot T}\right)^2 + \left(\frac{x_2 - c_2}{0.5 \cdot FWHM_2}\right)^2 - R^2 \leq 0.$$

- it is straightforward to extend this idea to n-dimensional spherical gate

$$\left(\frac{x_1 - c_1}{0.5 \cdot FWHM_1 \cdot T}\right)^2 + \left(\frac{x_2 - c_2}{0.5 \cdot FWHM_2}\right)^2 + \ldots + \left(\frac{x_n - c_n}{0.5 \cdot FWHM_n}\right)^2 - R^2 \leq 0 \text{ OR}$$

$$\left(\frac{x_1 - c_1}{0.5 \cdot FWHM_1}\right)^2 + \left(\frac{x_2 - c_2}{0.5 \cdot FWHM_2 \cdot T}\right)^2 + \ldots + \left(\frac{x_n - c_n}{0.5 \cdot FWHM_n}\right)^2 - R^2 \leq 0 \text{ OR}$$

.
.
.

$$\left(\frac{x_1 - c_1}{0.5 \cdot FWHM_1}\right)^2 + \left(\frac{x_2 - c_2}{0.5 \cdot FWHM_2}\right)^2 + \ldots + \left(\frac{x_n - c_n}{0.5 \cdot FWHM_n \cdot T}\right)^2 - R^2 \leq 0.$$

Reference: Theisen Ch., Kintz N., Stezowski O., Vivien J.P., Improvement of high-fold γ-ray data processing: the spherical gate method, NIM A 432 (1999) 249.
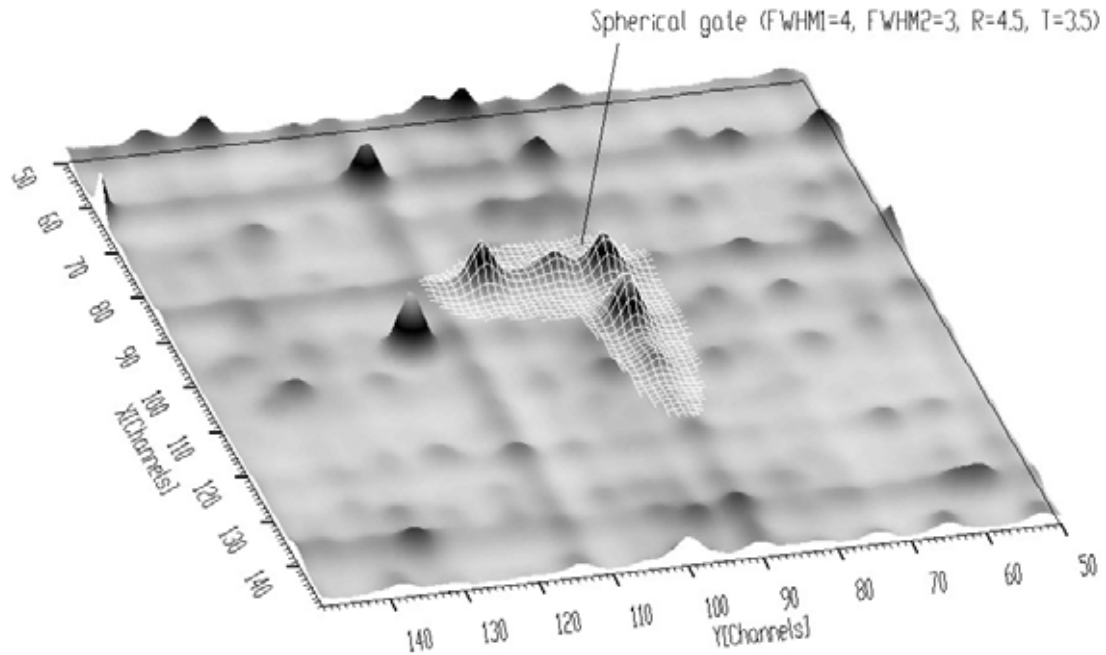
Figure 5 Example of two-dimensional spherical gate

- in Figure 6 we see three-dimensional γ-γ-γ-ray spectrum. The gate is shown in the form of three-dimensional surface in Figure 7. By changing parameters of the gate we can select any part of the spectrum of this shape.
- one example is given in Figure 8 where the gate is shown as shaded balls inside of the spectrum, i.e., the shaded channels satisfy the condition connected with the gate.
- one can observe that the shape of the gate coincides with the distribution of events in the spectrum. This way of the display of the gate allows to see the distribution of events inside of the gate.
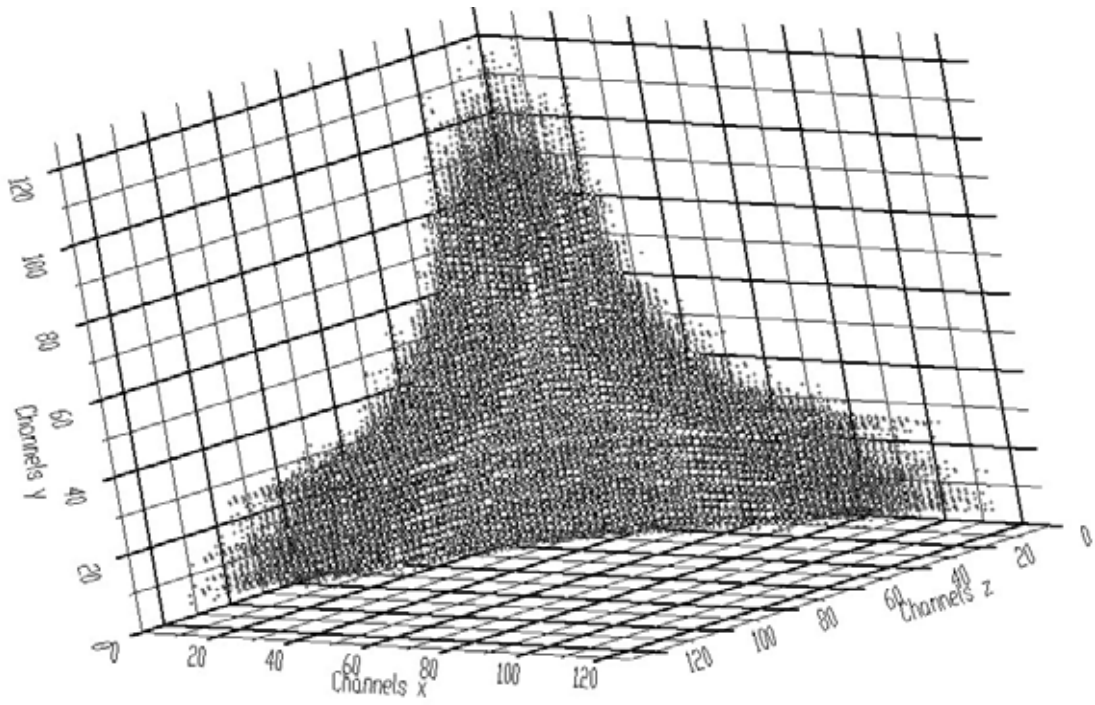
Figure 6 Three-dimensional $\gamma - \gamma - \gamma$ ray spectrum
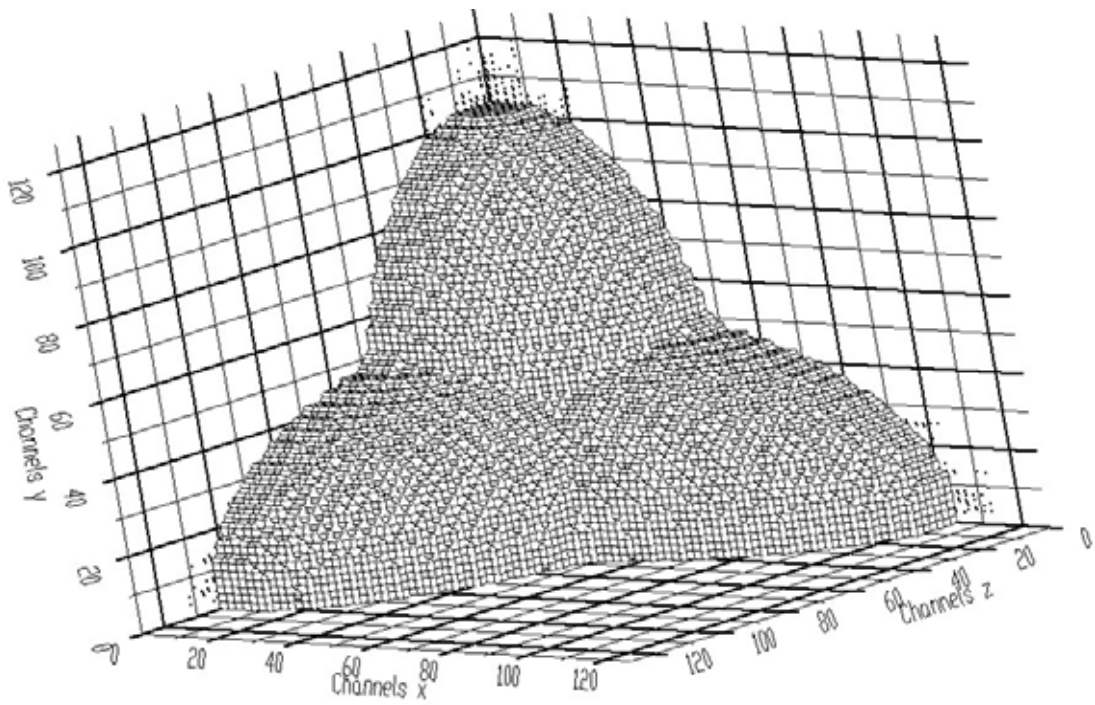
Figure 7 Three-dimensional spherical gate
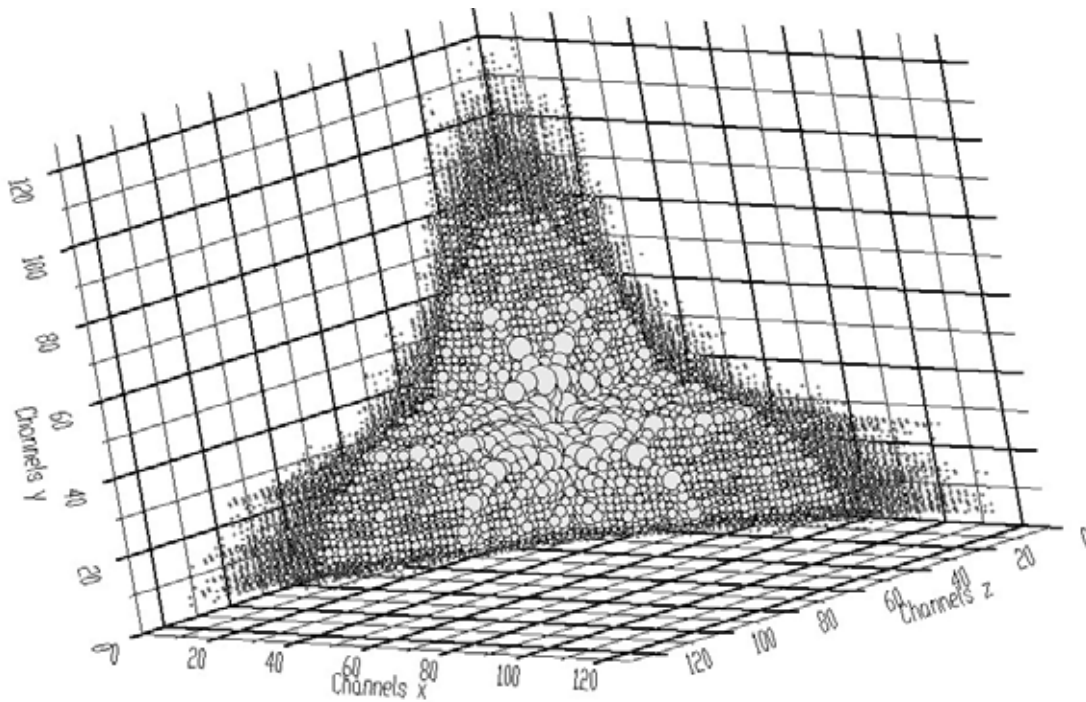
Figure 8 An example of the application of three-dimensional spherical gate to three-dimensional spectrum

- the proposed model of the gate allows one to change the width of spherical Gaussians (see Figure 9).
- however according to this model one cannot change independently tailings for individual dimensions and angles between the Gaussians.
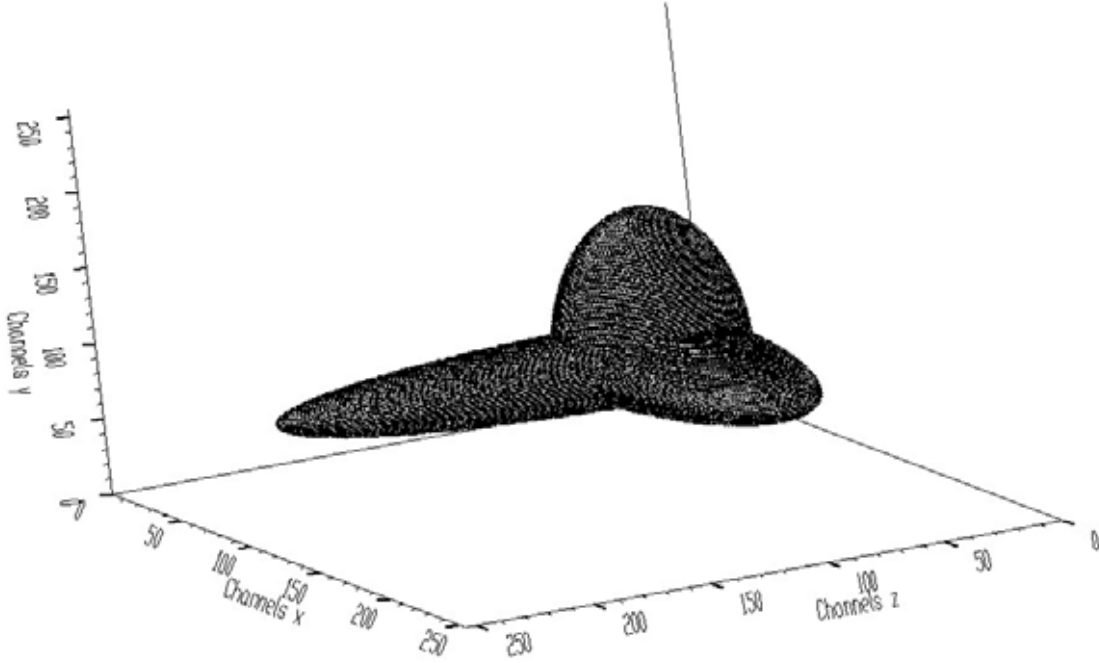
Figure 9 An example of the spherical gate with different width of Gaussians in different directions

f. Ellipsoids

- to remove the above mentioned limitations of the spherical gates and to make the design of the shape of the gates more flexible we proposed ellipsoid gates.
- let us express n-dimensional k-th ellipsoid E_k with center positioned at c_1, c_2,..., c_n and lengths of half-axes a_1, b_1, a_2, b_2, ..., a_n, b_n, in the parametric form

$$x_1 = b_1 \cos(t_{n-1})\cos(t_{n-2})....\cos(t_1) + c_1$$
$$\vdots$$
$$x_{k-1} = b_k \cos(t_{n-1})\cos(t_{n-2})....\cos(t_{k-3})\sin(t_{k-2}) + c_{k-1}$$
$$x_k = A_k(t_{k-1})\cos(t_{n-1})\cos(t_{n-2})....\cos(t_{k-2})\sin(t_{k-1}) + c_k$$
$$x_{k+1} = b_{k+1}\cos(t_{n-1})\cos(t_{n-2})....\cos(t_{k-1})\sin(t_k) + c_{k+1}$$
$$\vdots$$
$$x_n = b_n \sin(t_{n-1}) + c_n.$$

- in order to describe tailings in the gate let us propose the change of radii in dependence on the parameters t_i
  for $i = 1$

$$A_1(t_1) = \frac{a_1 + b_1}{2} + \frac{a_1 - b_1}{2}\cos(2t_1) \quad \text{for } t_1 \in \langle 0, \frac{\pi}{2}\rangle \, \& \, \langle\frac{3\pi}{2}, 2\pi\rangle$$

12

$$A_1(t_1) = b_1 \text{ otherwise}$$

for $i > 1$

$$A_i(t_{i-1}) = \frac{a_i + b_i}{2} + \frac{a_i - b_i}{2}\sin(2t_{i-1}) \text{ for } t_{i-1} \in \langle 0, \pi \rangle$$
$$A_i(t_{i-1}) = b_i \text{ otherwise,}$$

where

$t_i = u_i + s_i$, $u_i \in \langle 0, 2\pi \rangle$ and s_i is angle shift of the axis. Finally the n-dimensional gate can be expressed as logical OR of the individual ellipsoids

E_1 OR E_2 OR.... OR E_n.

- using this gate one can define in more flexible way the region of interest. An example of a spectrum of nuclear multifragmentation with ellipsoid two-dimensional gate is shown in Figure 10.
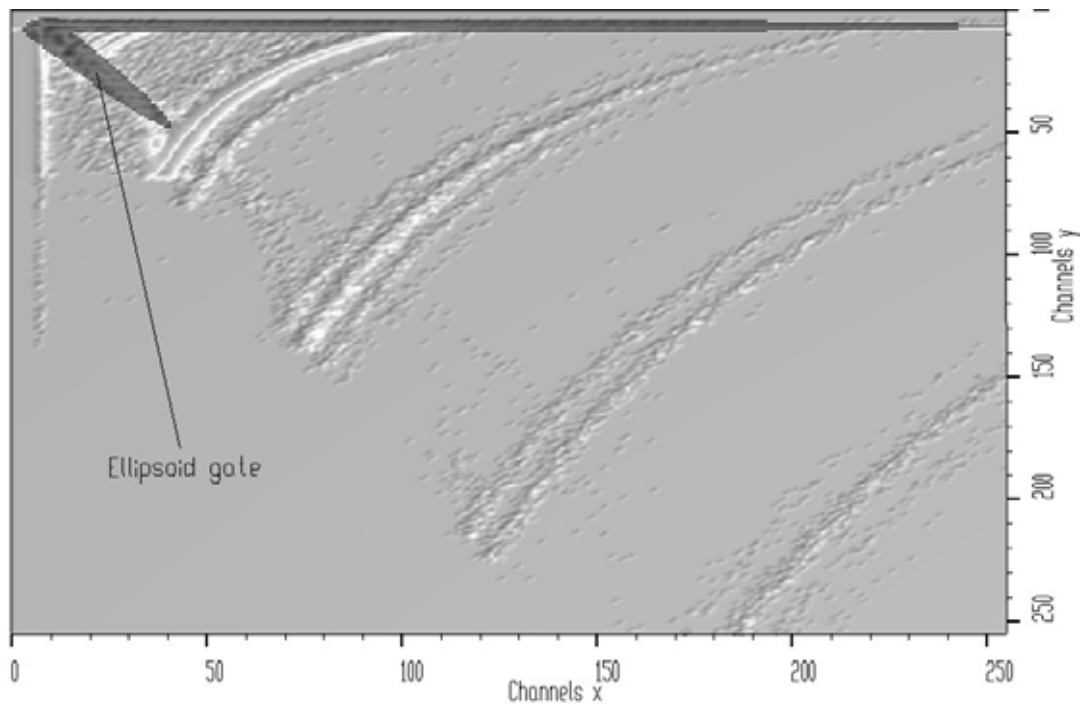
Figure 10 Two-dimensional ellipsoid gate applied to the spectrum of nuclear multifragmentation

- one can change freely lengths of half-axes, widths of ellipsoids as well as angle between them. For the sake of completeness we present also the three-dimensional gate of this type in Figure 11.

13
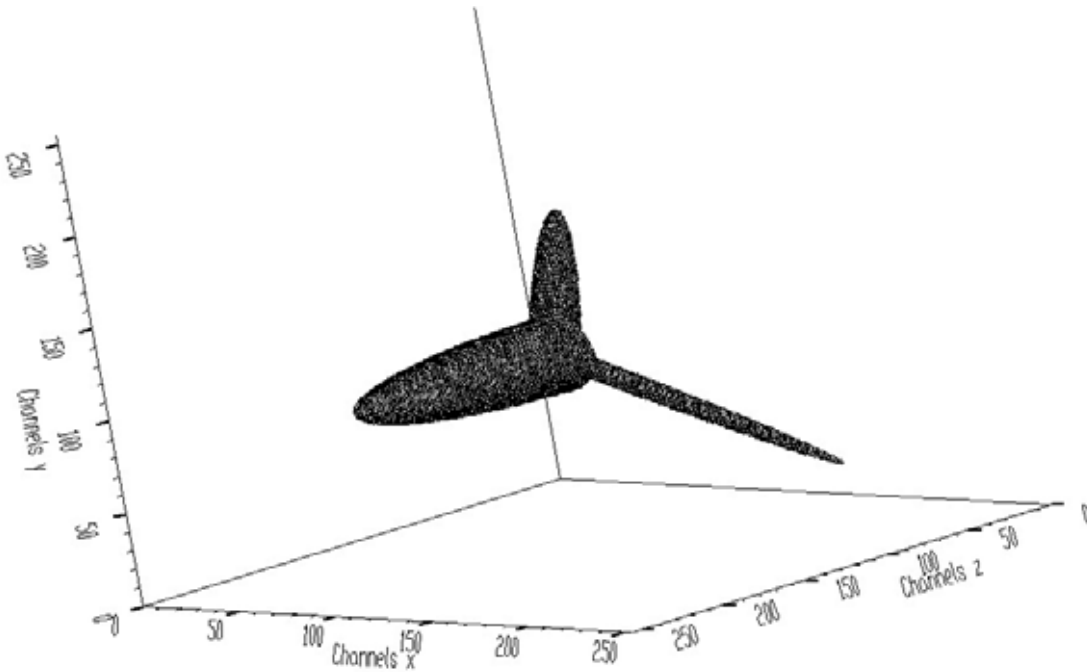
Figure 11 An example of three-dimensional ellipsoid gate

g. Composed gates

- the result of application of any of the above defined gates (conditions) is either the value „true", i.e., the event is accepted for further processing or the value „false" (event is ignored).
- every gate (also other objects) in DaqProVis has its own name. By applying logical operators (AND, OR, NOT) to operands (previously defined gate names) and using parantheses one can write very complex logical expressions defining the shape of the composed gate.
- the shape can be very complicated and can define even the composition of disjoint subsets.
- an example of composed gate applied to the two-dimensional spectrum of positron annihilation is illustrated in Figure 12, Figure13, Figure 14 and Figure 15, respectively. Let us denote the gate shown in Figure12 as A, the gate shown in Figure 13 as B and the gate shown in Figure 14 as C, respectively. Then the composed gate defined by logical function

(*A* OR *B*) AND *C*

is shown in Figure 15.
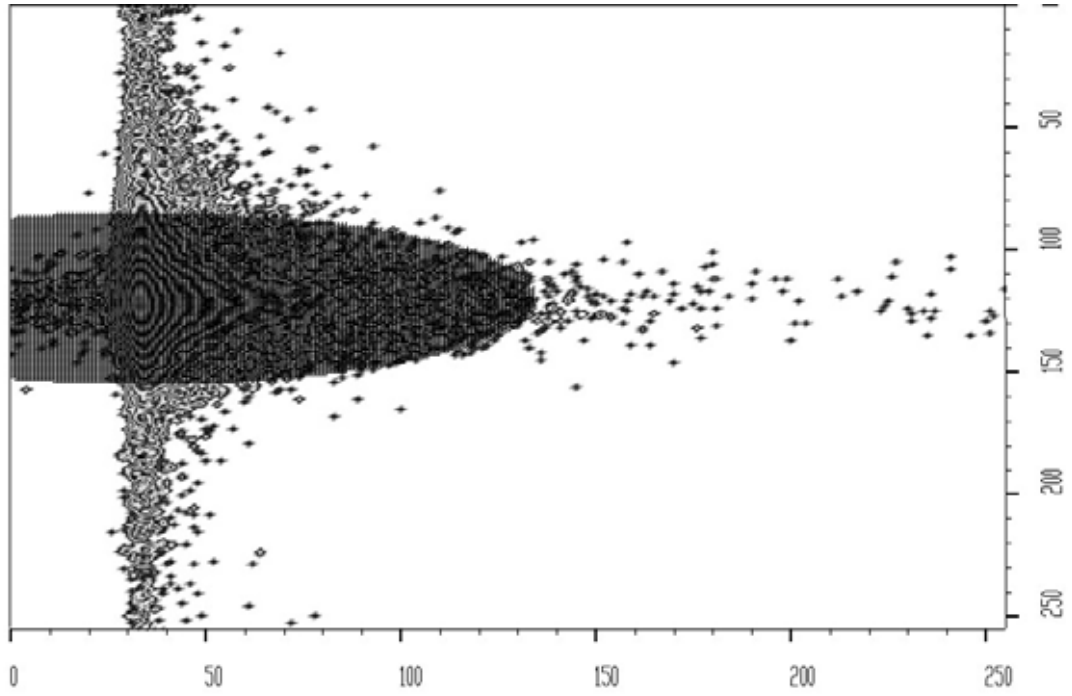
Figure 12 Two-dimensional gate A
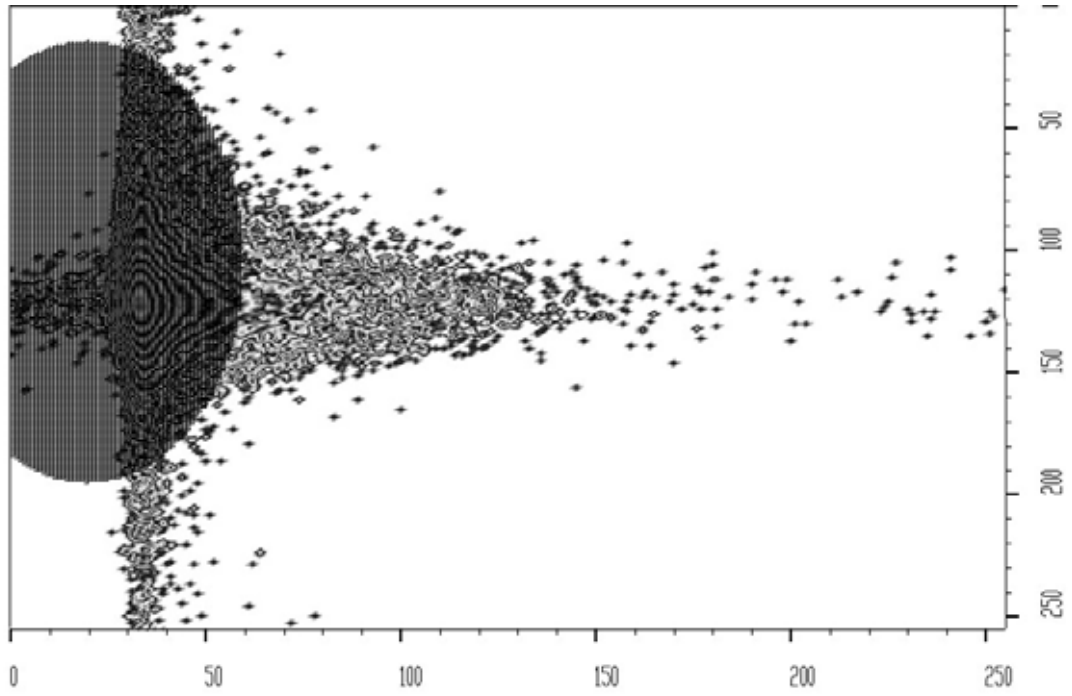
Figure 13 Two-dimensional gate B
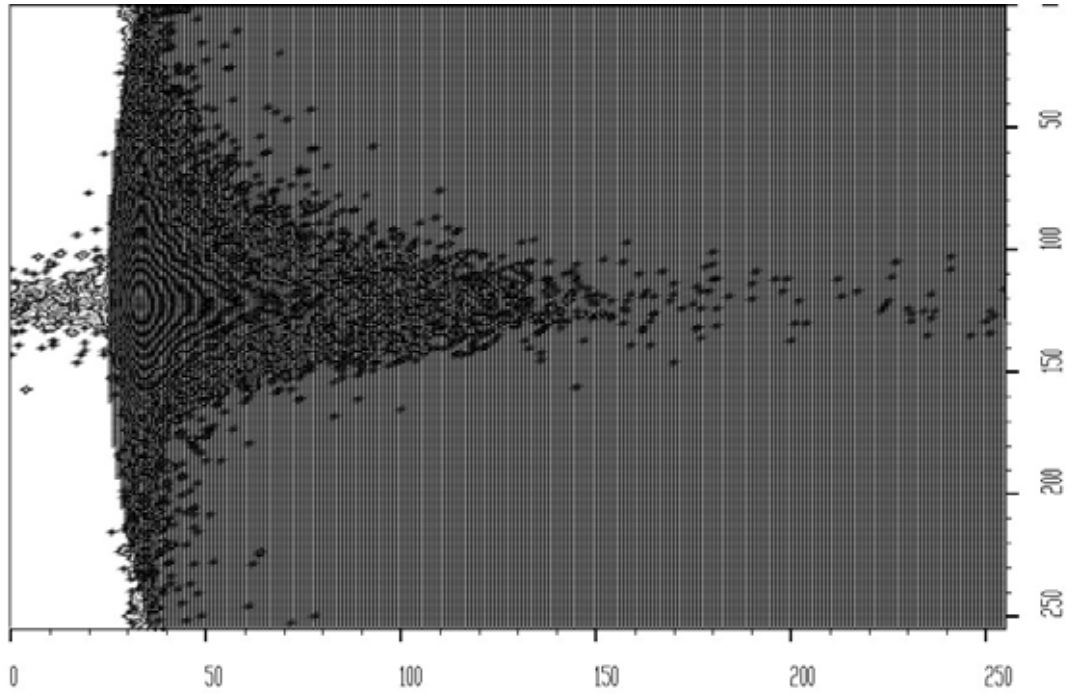
Figure 14 Two-dimensional gate C
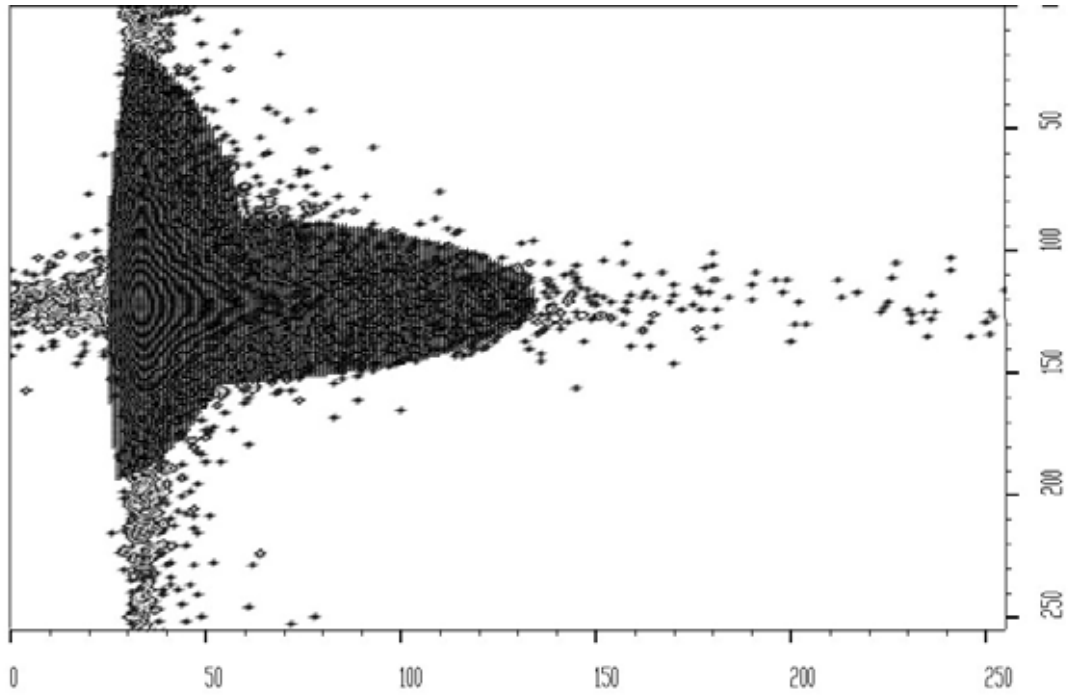
Figure 15 Resulting composed condition (A OR B) AND C

16

Storing and compression

Goal of compression: to make storing, handling and interactive analysis of multidimensional data possible in practice

- after eventual separating of interesting events from non-interesting ones the storing and possible compression, which is compelled by limited technical facilities, is the next element in the chain of processing of multidimensional experimental data arrays.
- it should be emphasized that because of practical reasons, e.g. interactive analysis, handling etc, the compression of large multidimensional arrays is in some situations unavoidable.
- methods of compression implemented in DaqProVis
    - o binning channels (very simple, but with loss of resolution in spectra)
    - o utilizing natural properties of data, e.g. multidimensional gamma-ray spectra are symmetrical. It allows, without the loss of information, to decrease the size of 2D data by factor 2, 3D data by factor 6 and k-dimensional data by factor k! However even if we utilized this property the volumes needed to store data are enormous. For instance assuming that for each element of the data array we need 4 bytes (e.g. float format) after the reduction according for resolution $R = 16384$ (14 bits ADC, e.g. data from Gammasphere) we get

$$4N_2 = 5.369 \cdot 10^8\, bytes \doteq 536.9 MB$$

$$4N_3 = 2.932 \cdot 10^{12}\, bytes \doteq 2.93 TB$$

$$4N_4 = 1.201 \cdot 10^{16}\, bytes \doteq 12.01 PB$$

$$4N_5 = 3.937 \cdot 10^{19}\, bytes.$$

Reference:
Radford D.C., NIM A 361 (1995) 290.

- o classical orthogonal transform (Fourier, Walsh, Haar, etc)
- o adaptive orthogonal transforms
    References:
    Morháč M., Matoušek V., An adaptive fast orthogonal transform algorithm for multi-dimensional data compression. Signal Processing 43 (1995) 29.
    Morháč M., Matoušek V., Fast adaptive Fourier-based transform and its use in multidimensional data compression. Signal Processing 68 (1998) 141.

Morháč M., Matoušek V., Multidimensional data compression using a new fast adaptive cosine transform, Applied signal processing 4 (1997) 16.

Morháč M., Matoušek V., New adaptive cosine-Walsh transform and its application to nuclear data compression, IEEE Transactions on Signal Processing 48 (2000) 2693.

Morháč M., Matoušek V., Data compression using new fast adaptive Cosine-Haar transforms, Digital Signal Processing 8 (1998) 63.

Morháč M., Matoušek V., Adaptive Hartley transform and its use in multidimensional data compression, Applied signal processing 6 (1999) 165.

Morháč M., Matoušek V., A new method of on-line multiparameter analysis with compression, NIM A 370 (1996) 499.

o randomizing transform - based on polynomial transforms, our new method modulo inverse numbers

References:

Bonačić V., Souček B., Čuljat K., Pseudo-random digital transformation, NIM 66 (1968) 213.

Souček B., Minicomputers in Data Processing and Simulation, Wiley-Interscience, New York, 1972.

Souček B., Bonačić V., Čuljat K., Million channel pulse height analyzer through pseudo-random digital transformation, NIM 66 (1968) 202.

- in both adaptive transforms as well as randomizing transform based method we utilized the property of symmetry
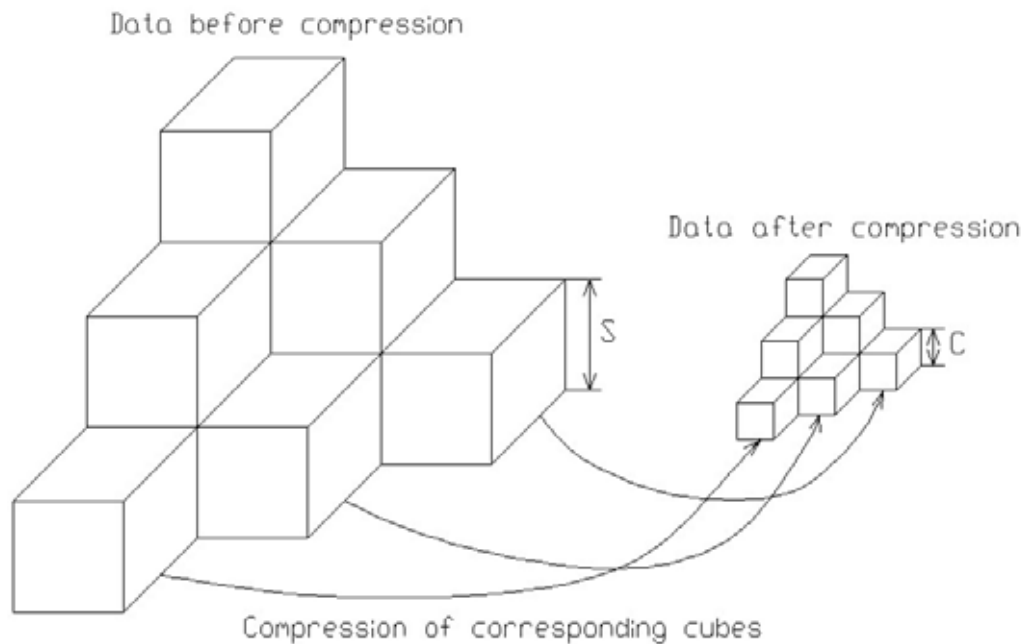
Figure 16 Principle of compression of three-dimensional symmetrical spectra using adaptive transforms

- for adaptive transforms we have created databases of compressed histograms for three-, four-, five-fold coincidences of the event data from Gammasphere.
- we have reduced the volume to 366MB for 3D data, 189.5MB for 4D data and 168.4MB for 5D data.
- it is worth noticing that the compression ratios expressed as a fraction of the data volume before and after compression are enormous

$$CR_3 = 8010, \; CR_4 = 63377308, \; CR_5 = 2.3378859 \cdot 10^{11}.$$

Examples of compression using adaptive transforms
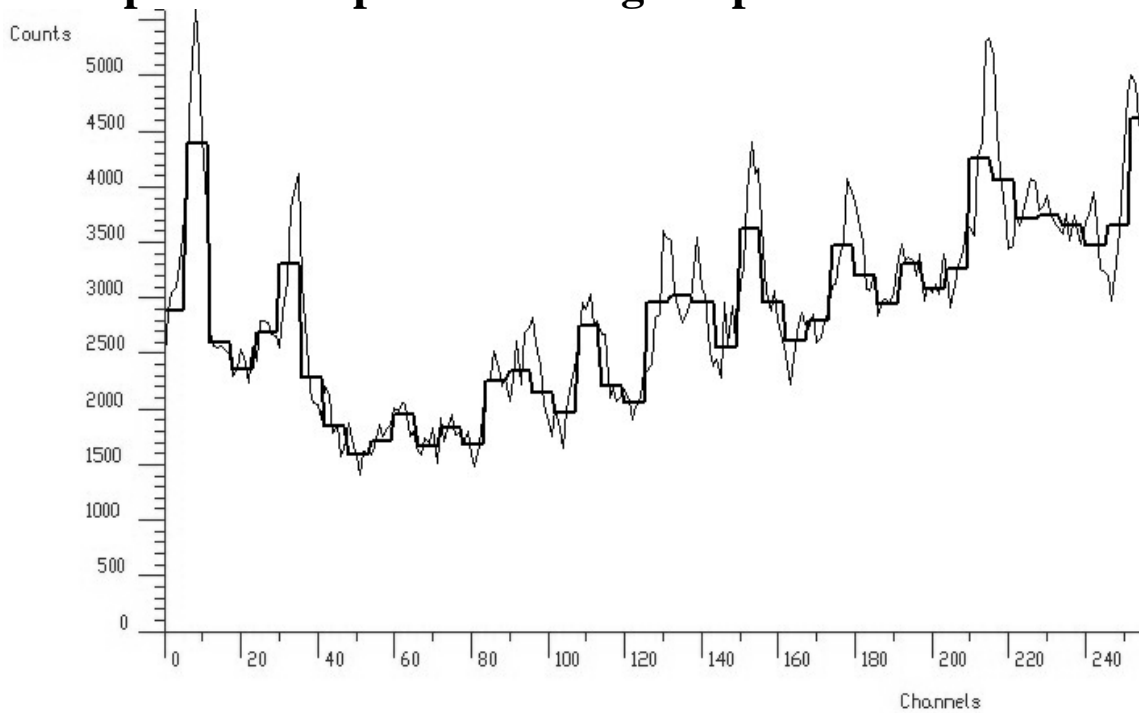
Figure 17 Slice from original data (thin line) and decompressed slice (thick line) from data compressed by employing binning operation (Radware)
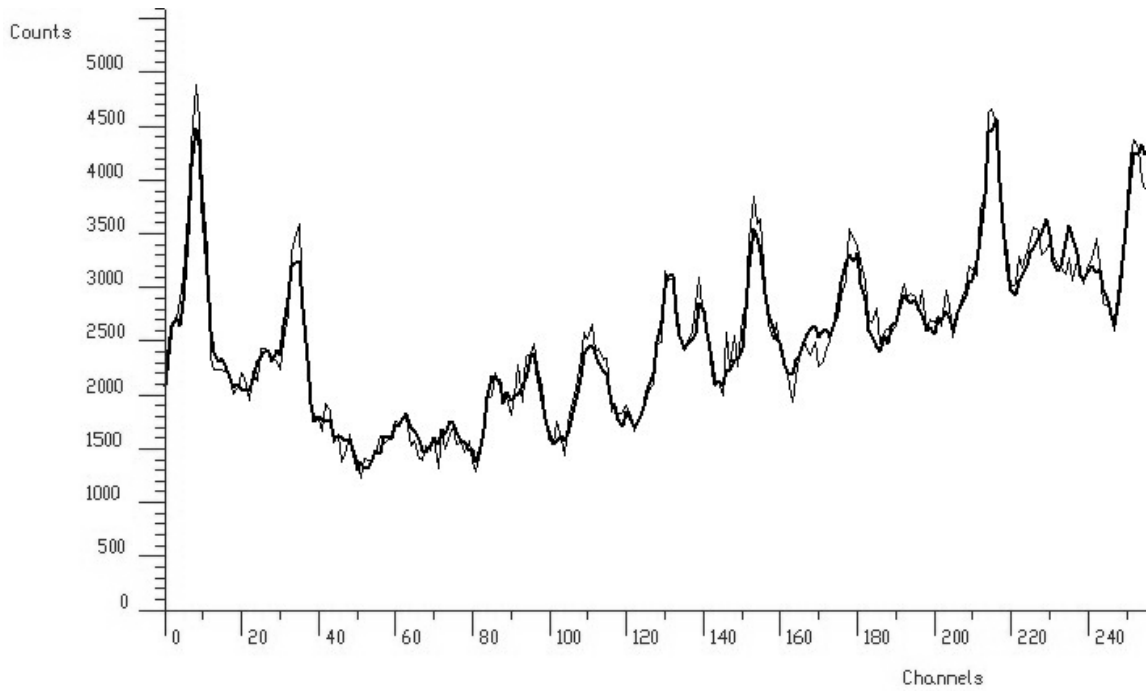
Figure 18 Slice from original data (thin line) and decompressed slice (thick line) from data compressed by employing adaptive Walsh transform
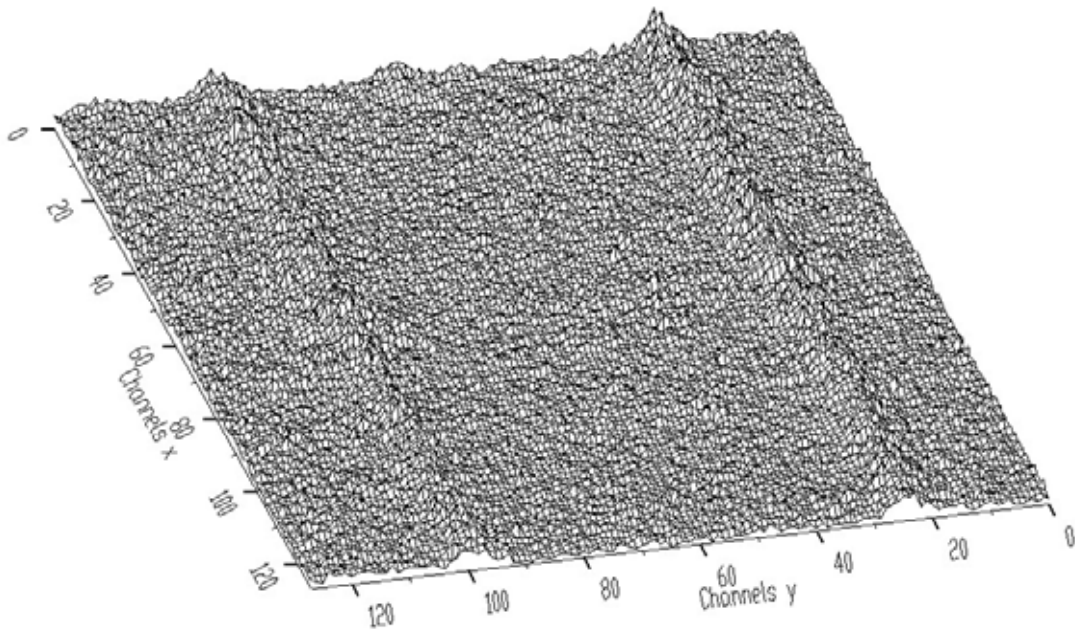
Figure 19 Two-dimensional slice from original data
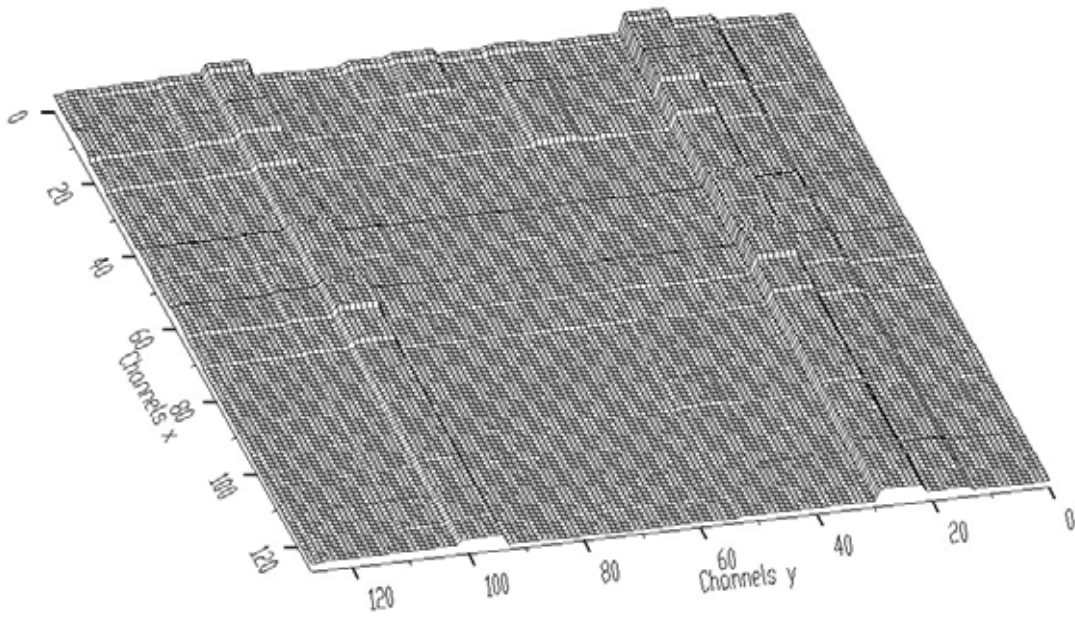
Figure 20 Two-dimensional slice from data compressed by employing binning operation (Radware)
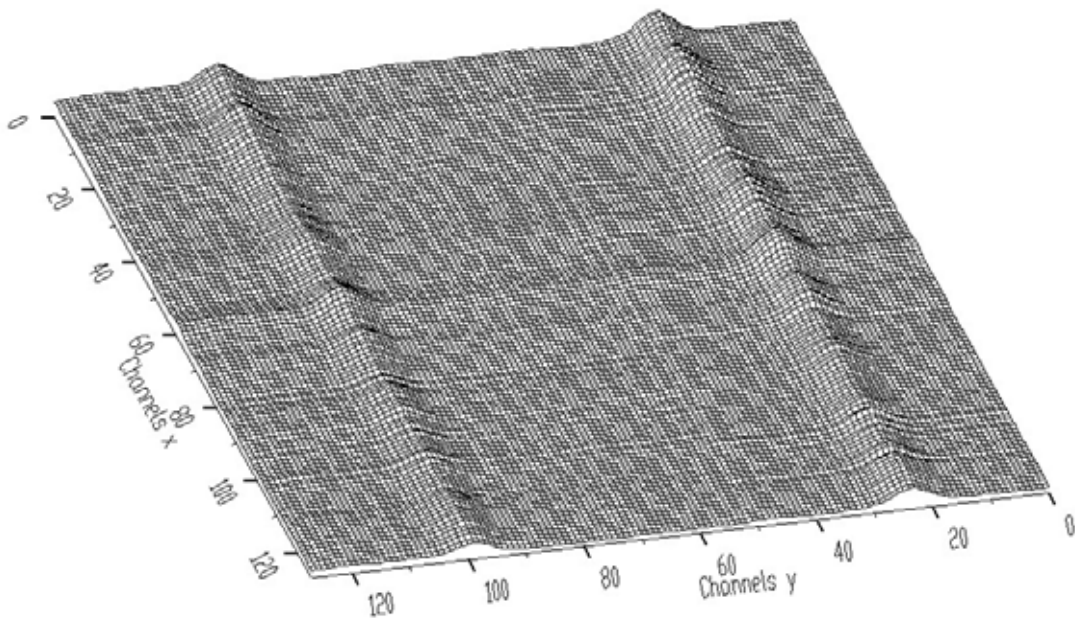
Figure 21 Two-dimensional slice from data compressed via adaptive Walsh transform

21
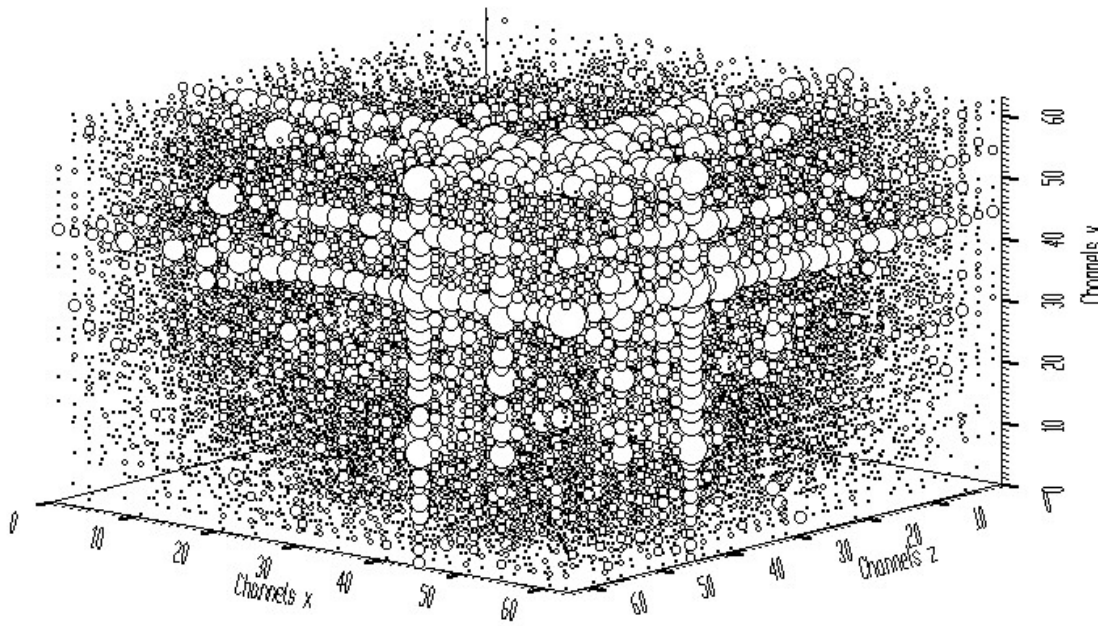
Figure 22 Three-dimensional original spectrum (sizes of spheres are proportional to counts the channels contain)
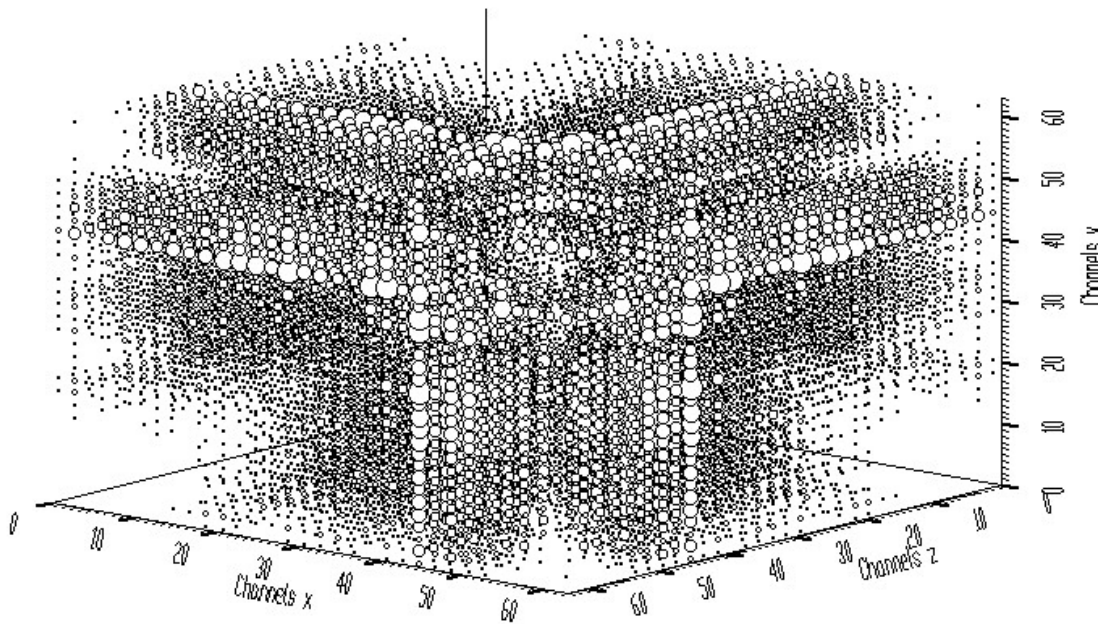
Figure 23 Three-dimensional spectrum decompressed from data compressed via adaptive Walsh transform
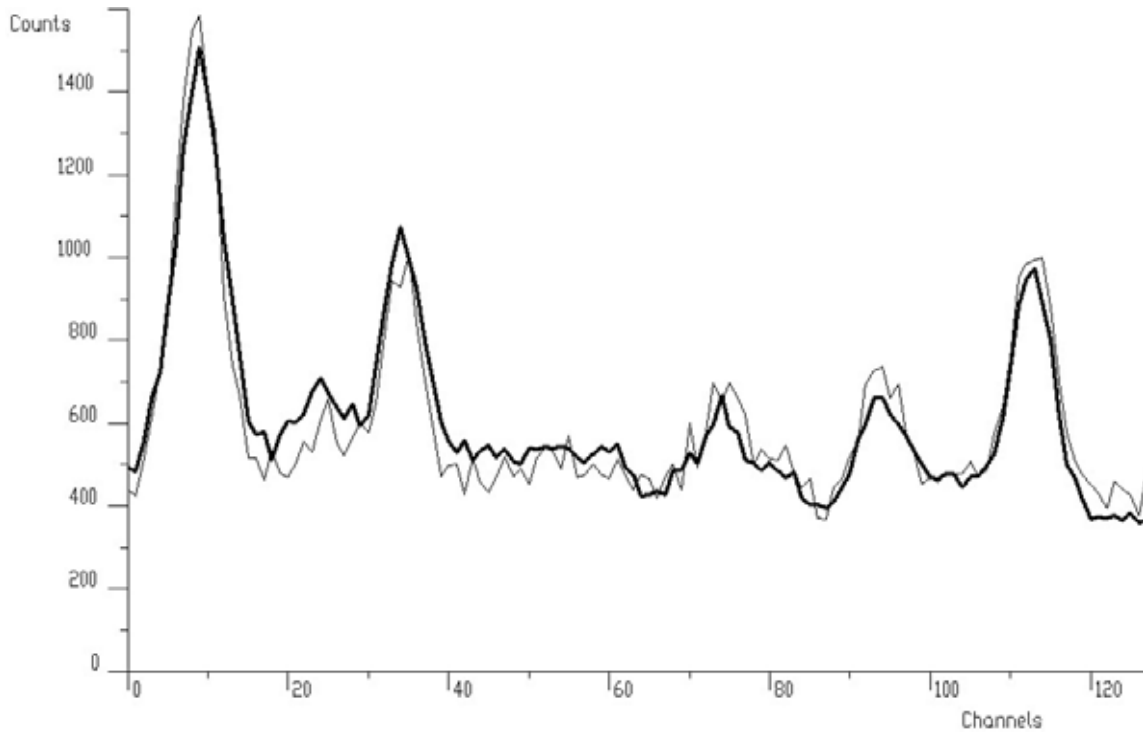
Figure 24 One-dimensional slice from original four-dimensional spectrum (thin line) and the same slice decompressed from data compressed via adaptive Walsh transform (thick line)
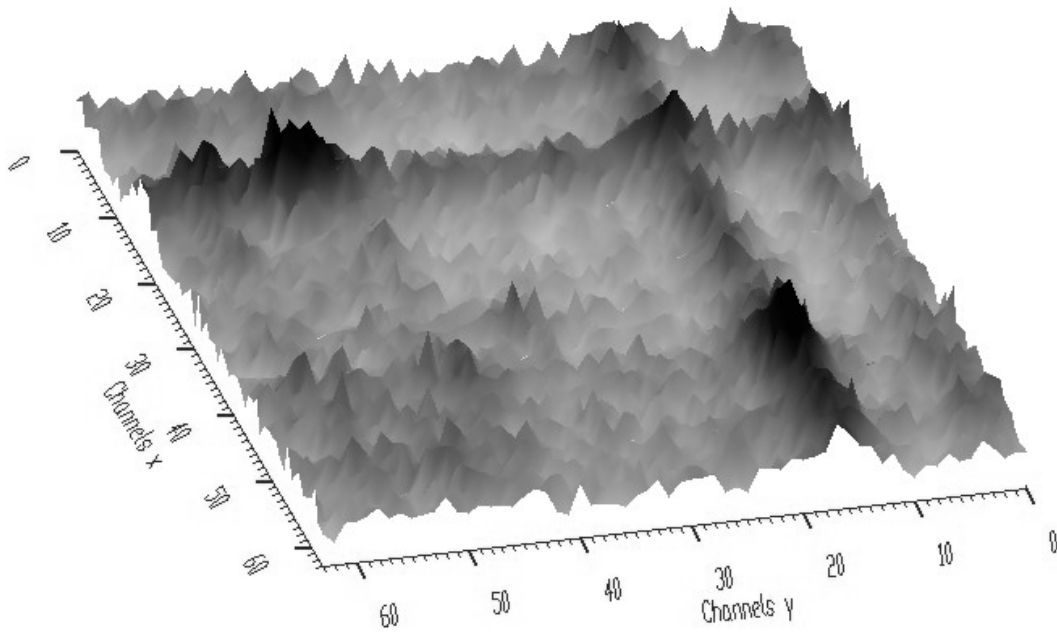
Figure 25 Two-dimensional slice from original four-dimensional spectrum
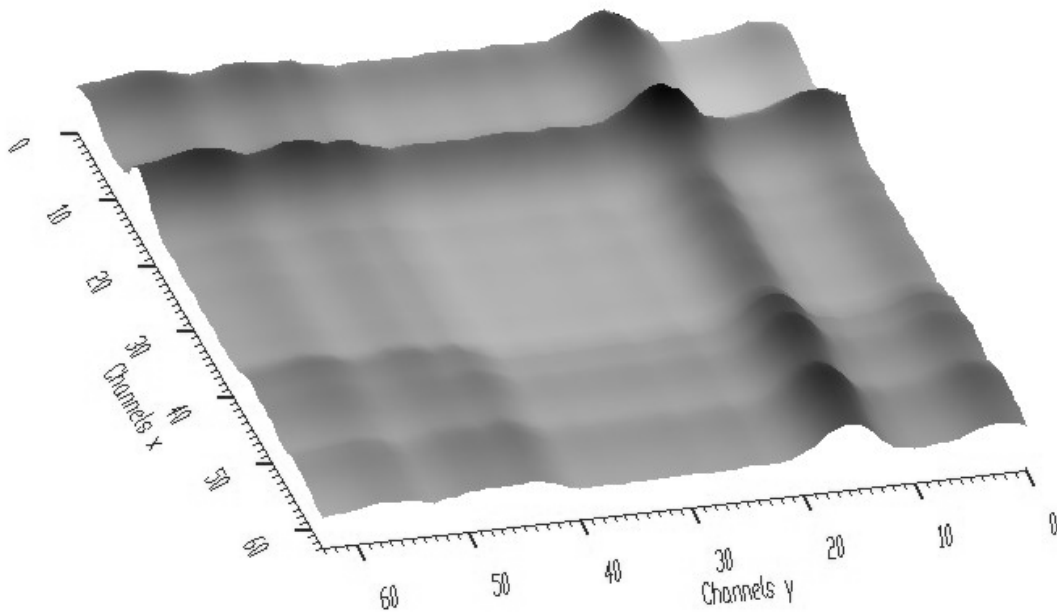
Figure 26 Two-dimensional slice decompressed from four-dimensional data compressed via adaptive Walsh transform

Examples of compression using randomizing transforms
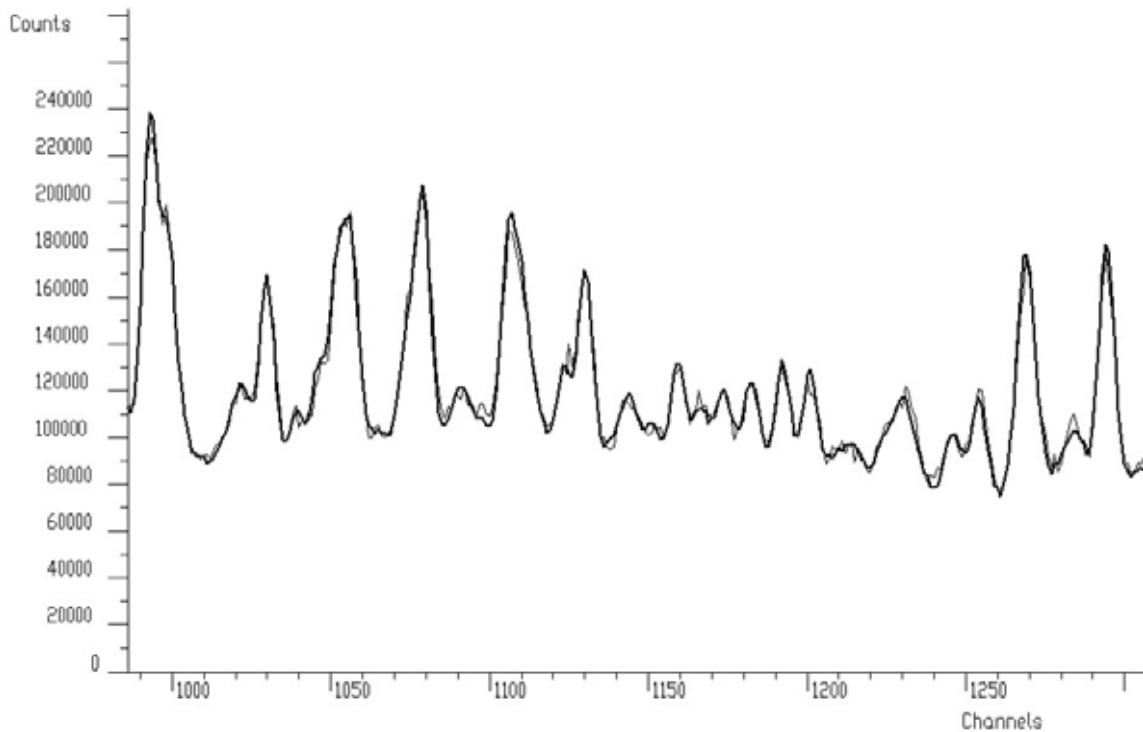
Figure 27 A part of one-dimensional slices from original (thick line) and compressed (thin line) four-dimensional data
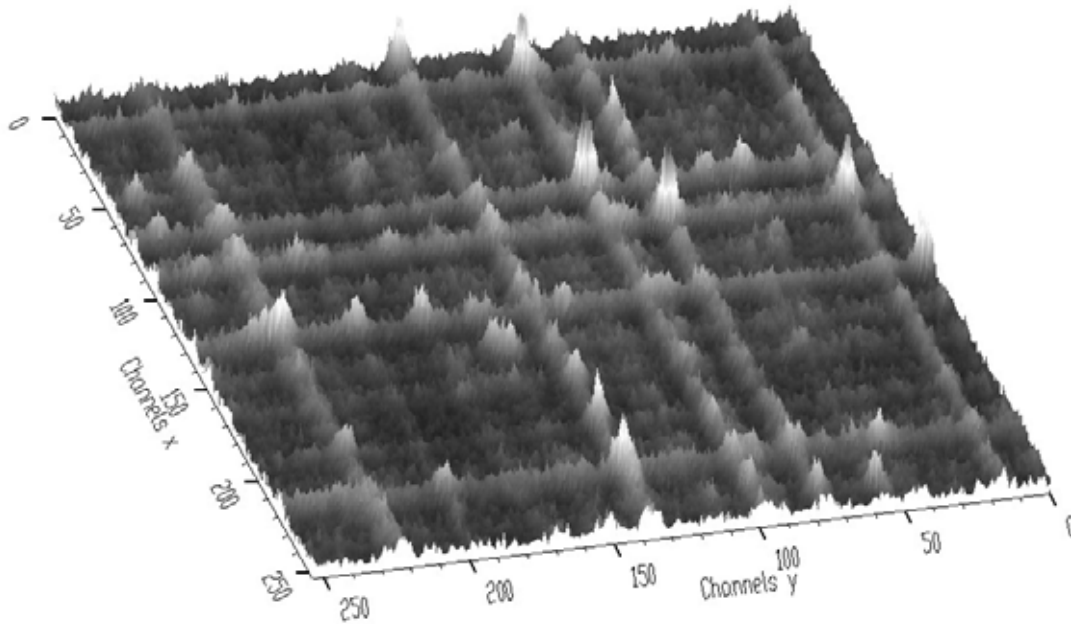
Figure 28 Two-dimensional slice from original four-dimensional data
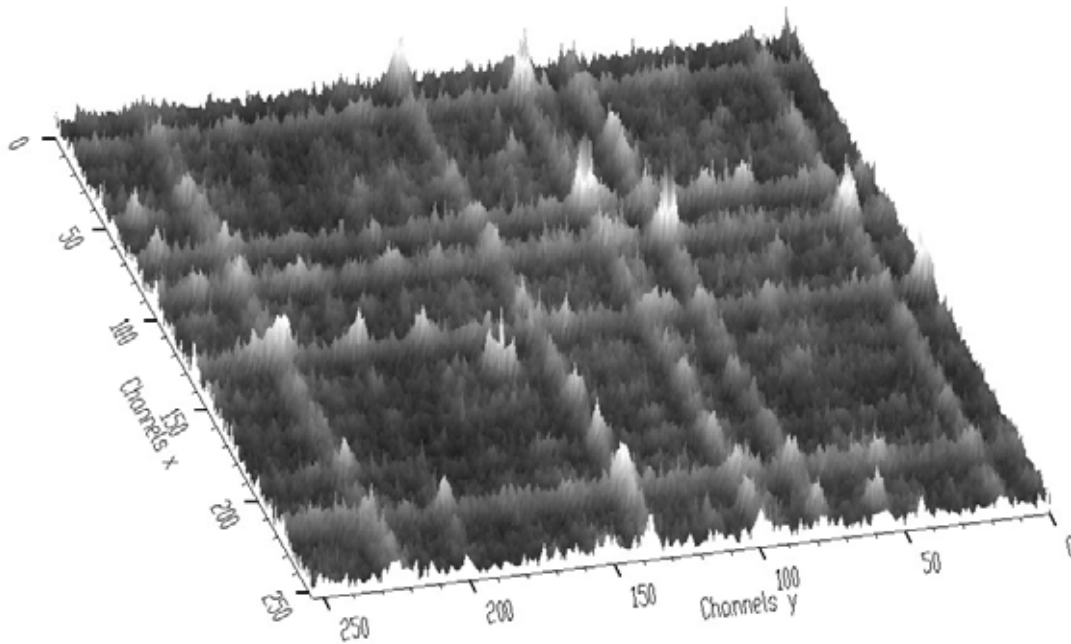
Figure 29 Two-dimensional slice from compressed four-dimensional data
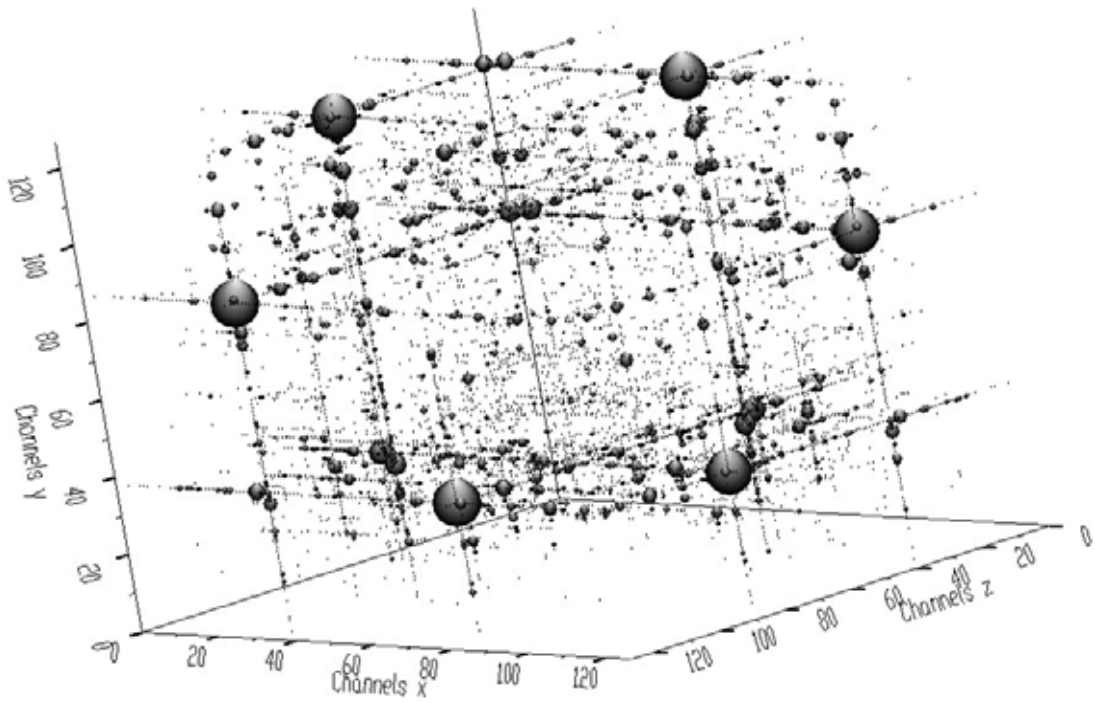
Figure 30 Three-dimensional slice from original four-dimensional data
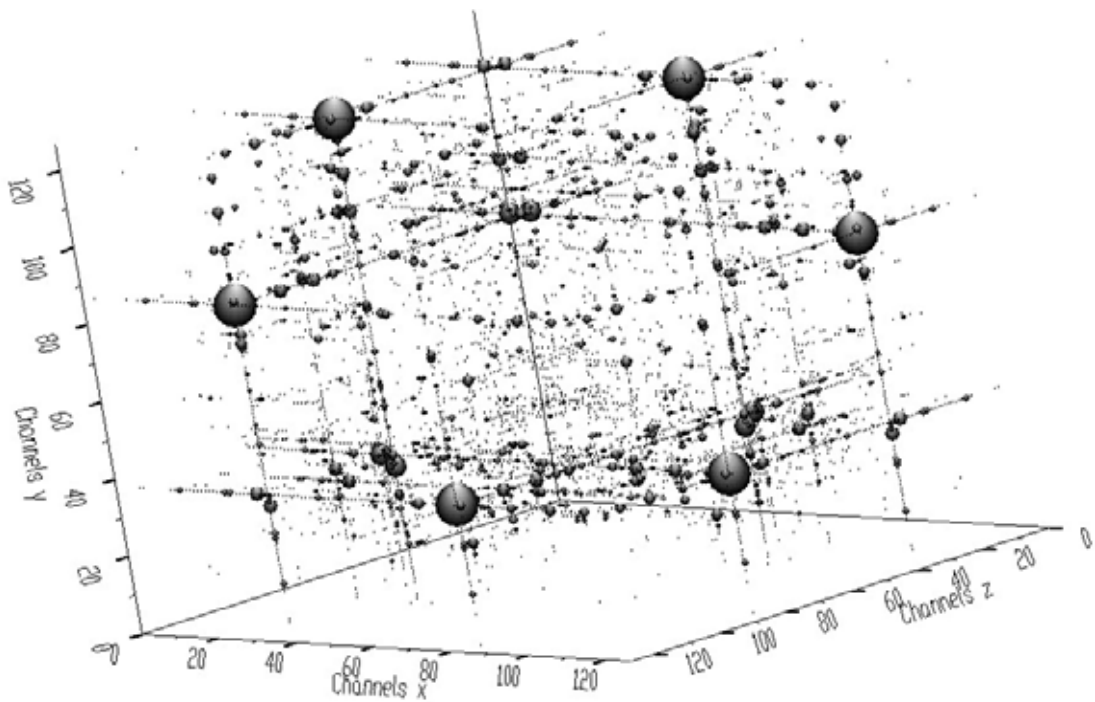
Figure 31 Three-dimensional slice from compressed four-dimensional data
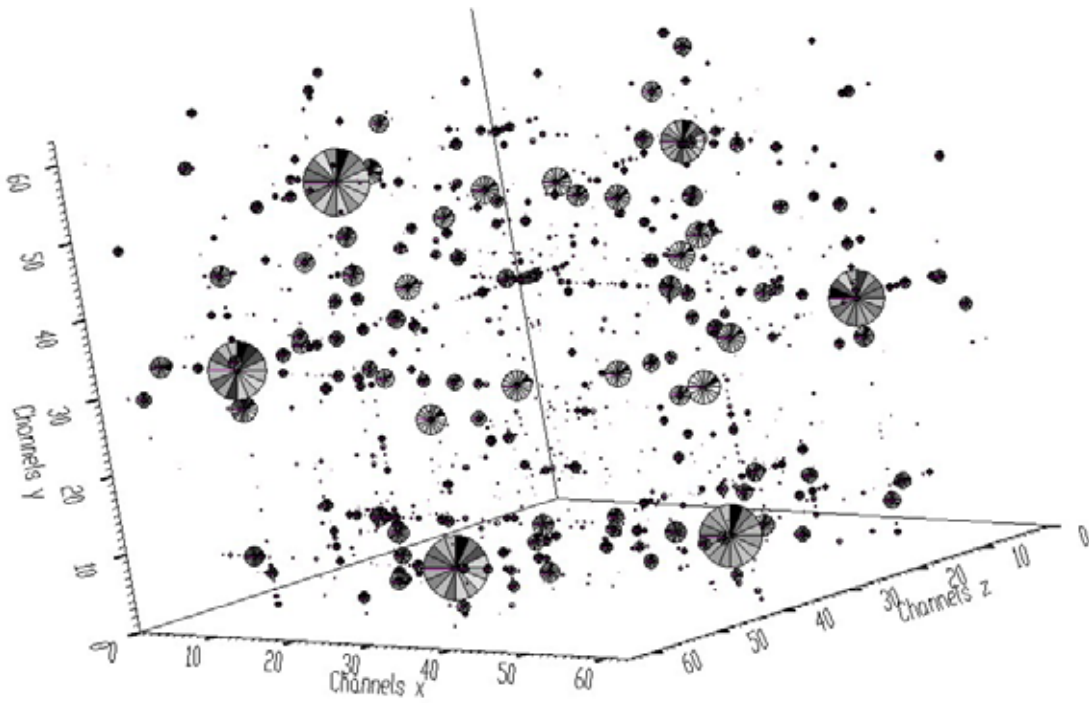
Figure 32 Four-dimensional slice from original four-dimensional data
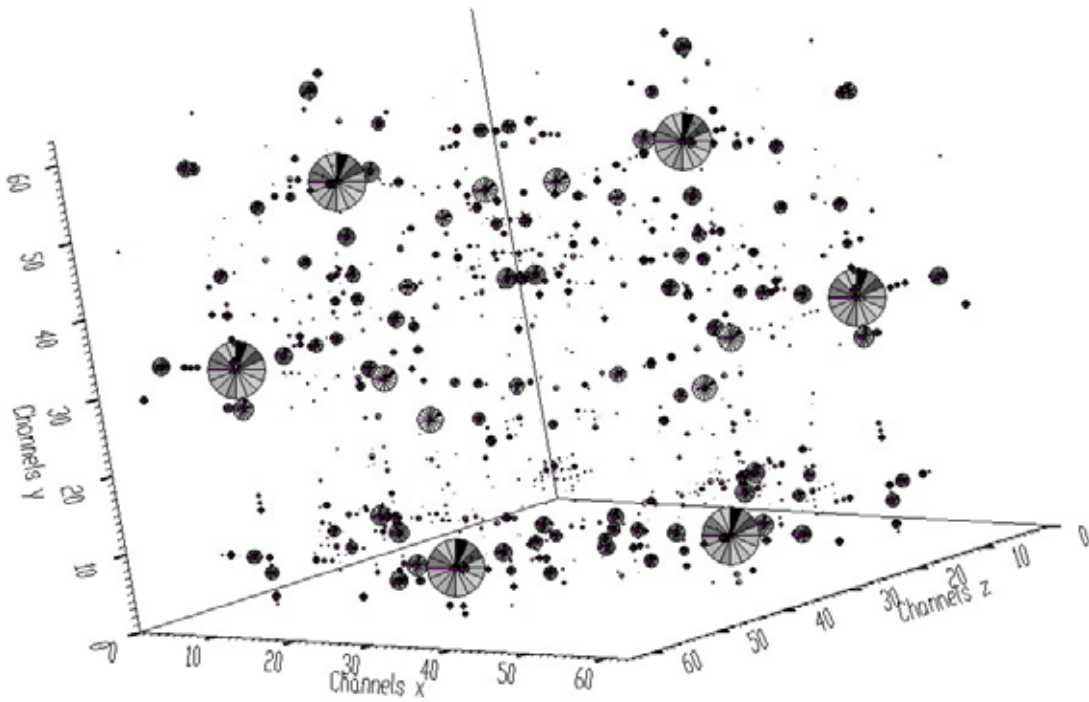
Figure 33 Four-dimensional slice from compressed four-dimensional data

Slicing and scanning - movies

Processing
- **Background estimation**
- **Deconvolution**
- **Peak identification**
- **Fit**

Background estimation

Goal: Separation of useful information (peaks) from useless information (background)

- we have derived an extension of the Sensitive Nonlinear Iterative Peak clipping (SNIP) algorithm to two-, and three-dimensional γ-ray spectra. We have generalized it to n-dimensional case.

Reference:
Morháč M., Kliman J., Matoušek V., Veselský M., Turzo I., Background elimination methods for multidimensional coincidence gamma-ray spectra, NIM A 401 (1997) 113.

- nevertheless, the algorithm suffers from several imperfections. In what follows we give some comparisons and results of improved and new proposed algorithms.

a. One- dimensional spectra
- the original SNIP algorithm and all the algorithms presented in the above-given reference were based on increasing clipping window principle.
- in the estimated background one can notice lobes at the edges of big peaks due to fluctuations present in the spectrum. Naturally, after subtraction of the estimated background from the spectrum the shapes of peaks are deformed.
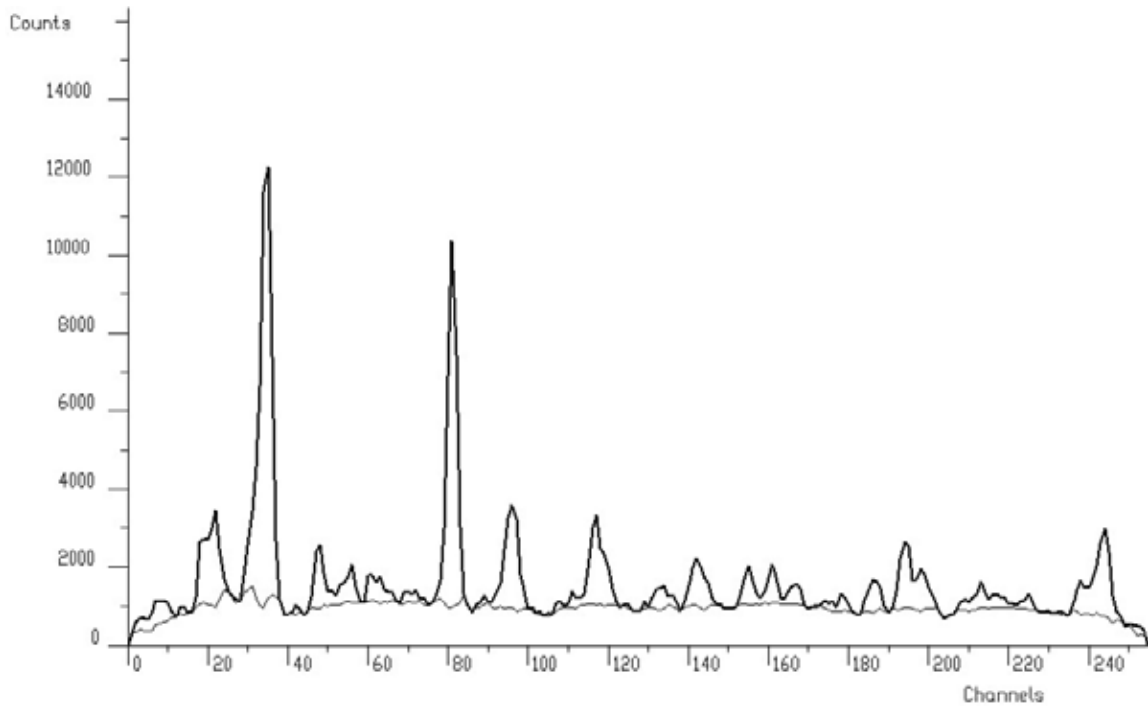
Figure 34 One-dimensional γ - ray spectrum and estimated background using increasing clipping window algorithm

- very simple, but efficient idea, how to improve the background estimate is to switch direction of the change of the clipping window to decreasing one
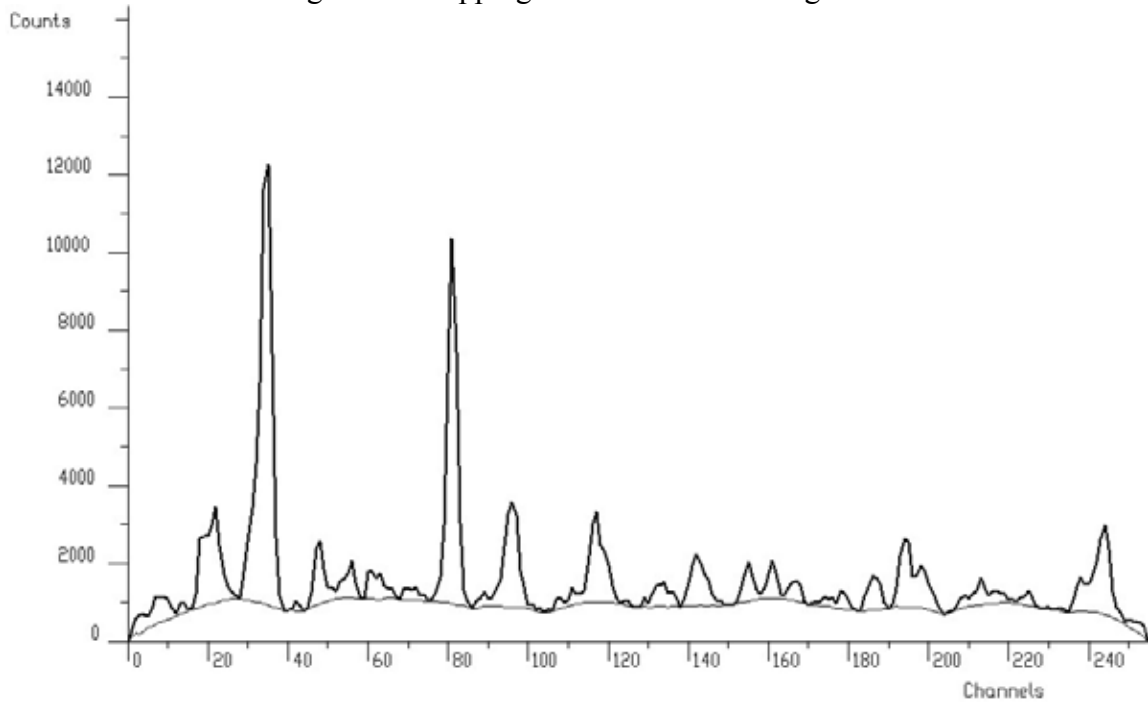
Figure 35 One-dimensional γ - ray spectrum and estimated background using decreasing clipping window algorithm

- let us illustrate the influence of the width of clipping window w on the estimated background. We take γ-ray spectrum with very complicated background and with many peaks .
- in the example we employed the algorithm with decreasing window for w=10, 20, 30, 40. Apparently, by changing the width one can substantially influence the estimated background.
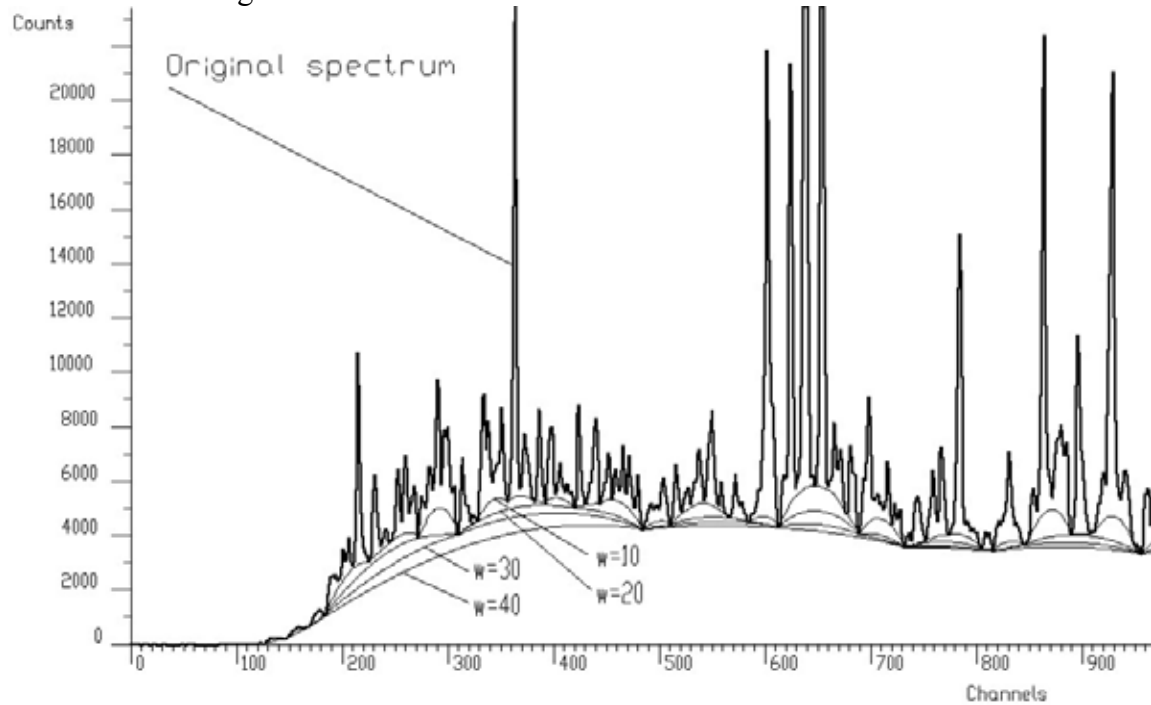
Figure 36 Illustration of clipping window width on estimated background

- the other way to improve the estimate of the background is to employ higher order clipping filters. The example of a portion of γ-ray spectrum for clipping filters of 2-nd, 4-th, 6-th, 8-th orders for w=40 are shown in Figure 37.

30
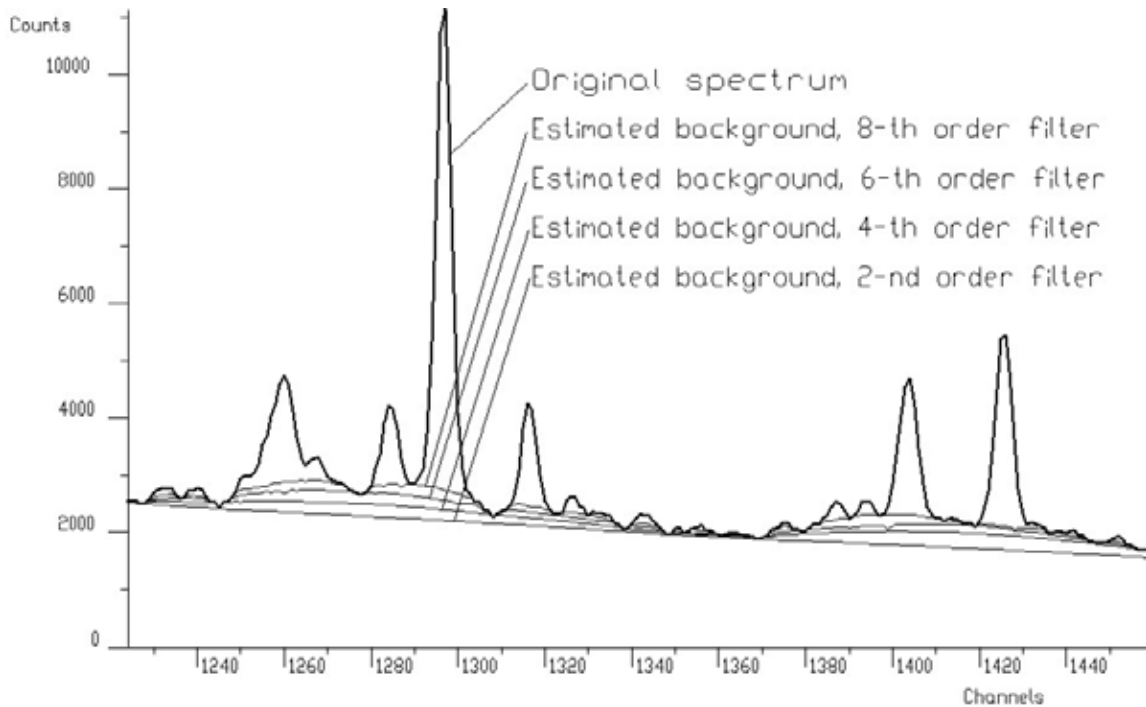
Figure 37 Illustration of the influence of clipping filter order on estimated background

- the estimate of the background can be influenced by noise present in the spectrum. We proposed the algorithm of the background estimate with simultaneous smoothing
- in the original algorithm without smoothing, the estimated background snatches the lower spikes in the noise. Consequently, the areas of peaks are biased by this error.
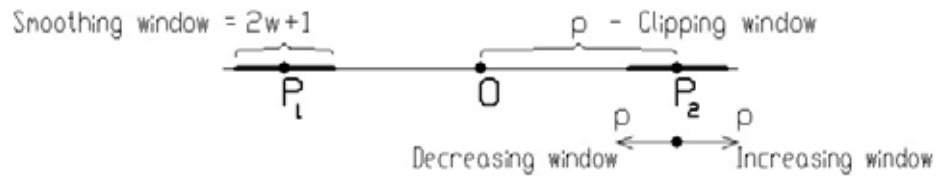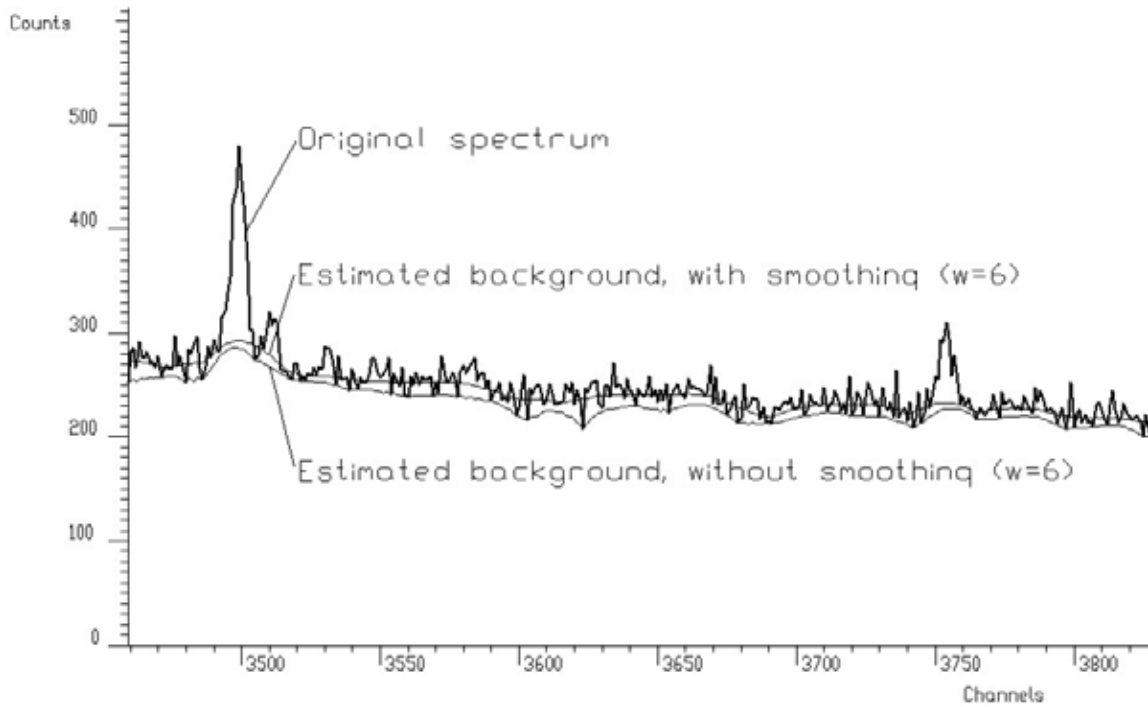
Figure 38 Illustration of non-smoothing and smoothing algorithm of background estimation

b. Two-dimensional spectra

- background estimation with simultaneous smoothing allows to improve the quality of the estimated spectrum
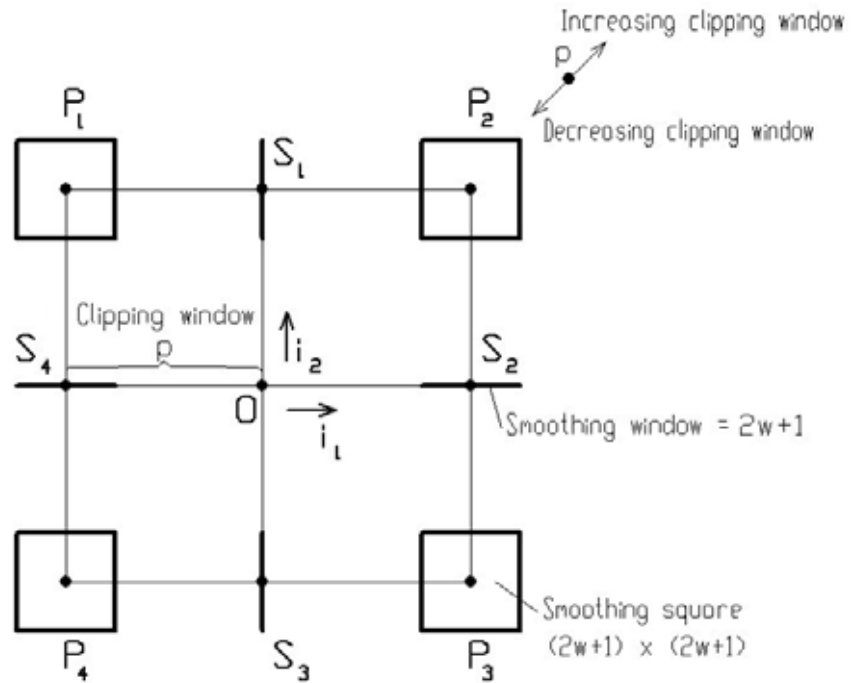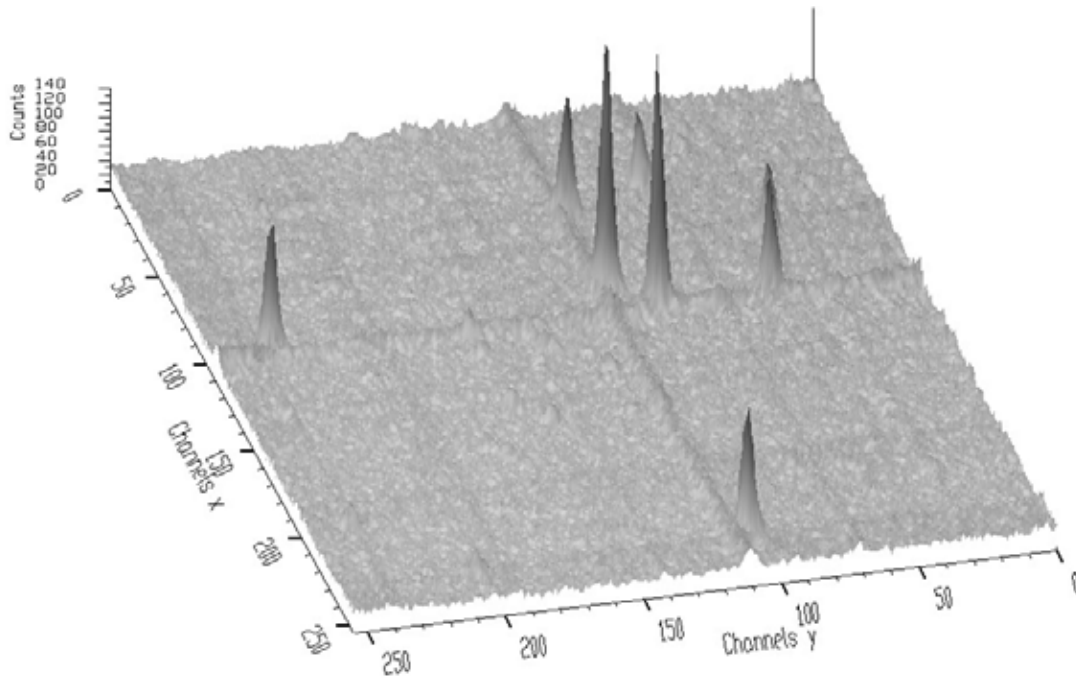
Figure 39 Original noisy two-dimensional γ-ray spectrum
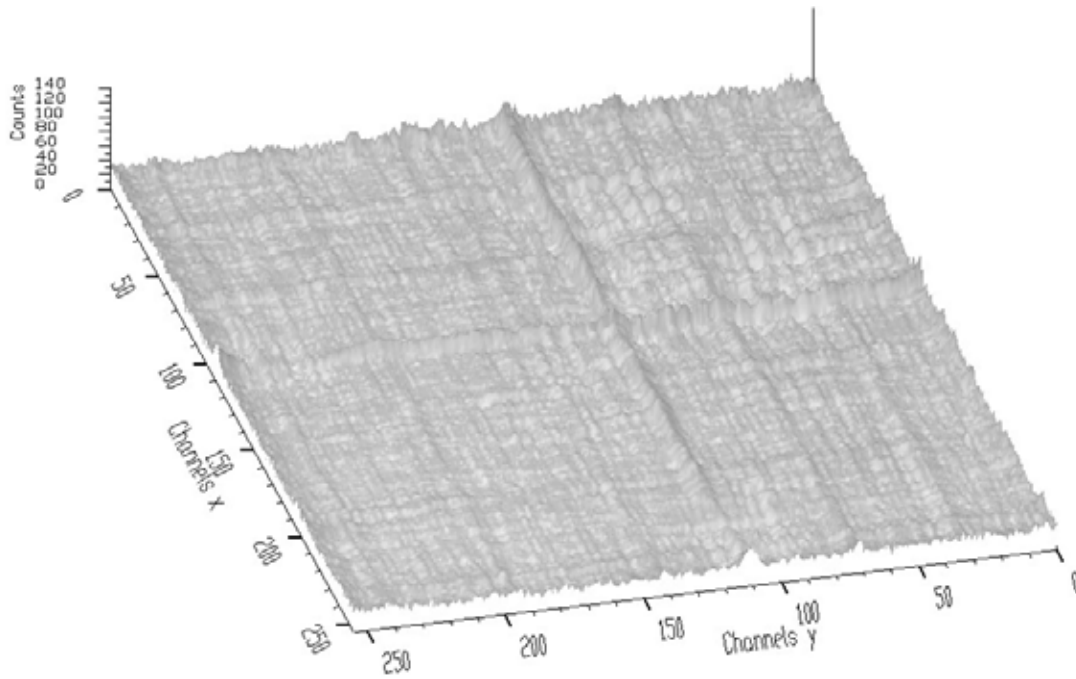
Figure 40 Estimated background of the spectrum from Figure 39 using the algorithm without smoothing
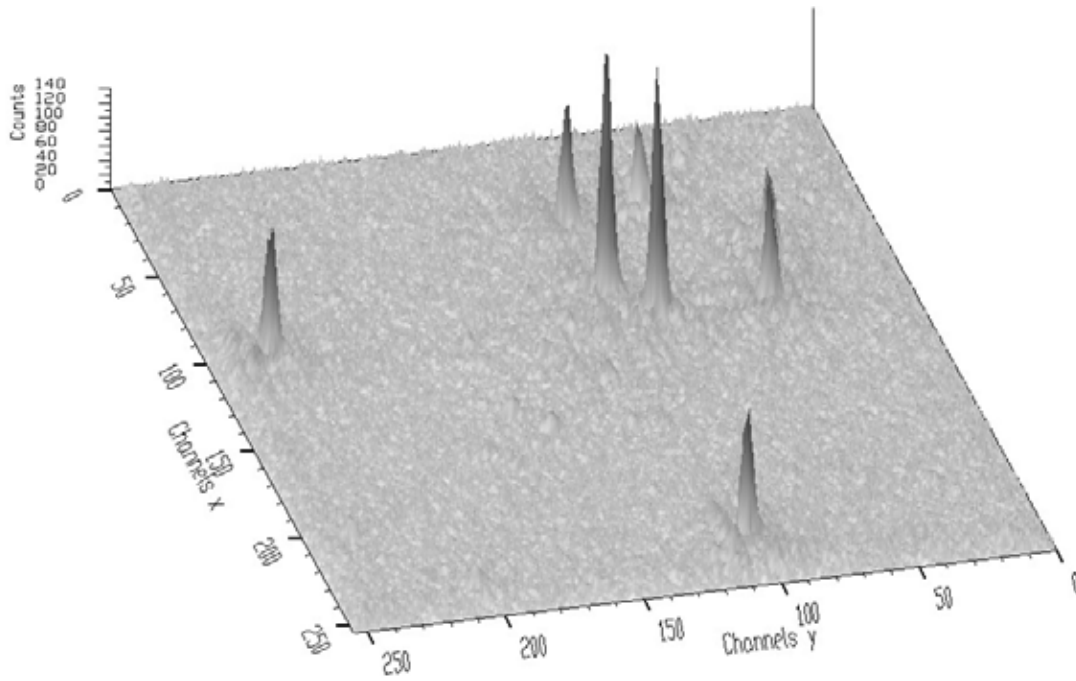
Figure 41 Spectrum from Figure 39 after background subtraction (Figure 40)
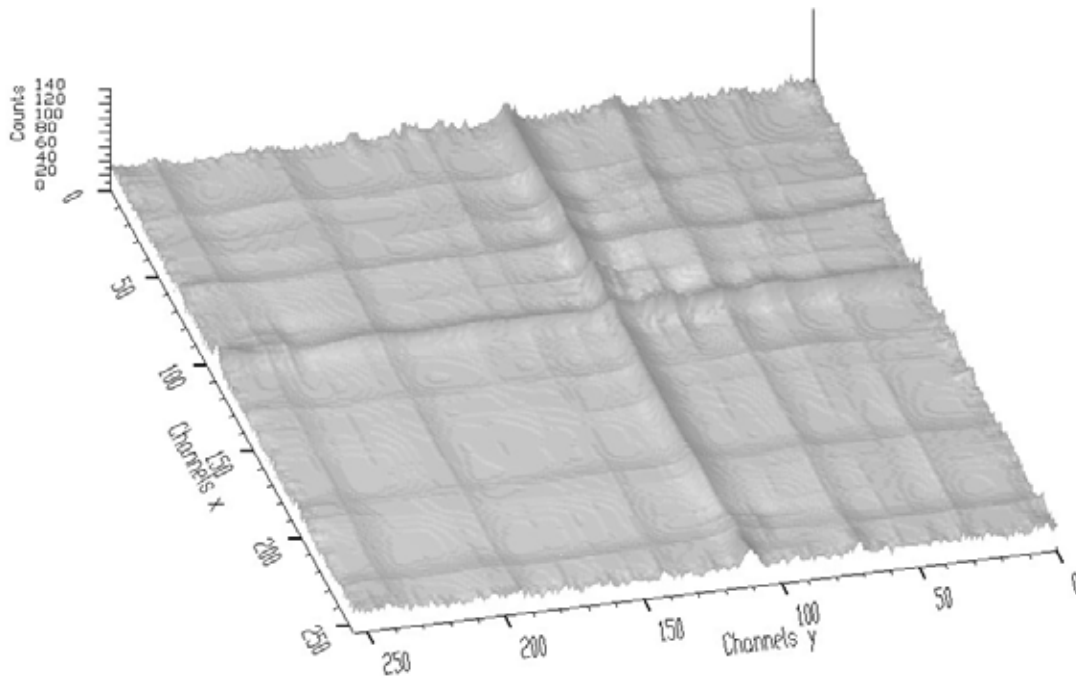
Figure 42 Estimated background of the spectrum from Figure 39 using the algorithm with simultaneous smoothing
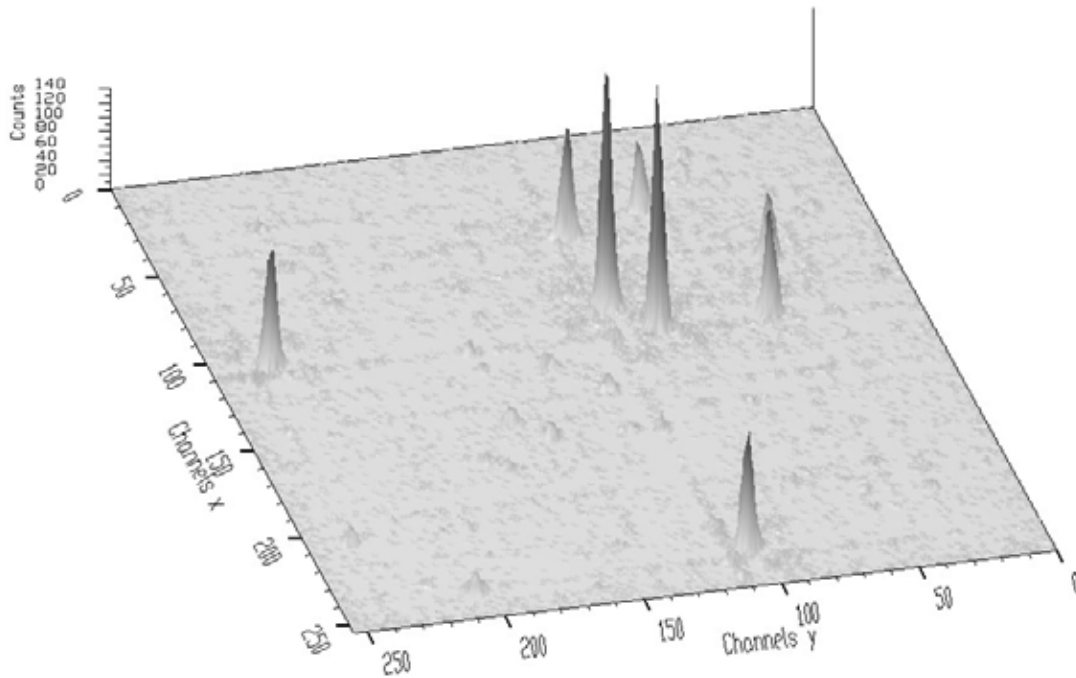
Figure 43 Spectrum from Figure 39 after subtraction of background estimated using the algorithm with simultaneous smoothing (Figure 42)

- so far we assumed that the width of the peaks was equal for both dimensions (we worked with γ-ray spectra). This is however not the case, e.g., for $\gamma - X$ spectra where the widths of peaks in both dimensions are different.
- we have generalized the algorithm even for this kind of data.
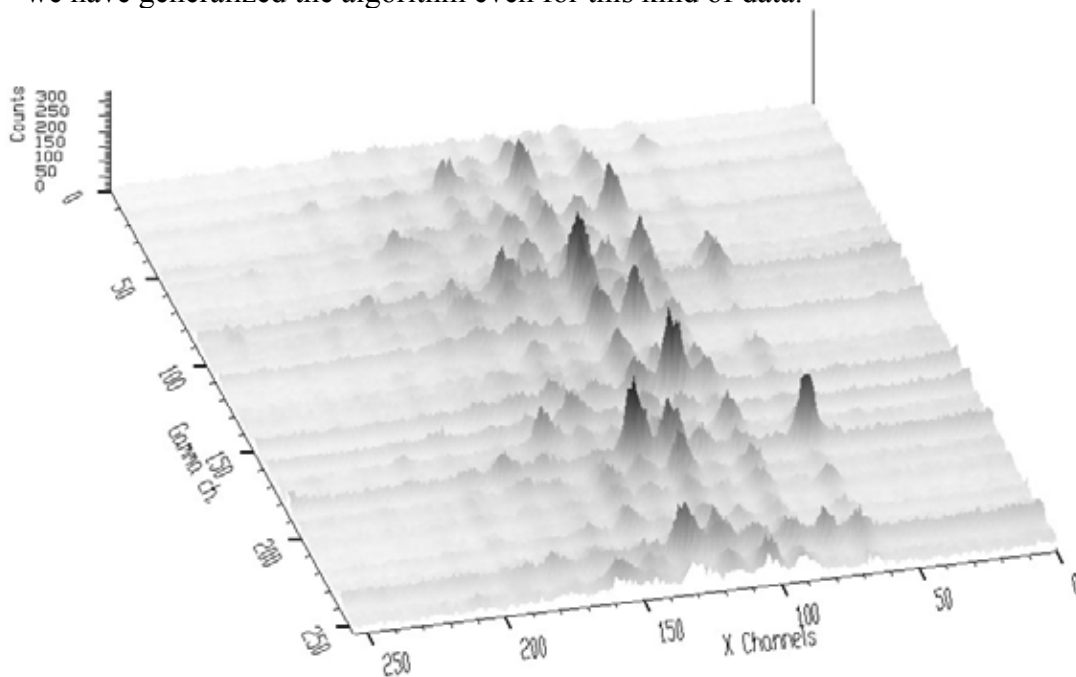
Figure 44 Original two-dimensional $\gamma - X$ spectrum
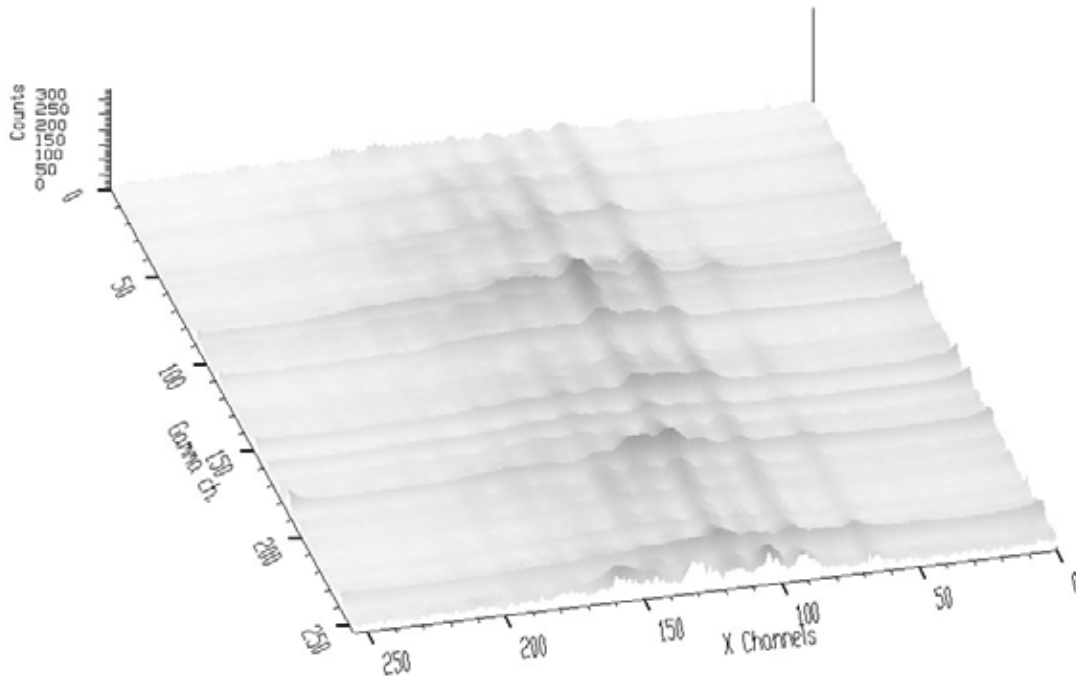
Figure 45 Estimated background of the spectrum from Figure 44 (decreasing clipping window w_γ =6, w_X =12)
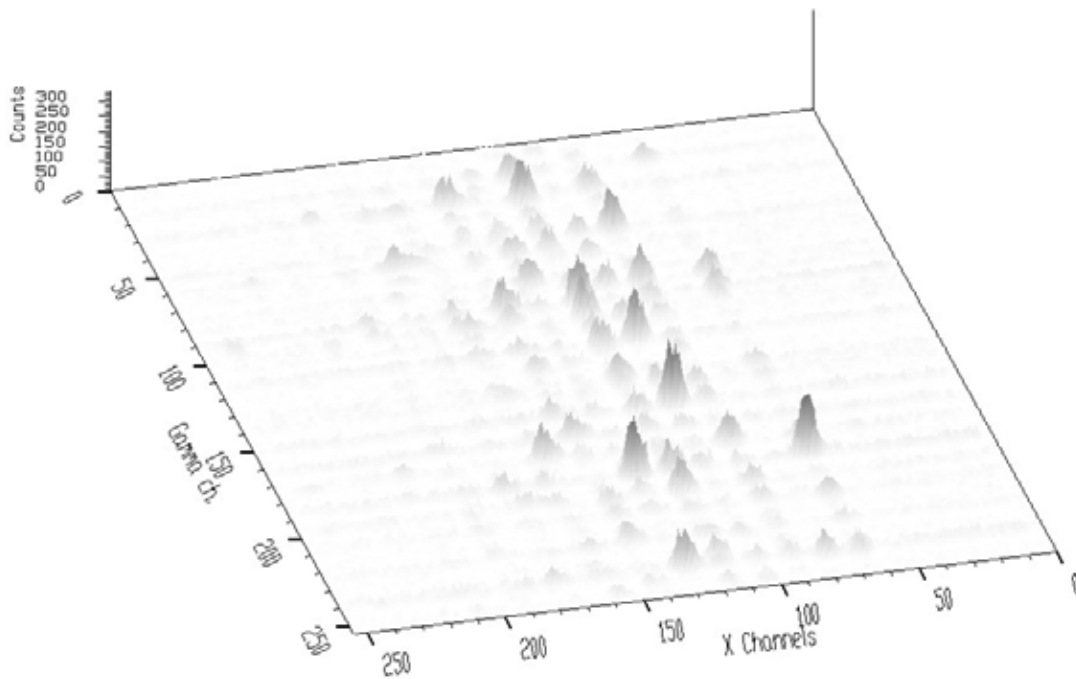
Figure 46 Spectrum from Figure 44 after background subtraction (shown in Figure 45)

- we derived the algorithm to estimate skew ridges in the two-dimensional spectrum.
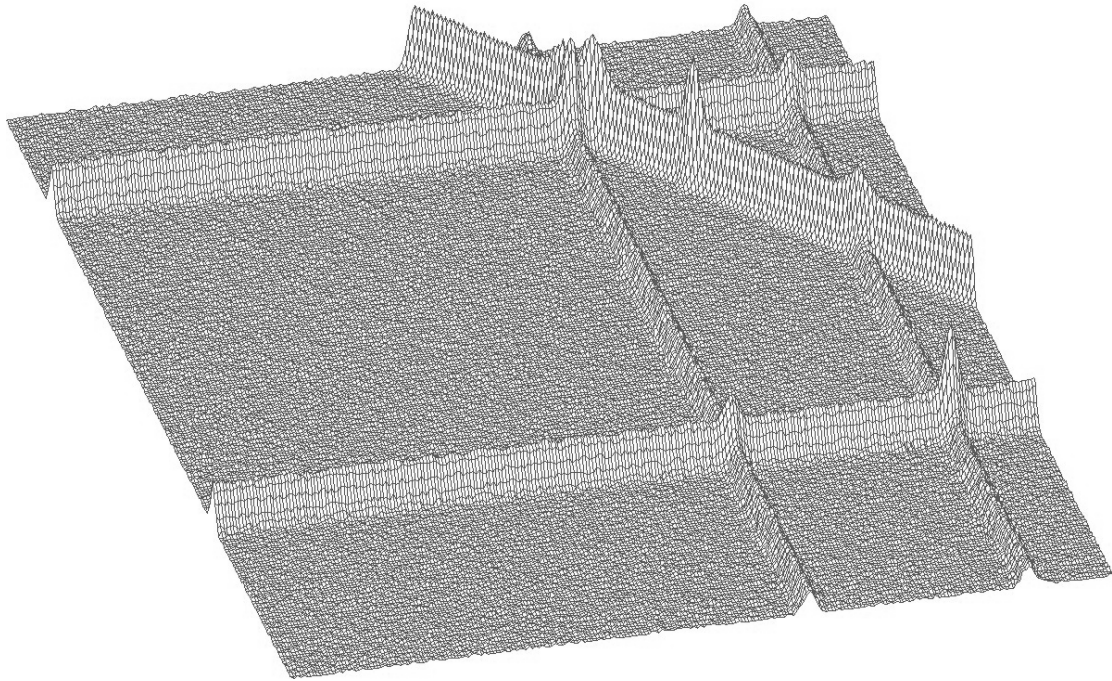
Figure 47 Two-dimensional synthetic spectrum containing skew ridges

- the goal is to remove rectangular as well as skew ridges from the spectrum and to leave only two-dimensional coincidence peaks.
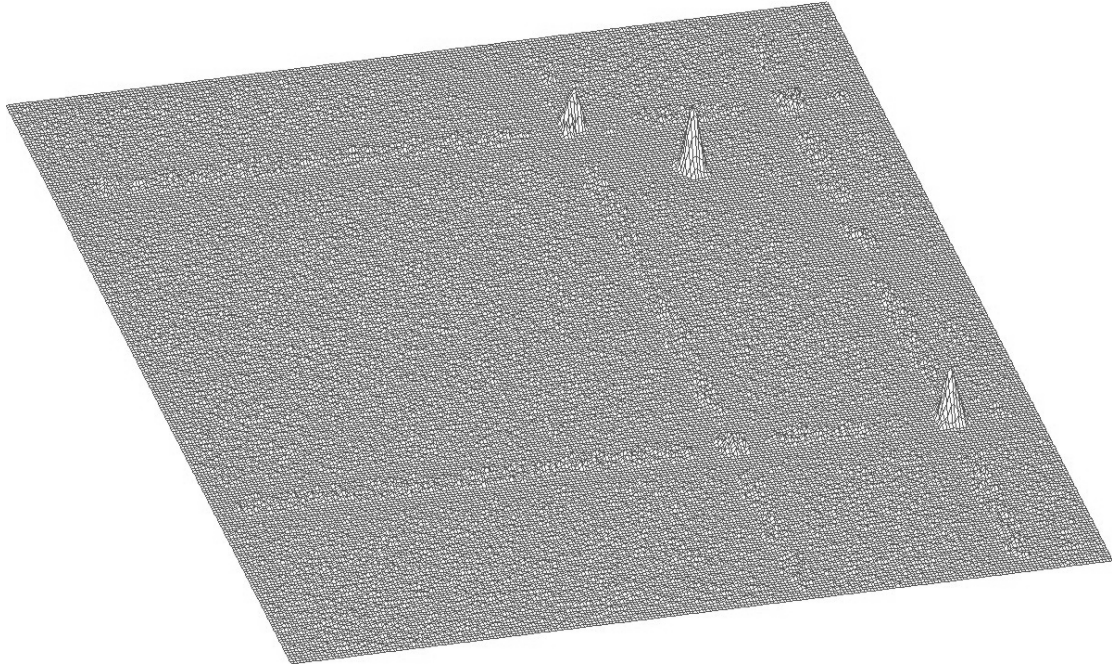
Figure 48 Spectrum from Figure 47 after subtraction of background

- in next two Figures we present the experimental spectrum with skew ridges and estimated background, respectively.
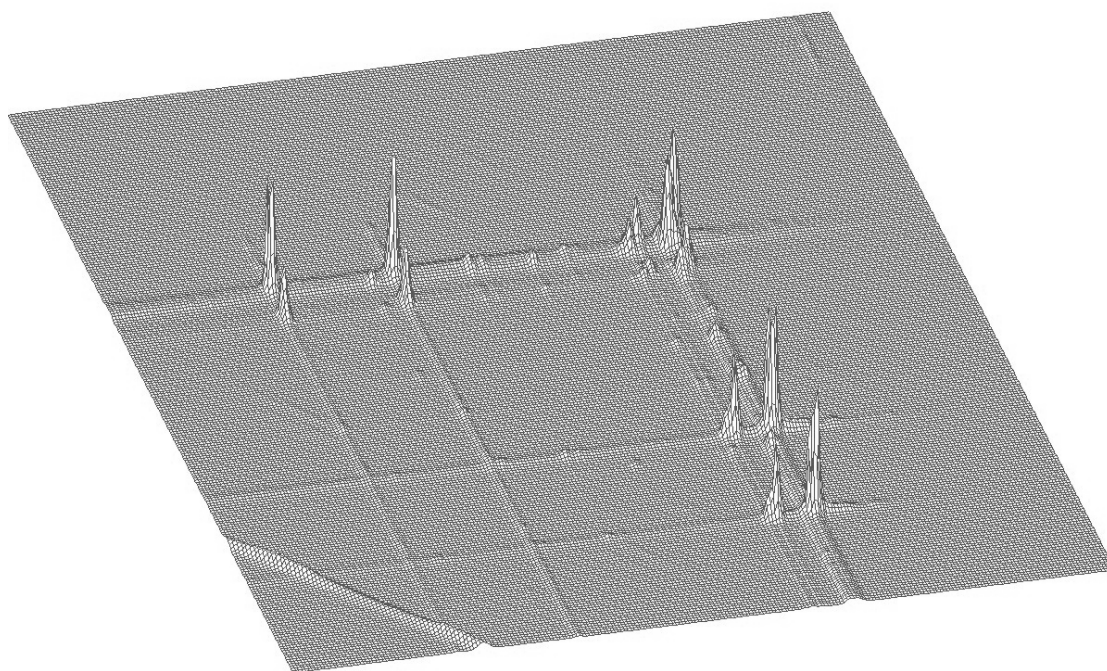
Figure 49 Experimental two-dimensional spectrum containing skew ridges
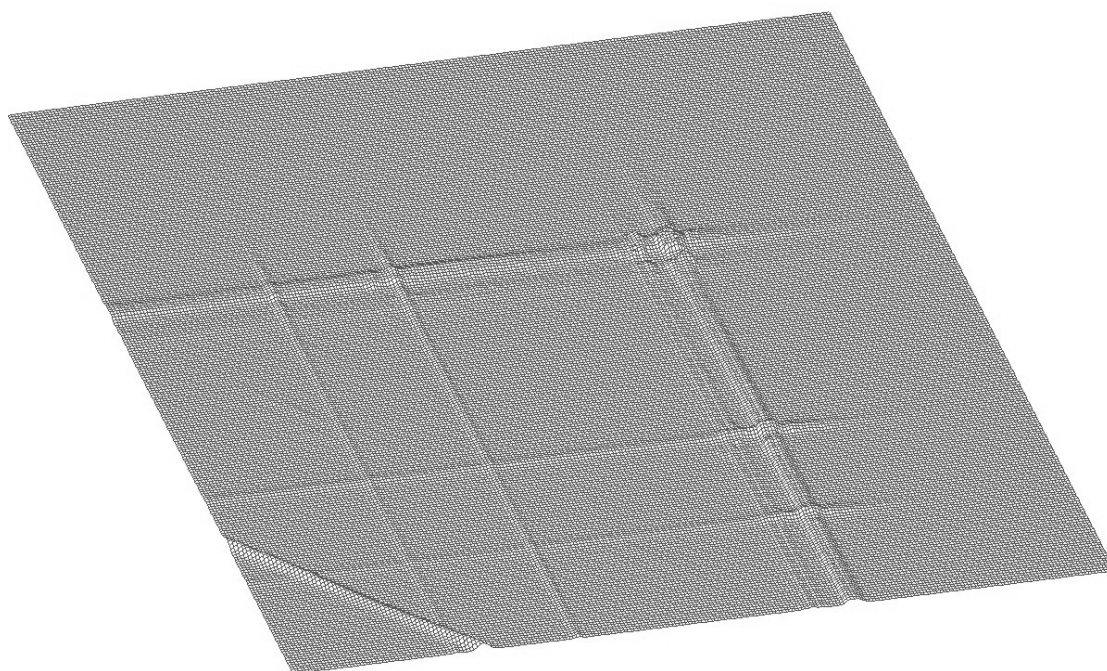
Figure 50 Estimated background (with skew ridges) of the spectrum from Figure 49

- finally, we present the algorithm that estimates the continuous background together with rectangular as well as with nonlinear ridges.
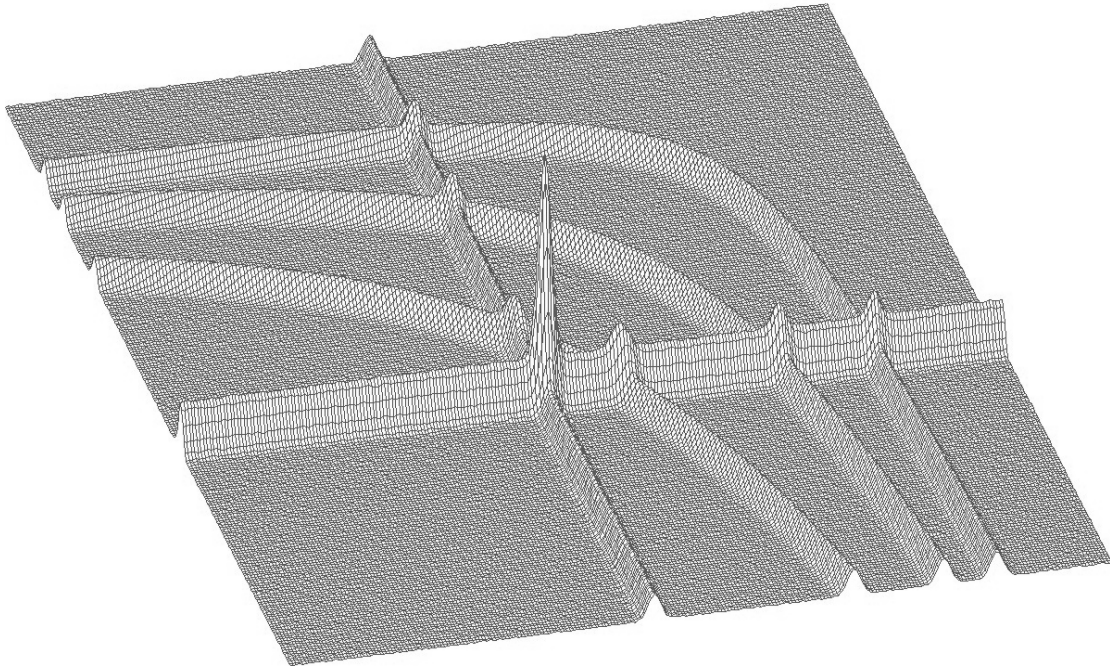
Figure 51 Synthetic two-dimensional spectrum containing rectangular as well as nonlinear ridges
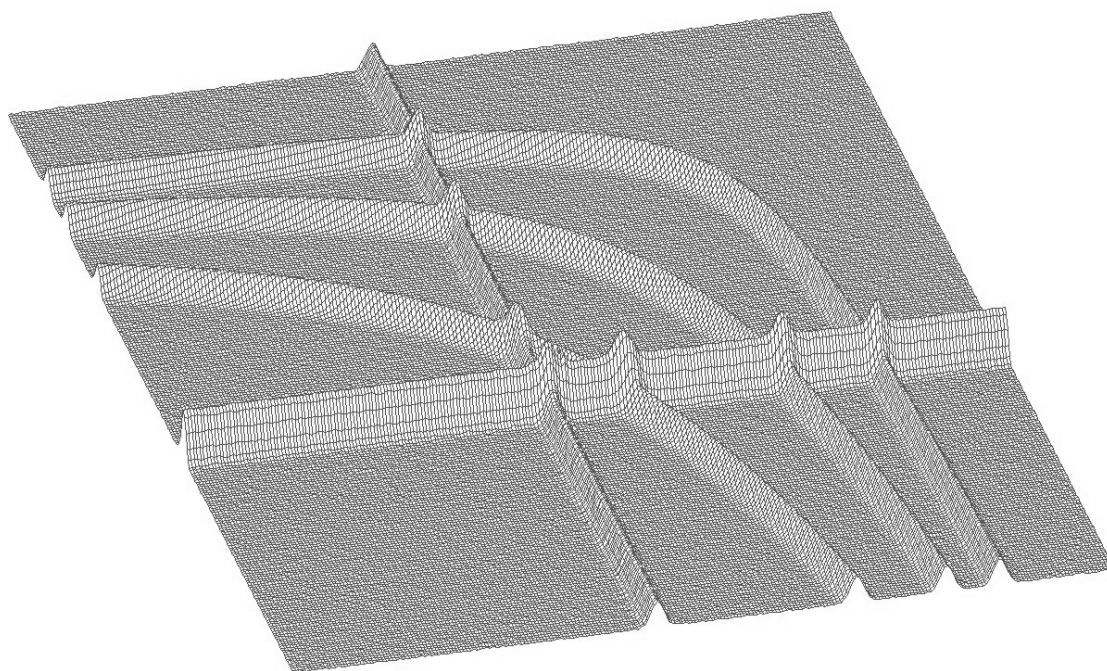
Figure 52 Estimated background (with nonlinear ridges) of the spectrum from Figure 51
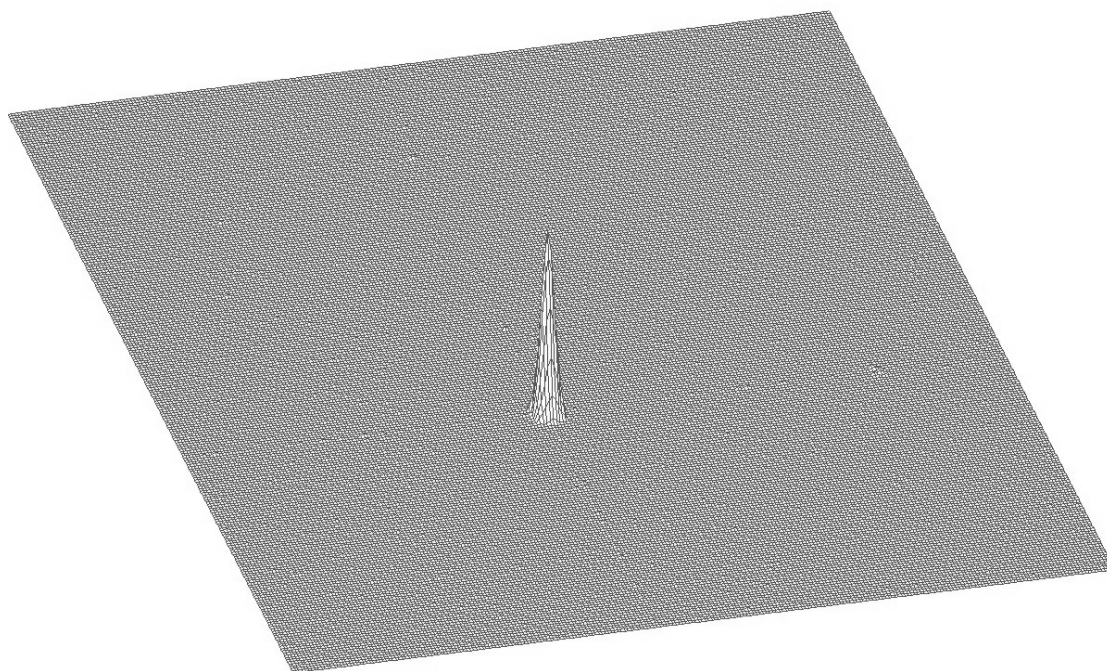
Figure 53 Two-dimensional peak after subtraction of background (Figure 52) from the spectrum shown in Figure 51

c. Three-dimensional spectra

- to illustrate the generalization of the background estimation algorithms we proceed to three-fold coincidence $\gamma - \gamma - \gamma$-ray spectra. In this case, we have to include to the estimated background its continuous component as well as one and two-fold coincidences in all dimensions.
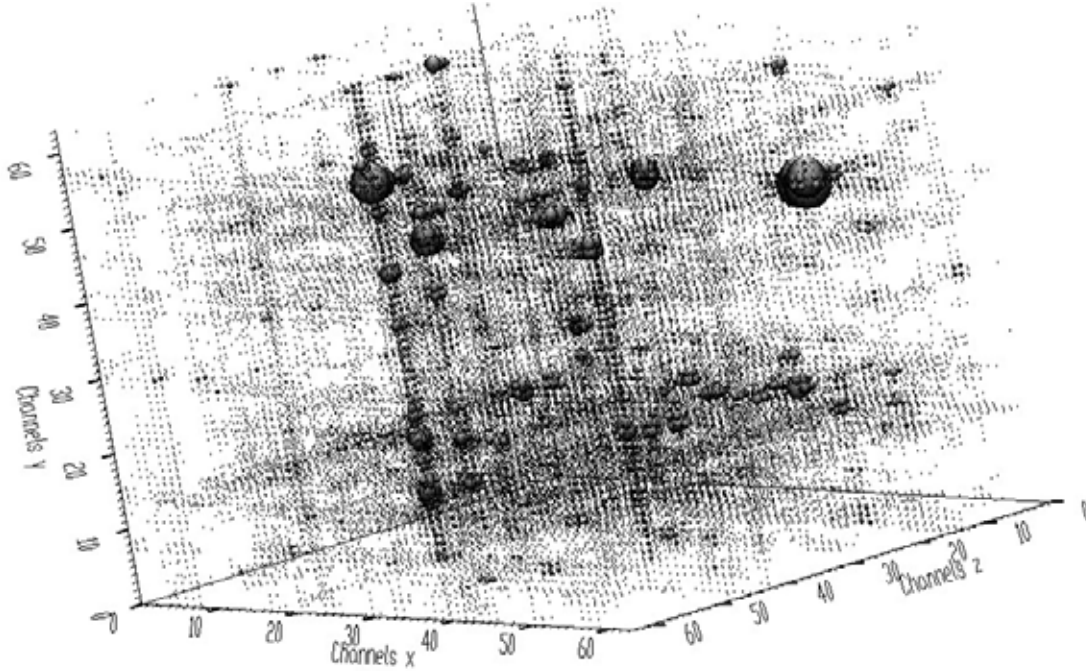
Figure 54 Original $\gamma - \gamma - \gamma$ ray spectrum
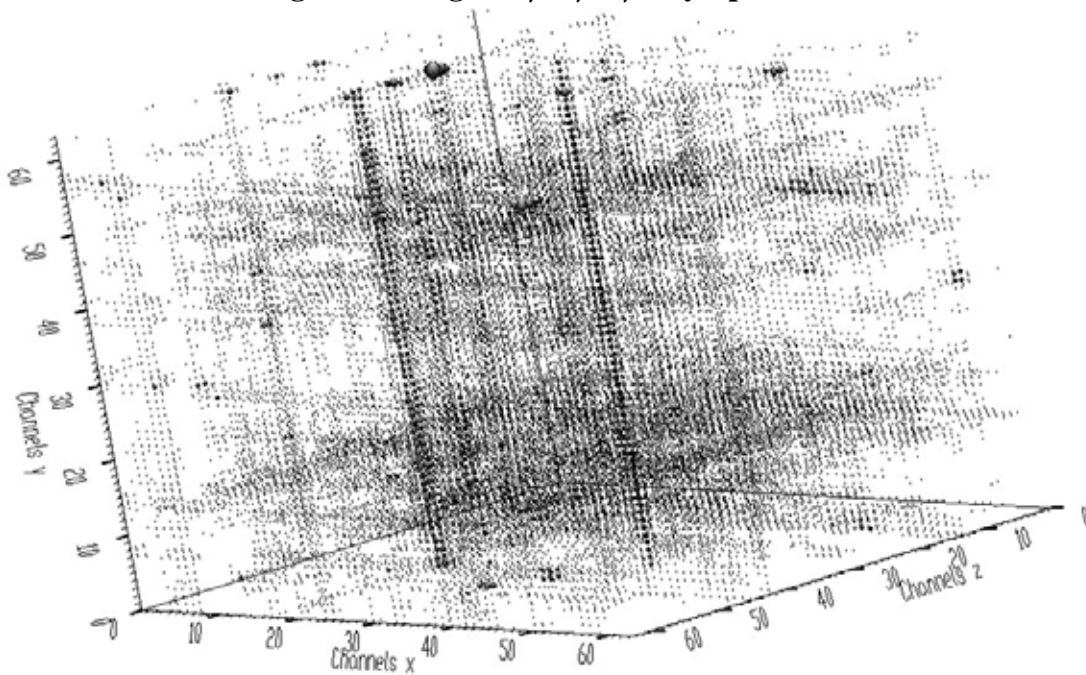
Figure 55 Estimated background (for decreasing clipping window, w =5) of the spectrum from Figure 54
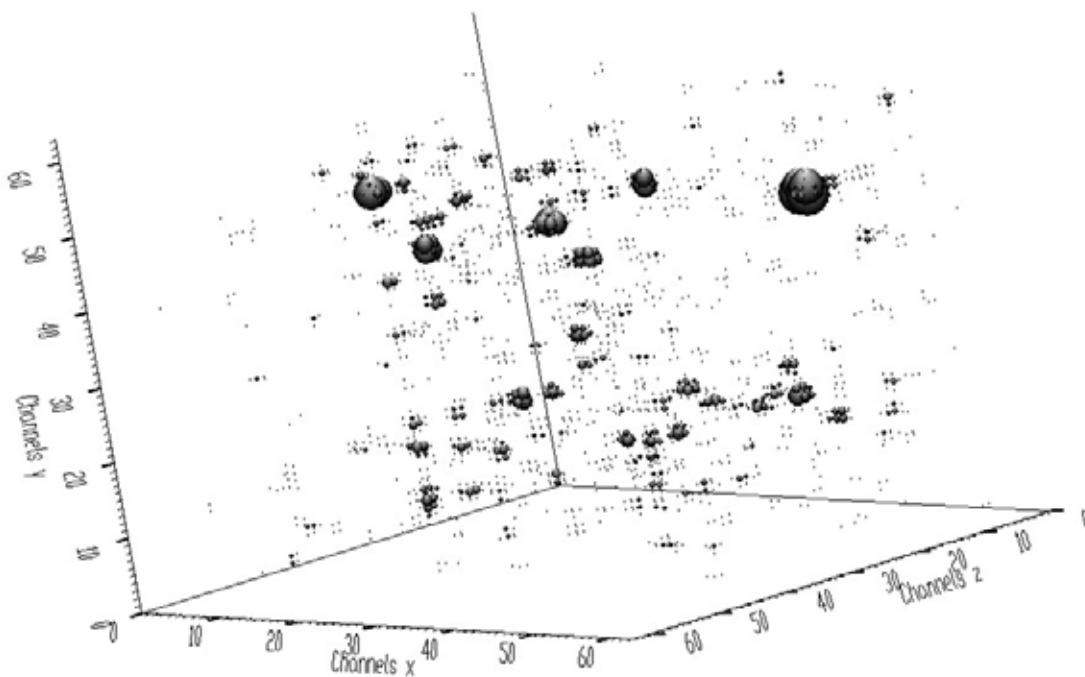
Figure 56 Spectrum from Figure 54 after background subtraction

d. Four-dimensional spectra

- we have implemented the algorithm of background determination even for four-dimensional spectra. The algorithm allows to separate four-fold coincidences from continuous background as well as from lower order concidences.
- three parameters determine the position of the center of the slice in the 4-th dimension. The channels of the slice are changing with the angle starting from 9 o'clock position. 2π angle of the slice is divided to appropriate number of channels in the 4-th dimension. The sizes of lines from the centre of the slice are proportional to the contents of channels.
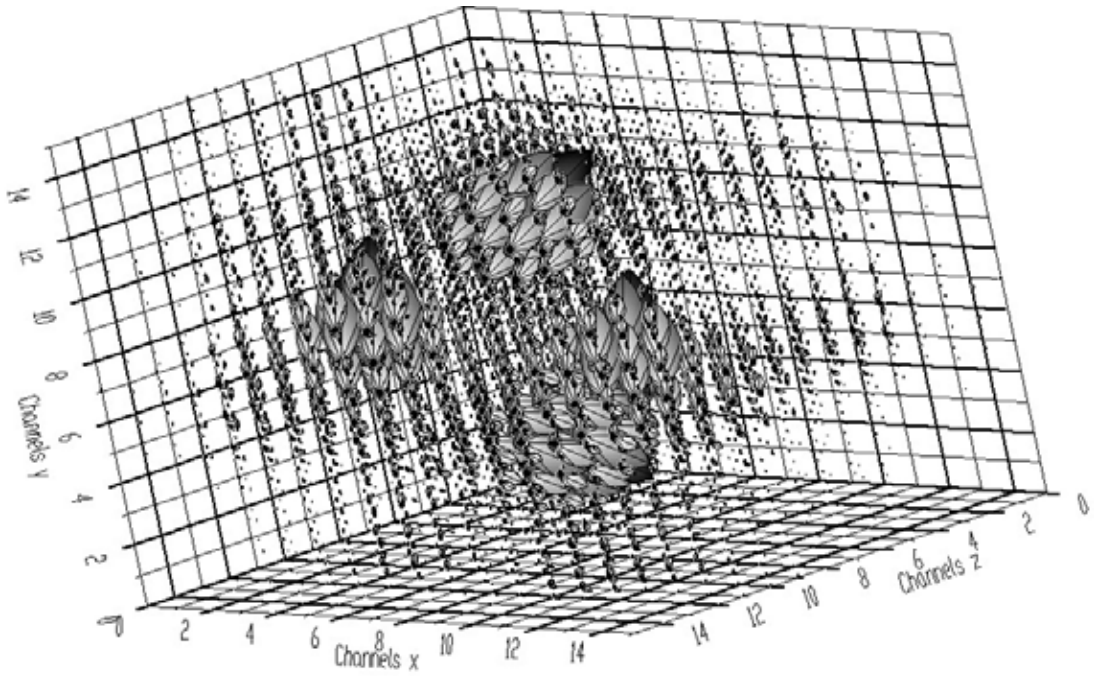
Figure 57 Synthetic four-dimensional spectrum
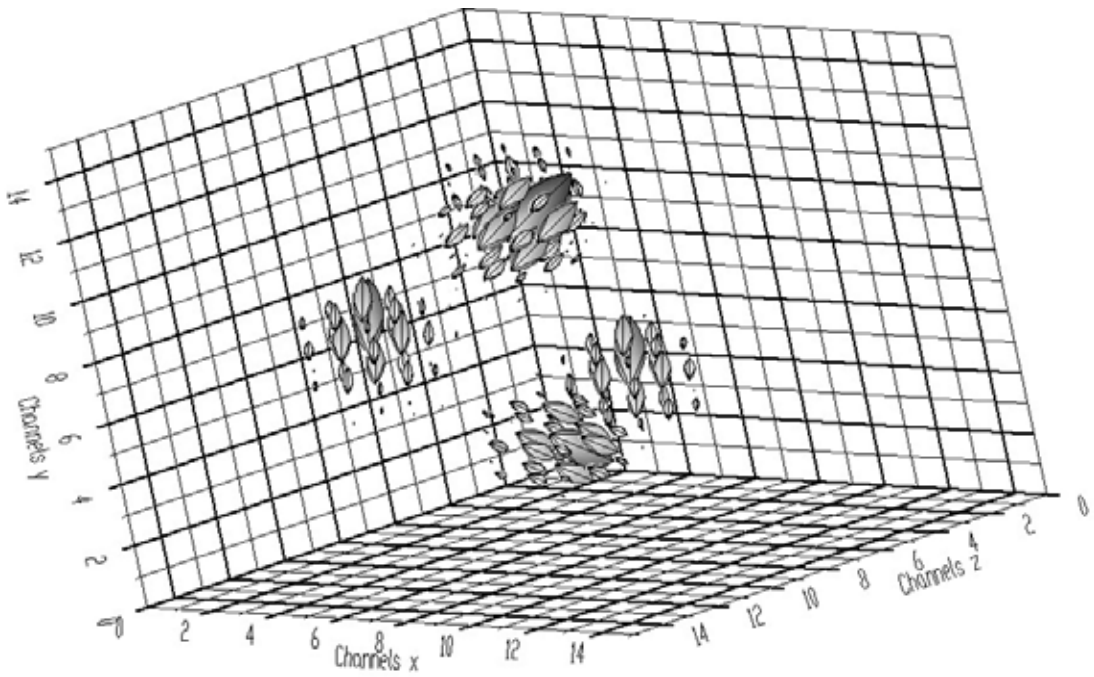
Figure 58 Spectrum from Figure 57 after background elimination

Movies

Deconvolution

Goal: Improvement of the resolution in spectra

- the principal results of the deconvolution operation were presented in

Reference:
Morháč M., Kliman J., Matoušek V., Veselský M., Turzo I., Efficient one and two dimensional Gold deconvolution and its application to gamma-ray spectra decomposition, NIM A 401 (1997) 385.

- later we have optimized the Gold deconvolution algorithm that allowed to carry out the deconvolution operation much faster and to extend it to three-dimensional spectra. The results of the optimized Gold deconvolution for all one-, two-, and three-dimensional data are given in

References:
Morháč M., Matoušek V., Kliman J., Efficient algorithm of multidimensional deconvolution and its application to nuclear data processing, Digital Signal Processing 13 (2003) 144.
Morháč M., Matoušek V., Kliman J., Optimized multidimensional nonoscillating deconvolution, Journal of Computational and Applied Mathematics 140 (2002) 639.

- we have proposed improvements, modifications, extensions of existing deconvolution methods as well as new regularization technique, e.g. one-fold Gold deconvolution, boosted deconvolution, Tikhonov regularization with minimization of squares of negative values.

a. One - dimensional spectra
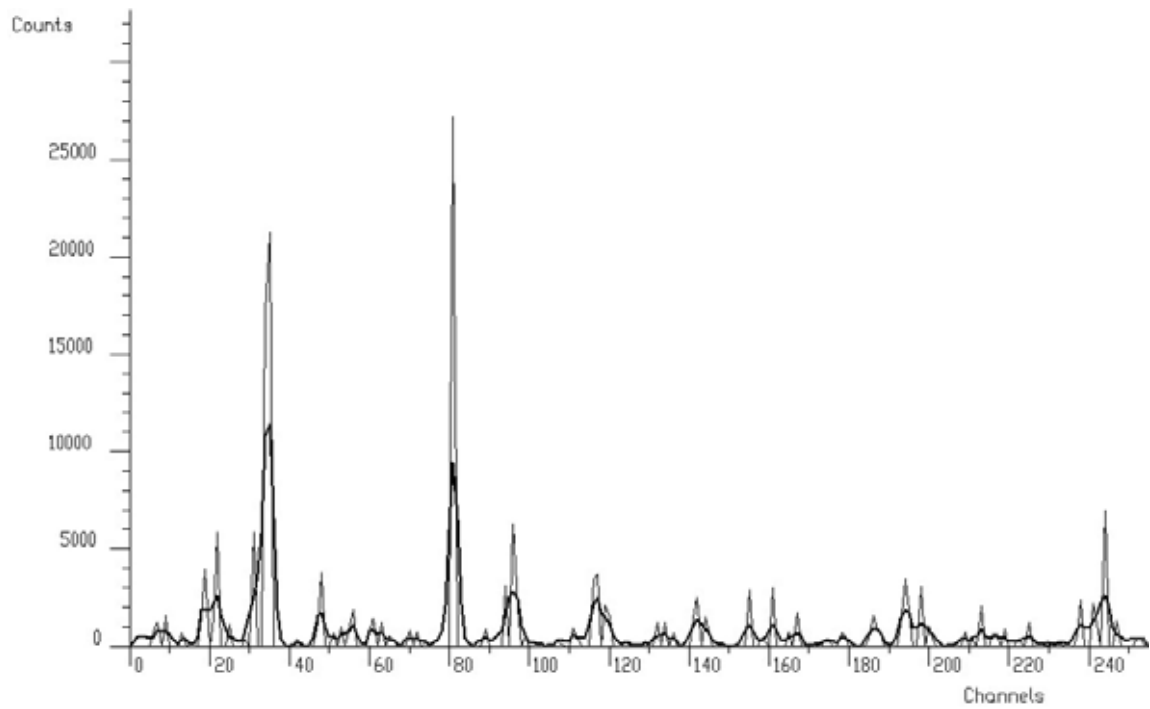
Figure 59 Experimental γ-ray spectrum before (thick line) and after (thin line) boosted one-fold Gold deconvolution

b. Two - dimensional spectra
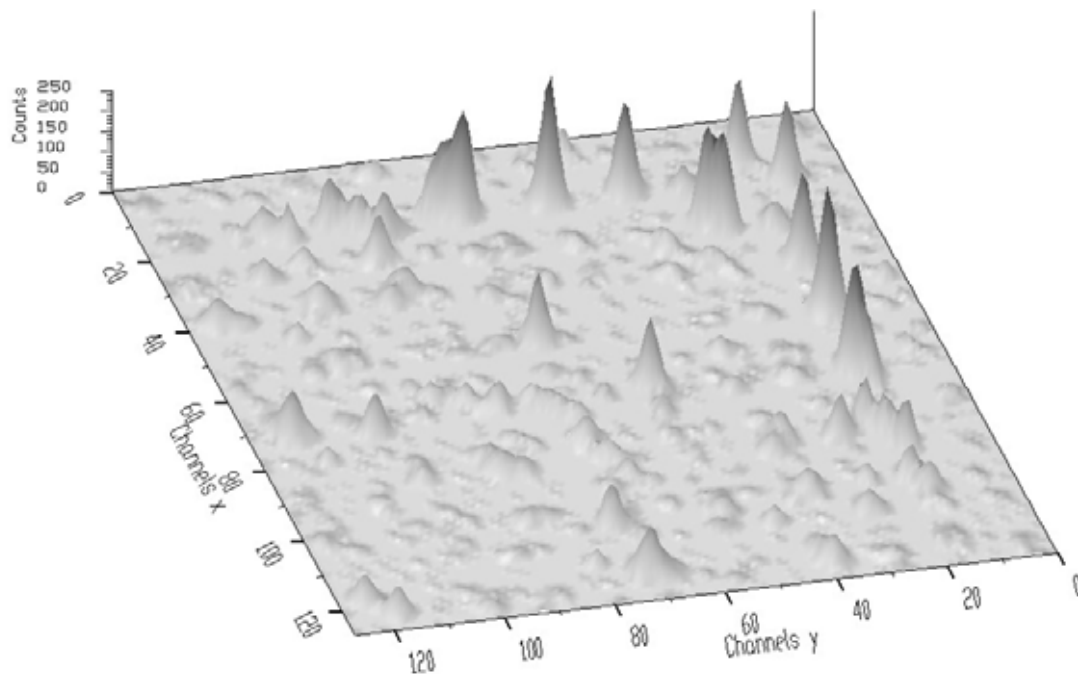
Figure 60 Part of original experimental two-dimensional $\gamma - \gamma$ coincidence spectrum
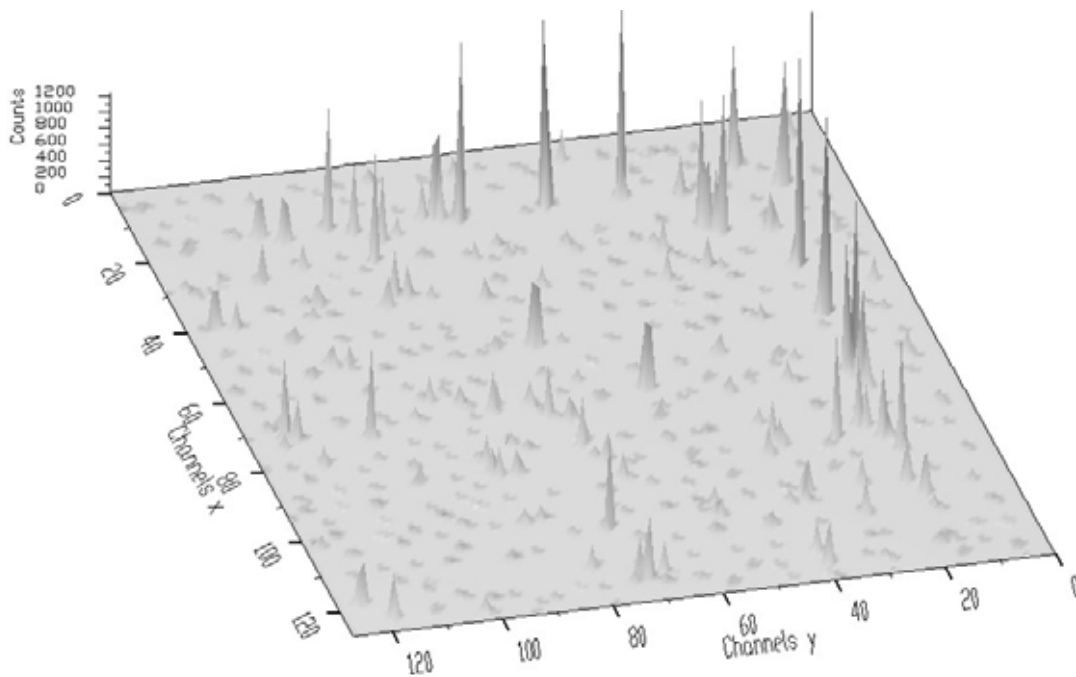
Figure 61 Spectrum from Figure 60 after boosted one-fold Gold deconvolution

c. Three - dimensional spectra
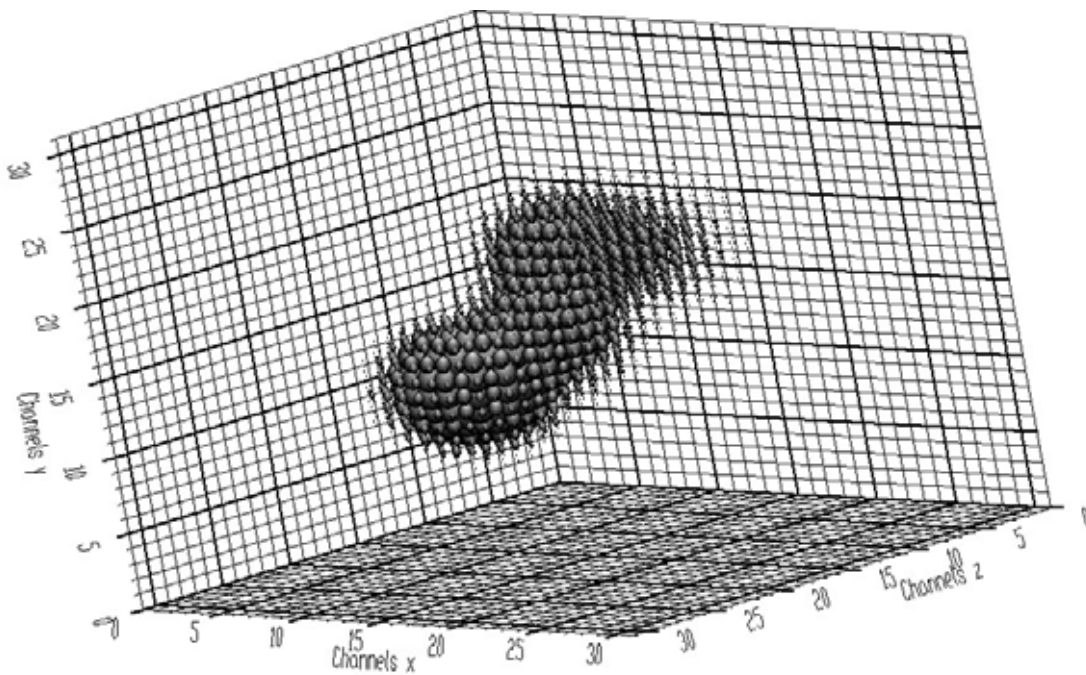
Figure 62 Three-dimensional synthetic spectrum
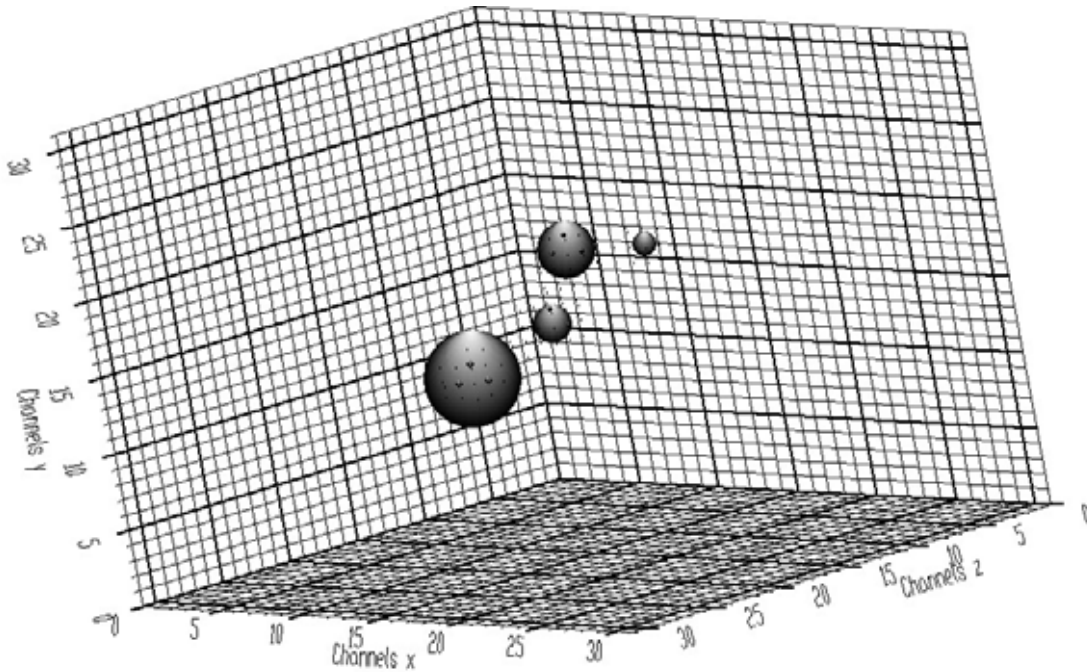
Figure 63 Spectrum from Figure 62 after boosted one-fold Gold deconvolution

Movies

Peak identification

Goal: to identify automatically peaks positions in spectrum with the presence of the continuous background and statistical fluctuations - noise

Peak searching algorithm based on smoothed second differences

a. One-dimensional spectra
- the essential peak searching algorithm is based on smoothed second differences (SSD) that are compared to its standard deviations.

Reference:
Mariscotti M.A., A method for automatic identification of peaks in the presence of background and its application to spectrum analysis, NIM 50 (1967) 309.
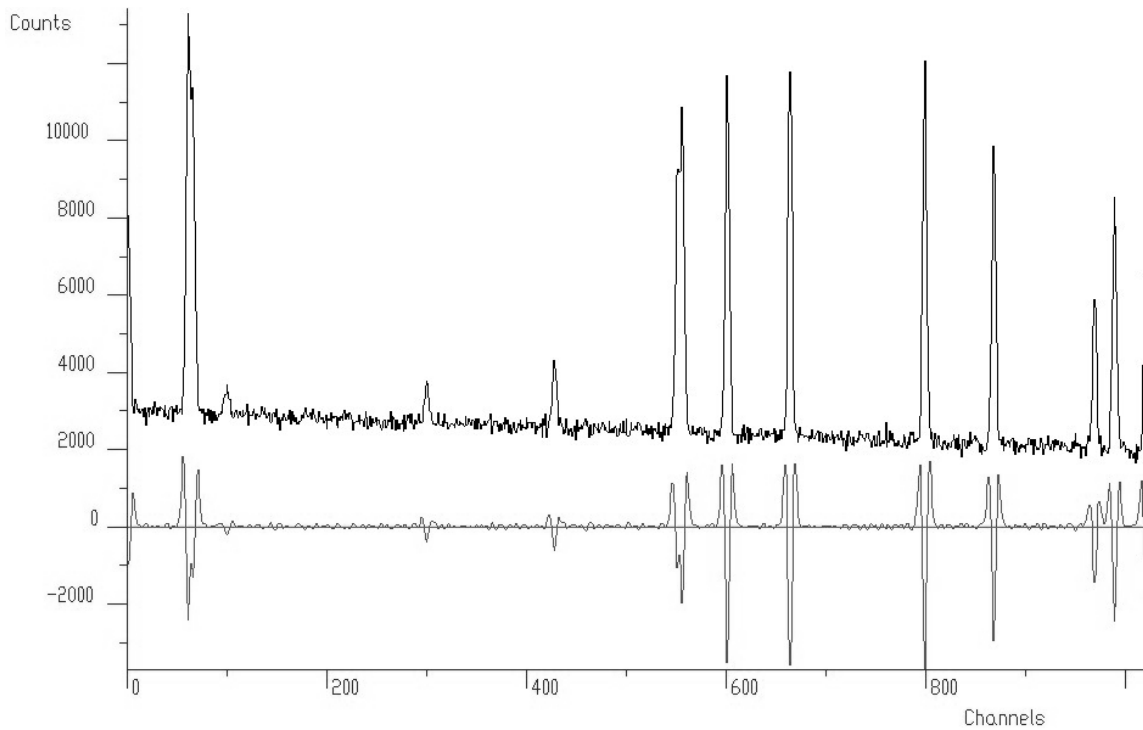
Figure 64 One-dimensional synthetic spectrum and its SSD spectrum
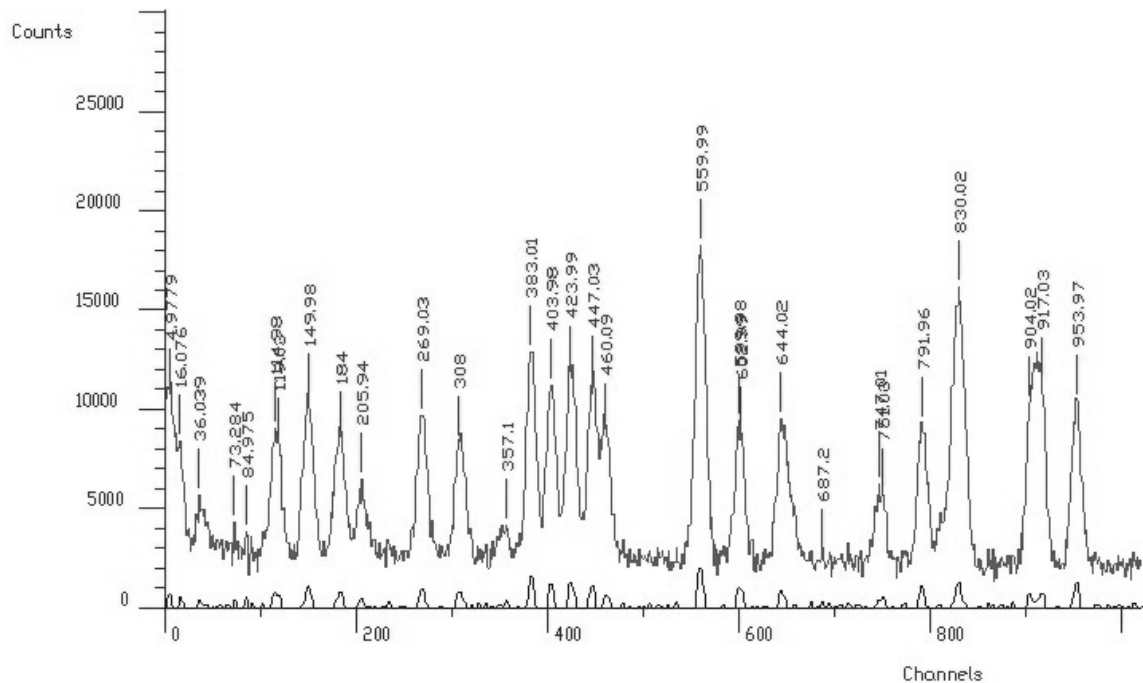
Figure 65 An example of one-dimensional γ-ray experimental spectrum with found peaks and its inverted positive SSD spectrum

b. Two-dimensional spectra

- we have extended the above presented SSD based method of peak identification for two-dimensional and in general for multidimensional spectra. In addition to the

49

above given requirements now the algorithm must be insensitive to the lower-fold coincidences peak-background (ridges) and their crossings.

Reference:
Morháč M., Kliman J., Matoušek V., Veselský M., Turzo I., Identification of peaks in multidimensional coincidence gamma-ray spectra, NIM A 443 (2000) 108.
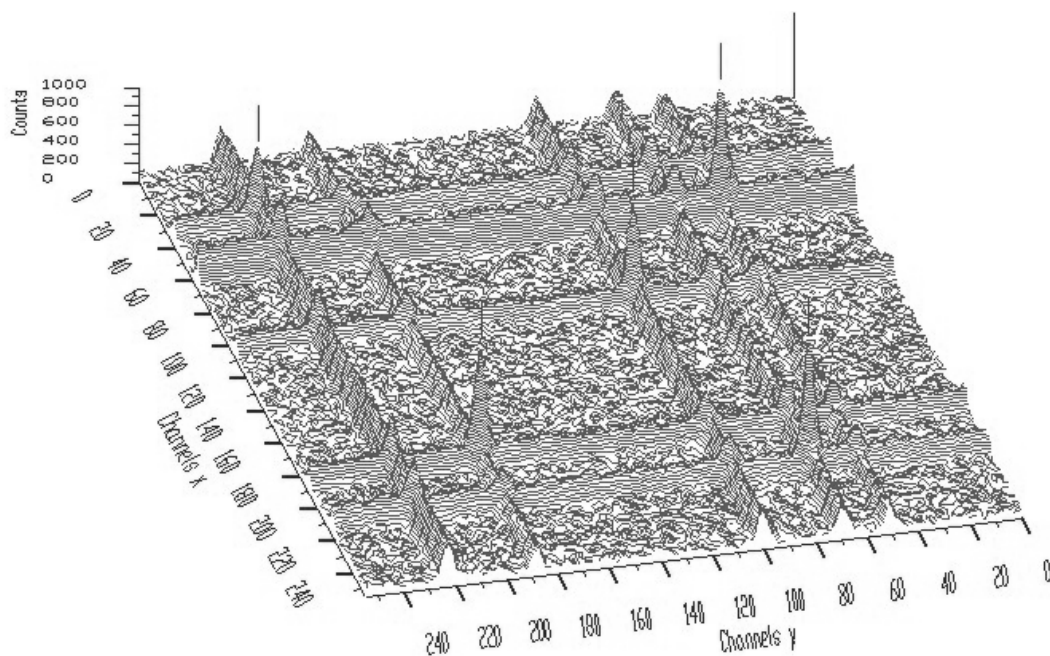
Figure 66 Two-dimensional noisy synthetic spectrum with peaks denoted by markers
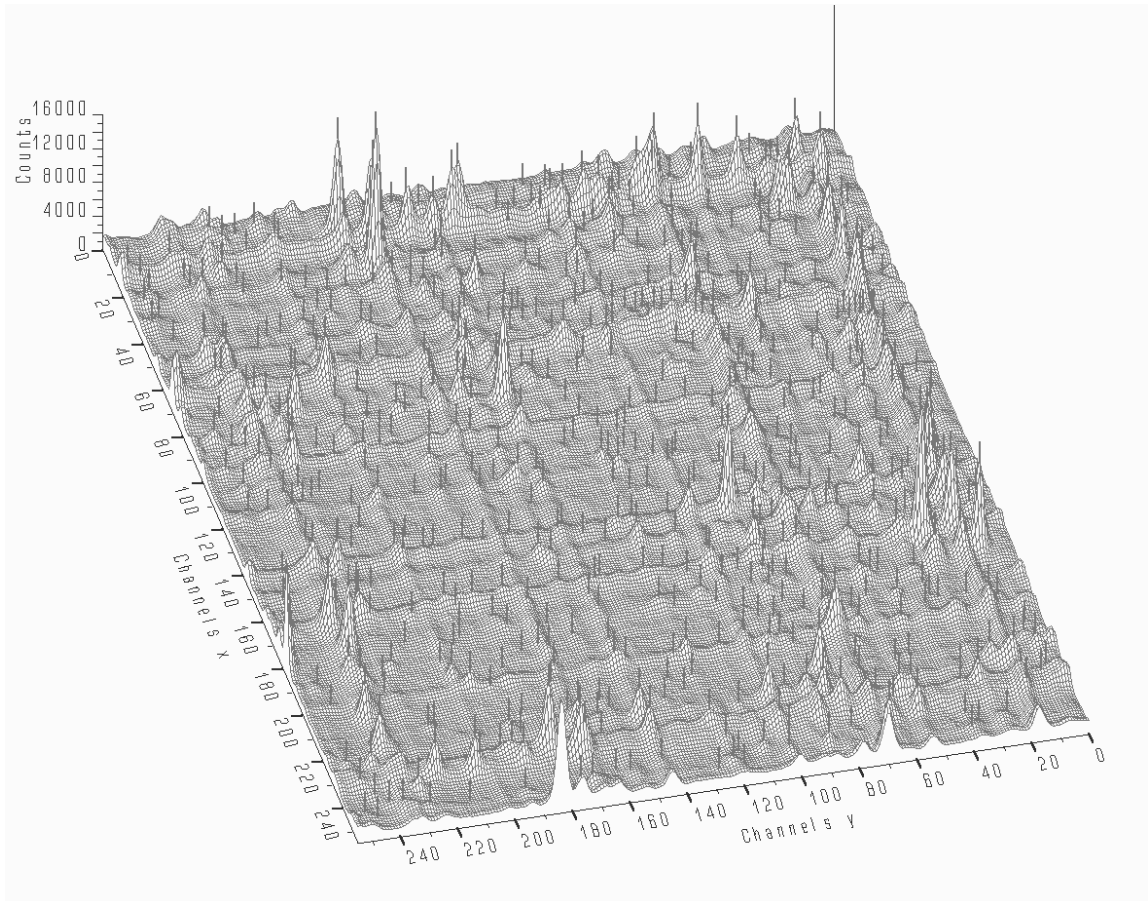
Figure 67 Two-dimensional experimental $\gamma - \gamma$-coincidence spectrum with found peaks denoted by markers

High resolution peak searching algorithm

- based on deconvolution methods (Gold deconvolution)
a. One-dimensional spectra
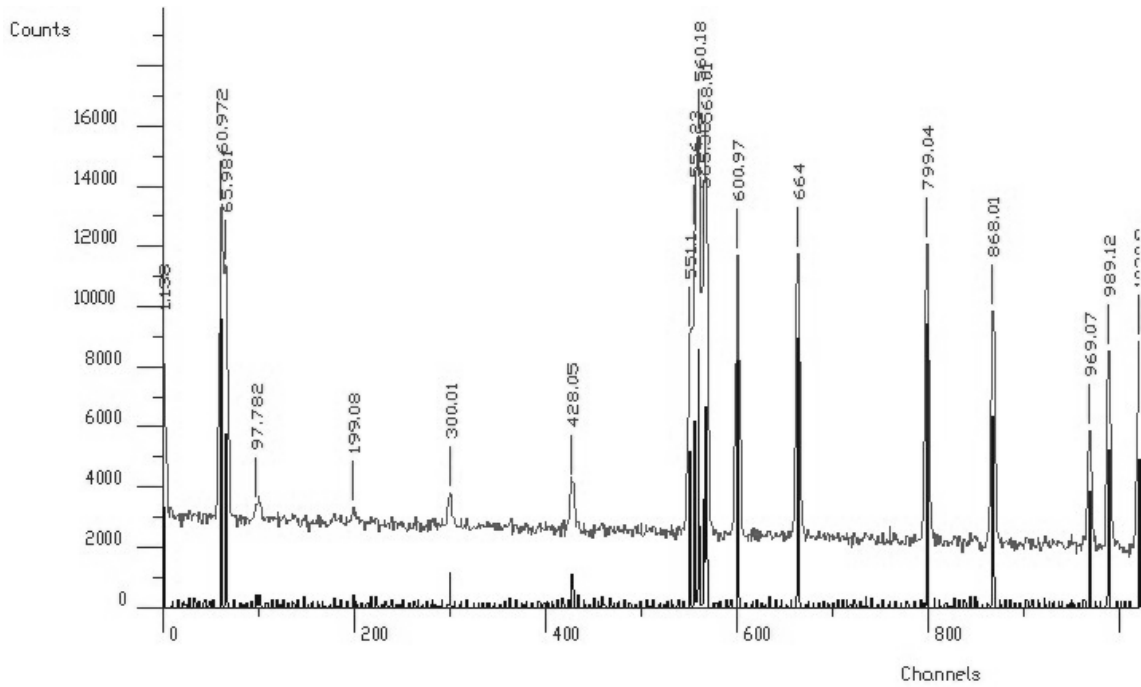
**Figure 68 Example of synthetic spectrum with doublet and multiplet and its
deconvolved spectrum (in bottom part of picture)**
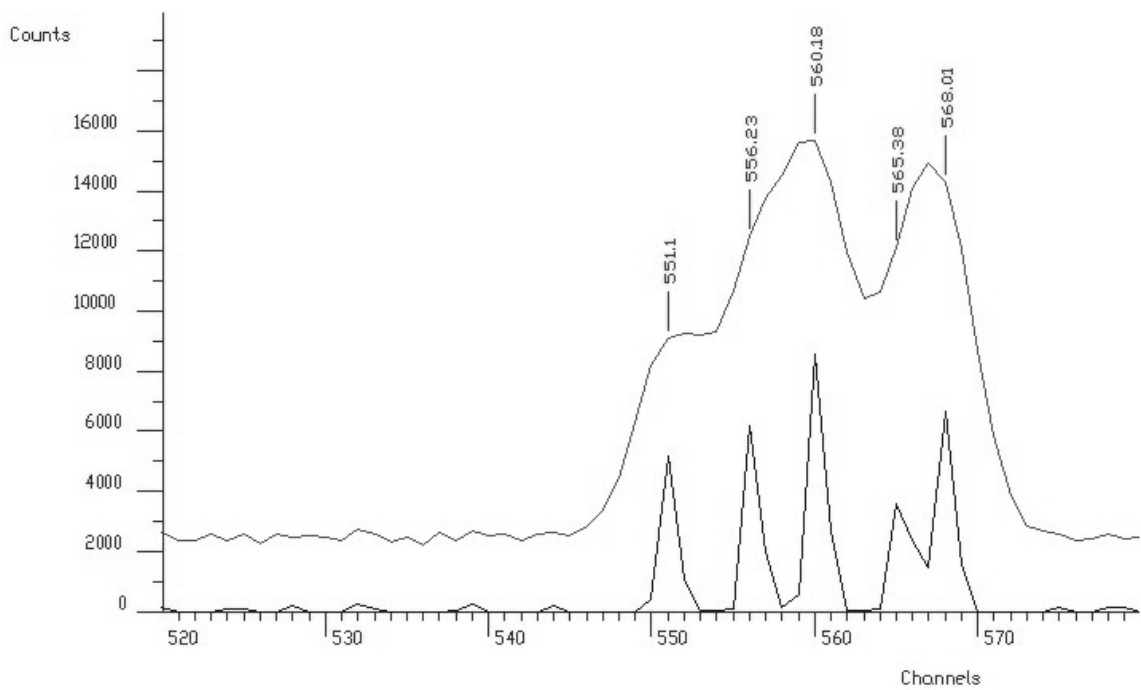
Figure 69 Detail of multiplet from Figure 68

b.   Two-dimensional spectra
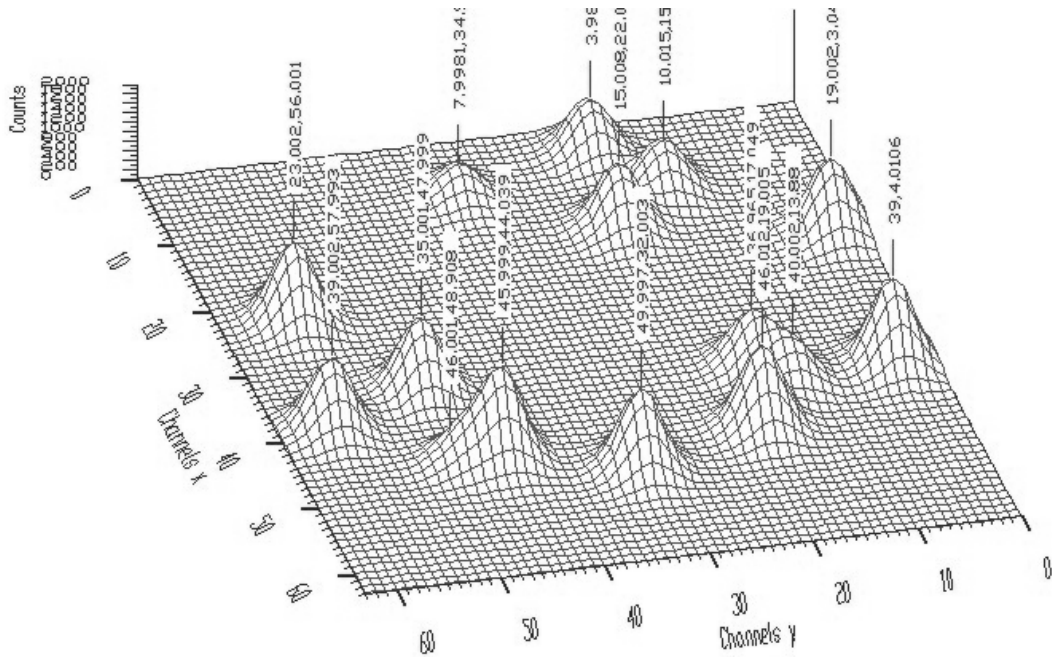
Figure 70 Result of the search using high resolution method based on Gold deconvolution
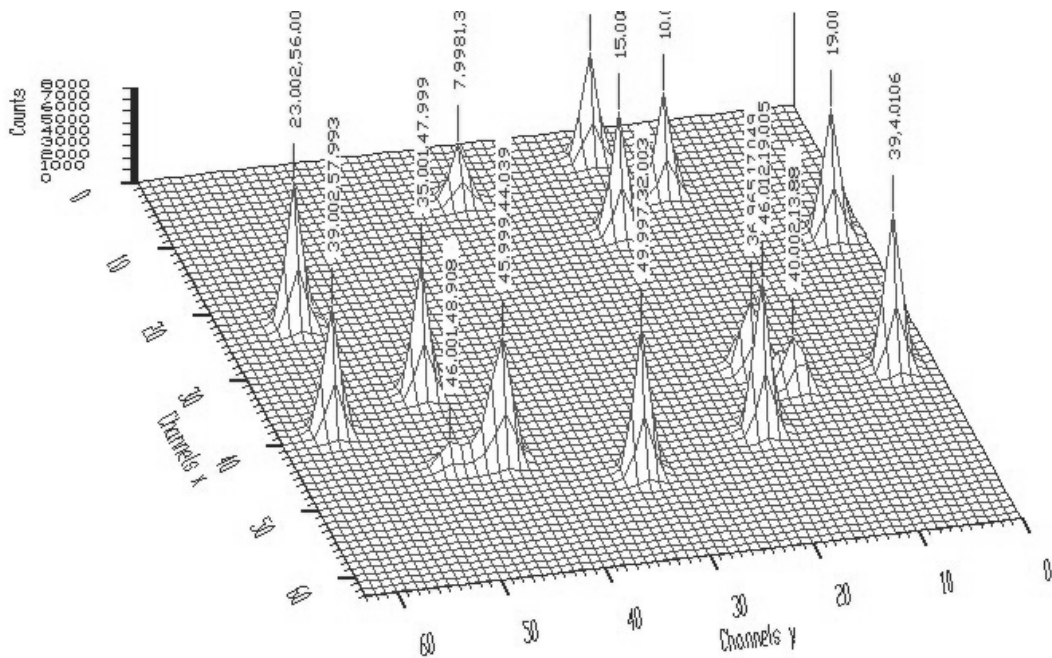
Figure 71 Deconvolved spectrum of the data from Figure 70

Sigma range peak search algorithm

- previous two algorithms are bound with a σ that should be passed as input parameter. To some extent they are robust to the variations of this parameter.

- however, for large scale of the range of σ and for poorly resolved peaks both previously designed algorithms fail to work properly.
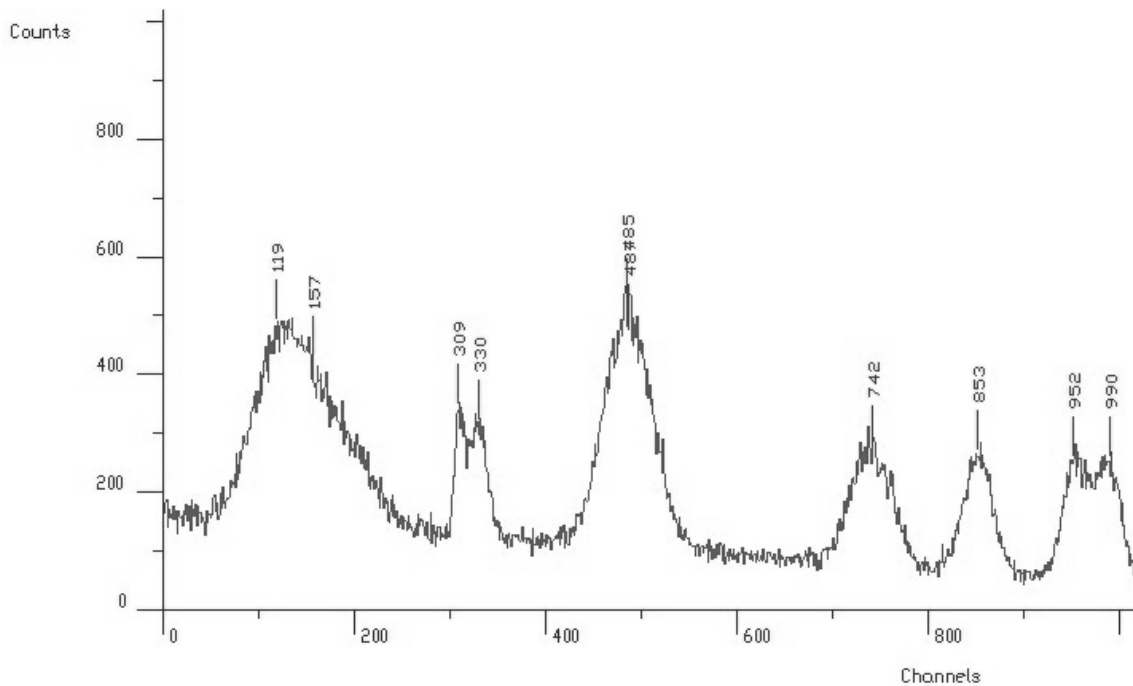
Figure 72 Original spectrum with found peaks denoted by markers

Identification of ridges in two-dimensional spectra

- in some applications one has to determine ridges of corresponding points from very sparsely distributed two-dimensional experimental data.
- we proposed sophisticated algorithm of the ridges identification based on application of SSD technique.
- the algorithm was applied to spectra of nuclear multifragmentation.

Reference:

Veselský M. et al., Phys. Rev. C 62 (2000) 64613.
Veselský M. et al., Progress in Research, 2000-2001, Cyclotron Institute, Texas A&M University College Station (2001) 13.
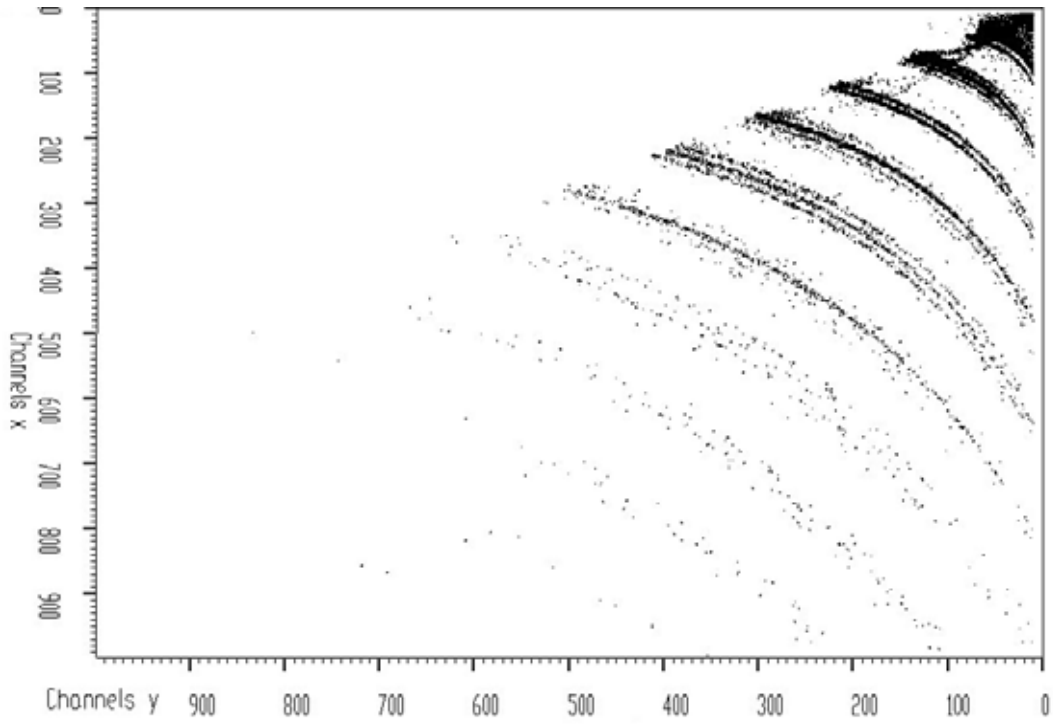
Figure 73 Original two-dimensional Si-Si spectrum

- to illustrate the complexity and statistical fluctuations in the data in next Figure we show detail at the beginning of the coordinate system.
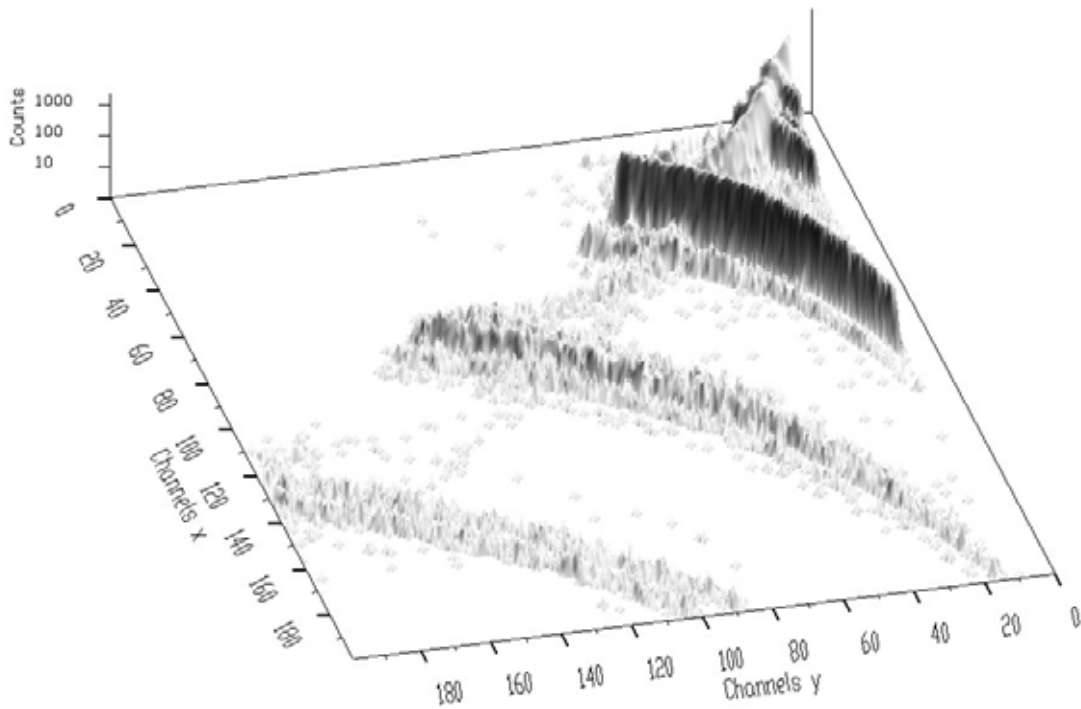
Figure 74 Detail of the spectrum from Figure 73
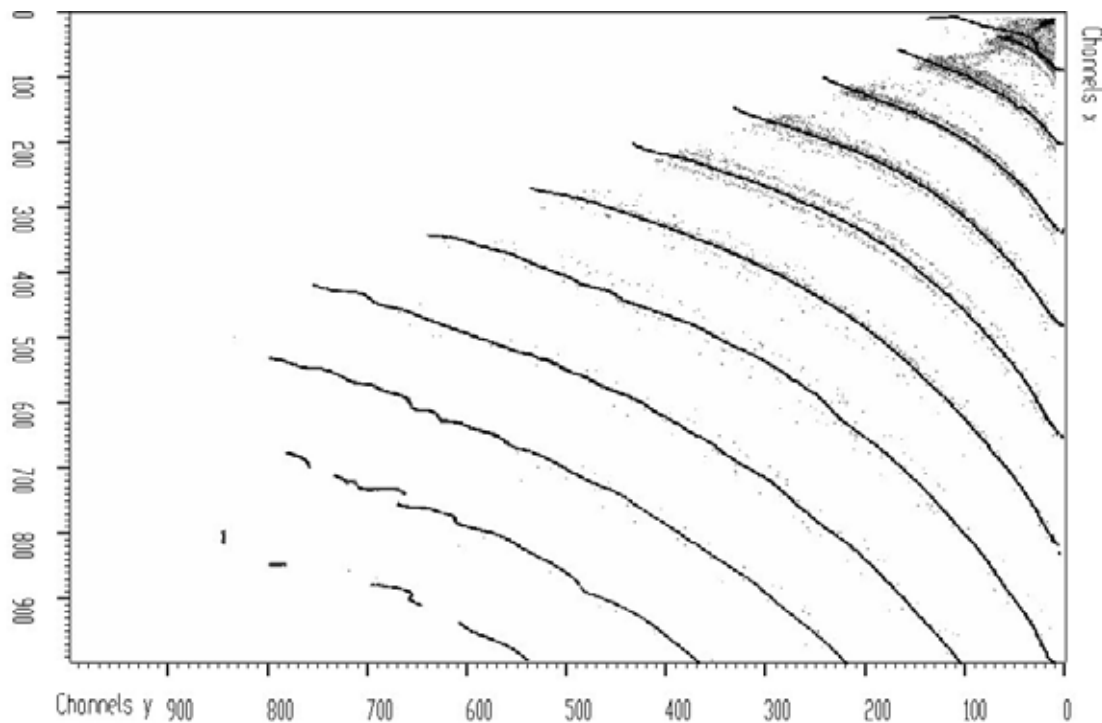
Figure 75 Original Si-Si spectrum and identified ridges

Fitting and analysis

Goal: to estimate peak shape parameters of the identified peaks

- we have implemented several methods of fitting (Newton, conjugate gradients, Stiefel-Hestens, algorithm without matrix inversion, etc)
- specific problem in the analysis of multidimensional γ-ray spectra is that connected with simultaneous fitting of large number peaks in large blocks of multidimensional γ-ray spectra and hence enormous number of fitted parameters.
- we have proposed and studied the fitting algorithms without matrix inversion, which allow a large number of parameters to be fitted

Reference:
Morháč M., Kliman J., Jandel M. Krupa L., Matoušek V., Study of fitting algorithms applied to simultaneous analysis of large number of peaks in gamma-ray spectra, Applied Spectroscopy 57 (2003) 753.

- the fitting procedure has been applied to the determination of relative yields of correlated fragment pairs in ternary fission of ^{252}Cf. One example of the results of the fit of the one-dimensional spectrum obtained by gating on ^{138}Xe $2^{+} \rightarrow 0^{+}$ (588.8 keV) transition in γ-γ matrix of coincidences in ^{4}He ternary fission of ^{252}Cf is shown in next Figure.

56

- the high accuracy and resolution of the fitting procedure can be observed. The transitions in fragments Mo, their doublets and multiplets are well resolved.
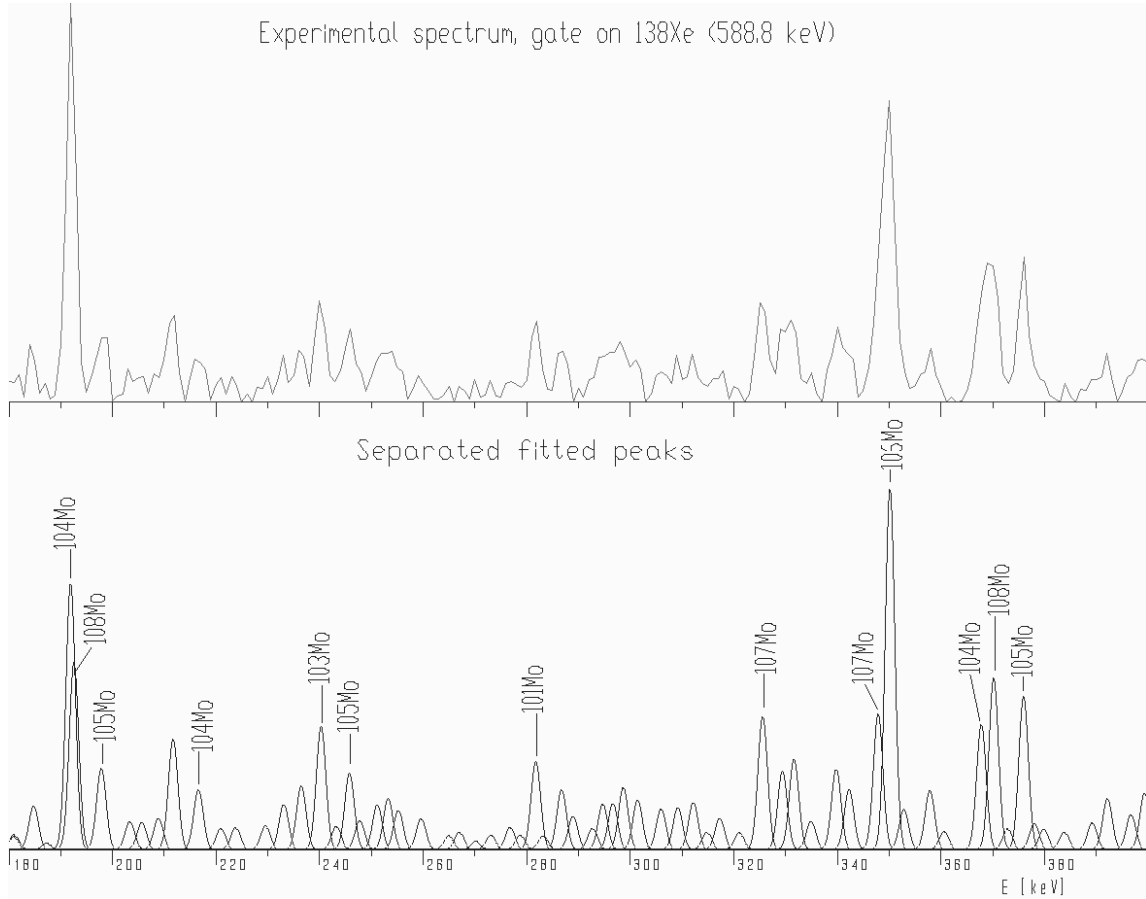
Figure 76 Experimental spectrum and separated fitted peaks (below)

- we have extended the fitting procedures to higher dimensions.
- let us analyze a two-dimensional spectrum (256 x 256 channels) with a large number of overlapped peaks shown in Figure 77. Using this example let us illustrate the entire procedure of the analysis, which consists of the following steps
  - background elimination
  - deconvolution – improving the resolution
  - identification of peaks
  - fit.
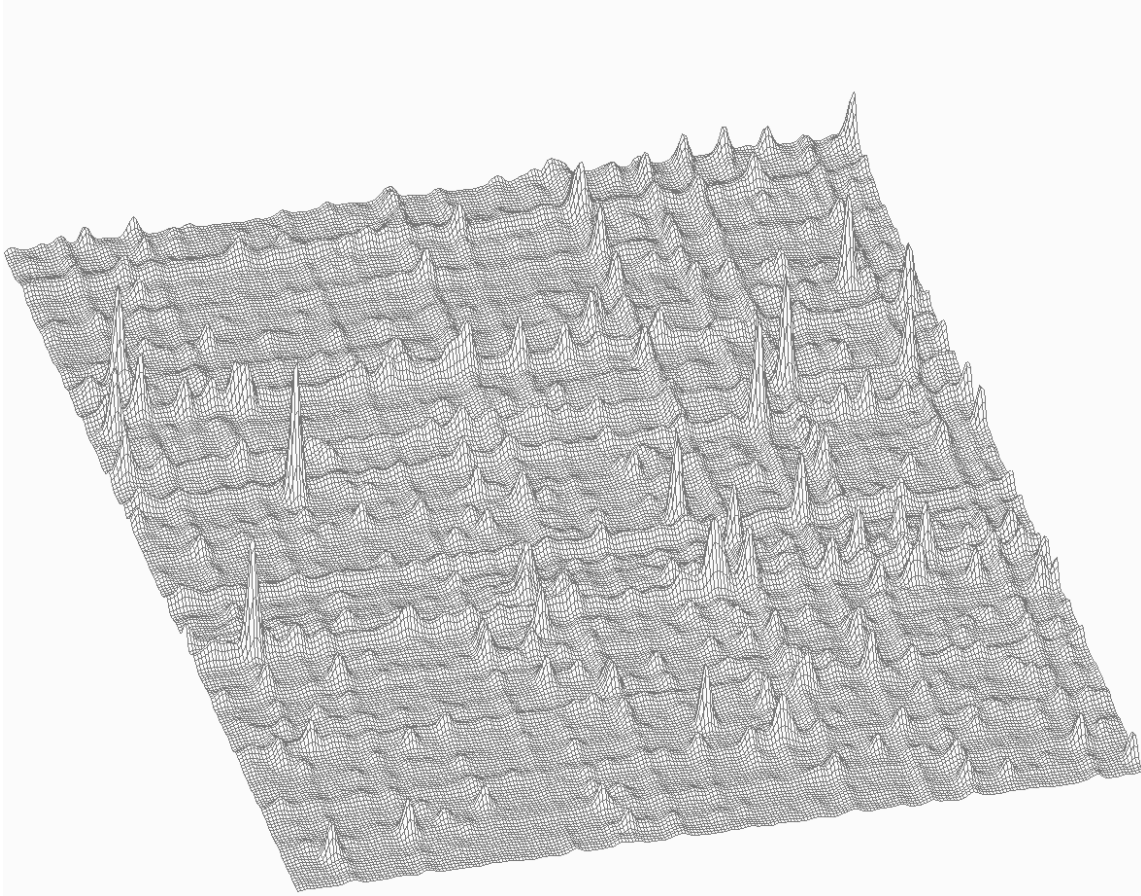
Figure 77 An example of two-dimensional $\gamma - \gamma$ coincidence spectrum with large number of peaks (some of them are overlapping)
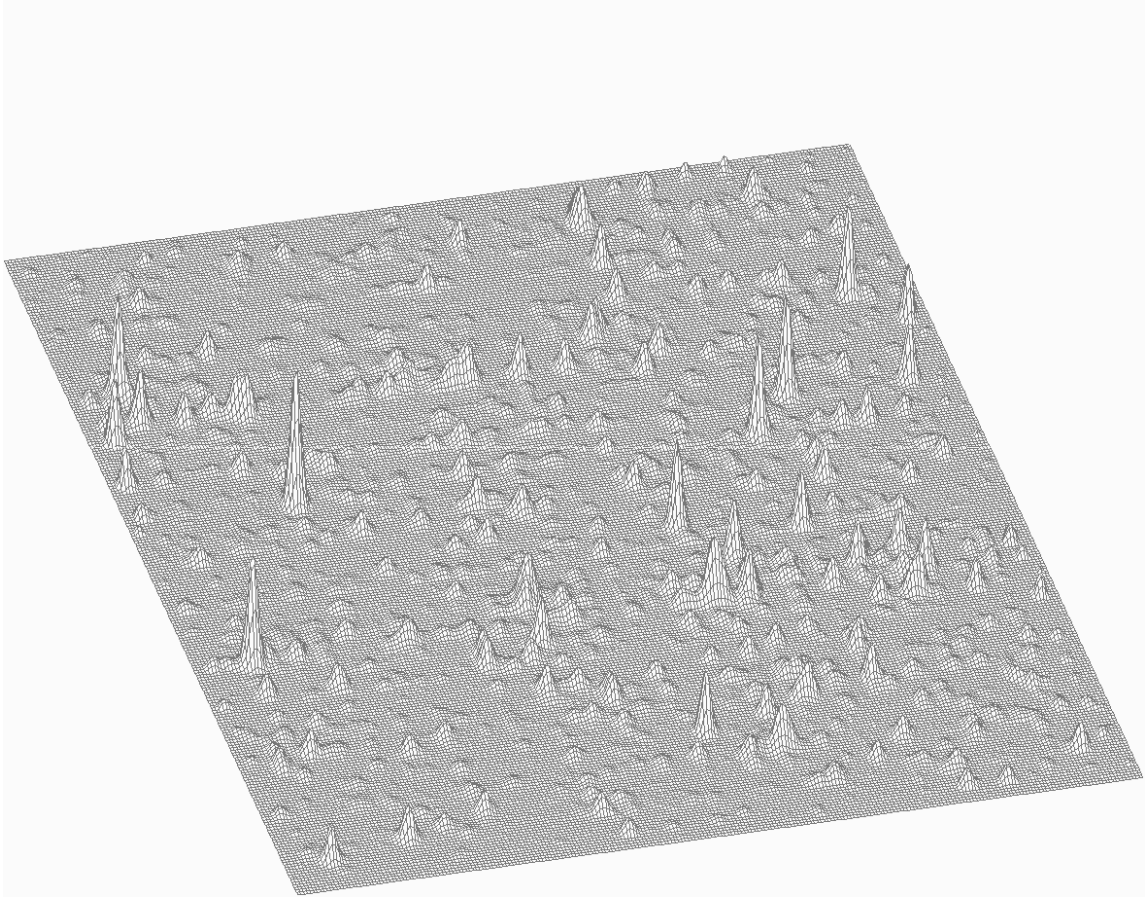
Figure 78 Spectrum from Figure 77 after background elimination
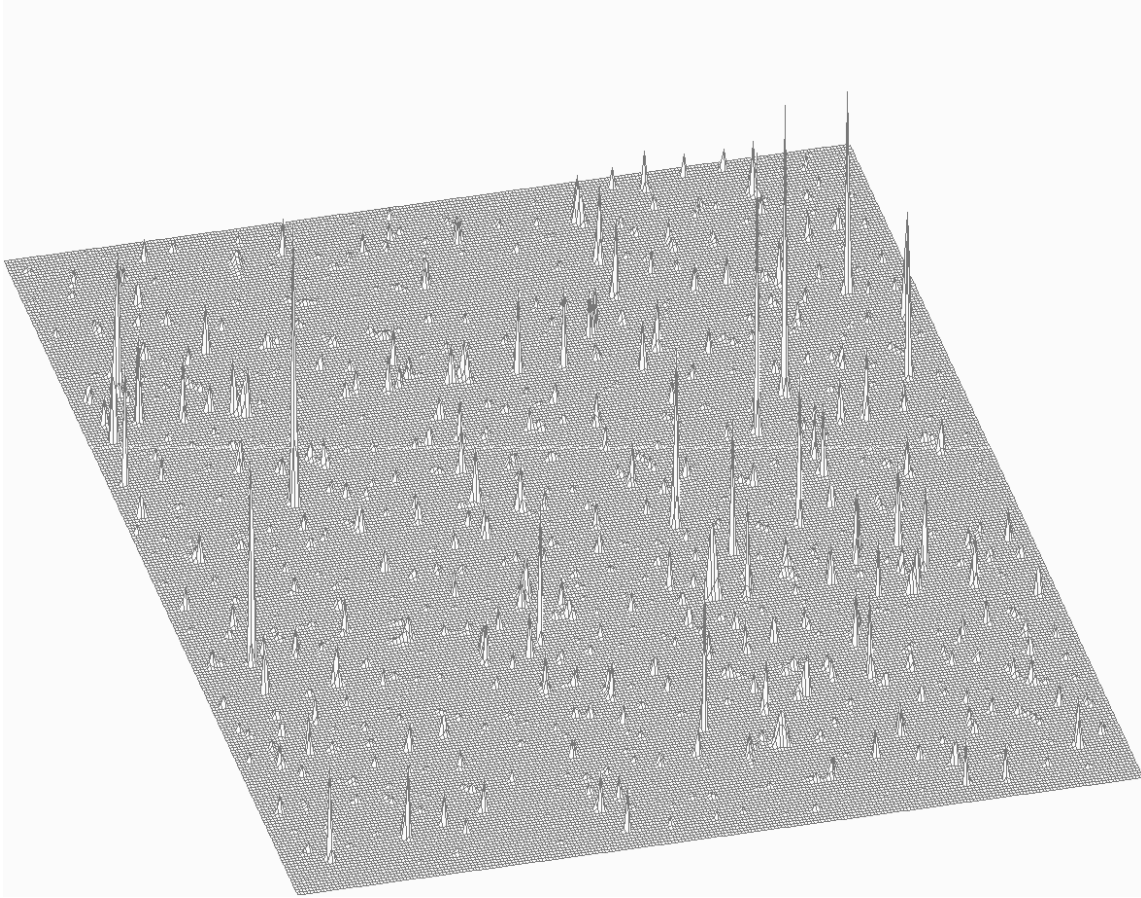
Figure 79 Deconvolved spectrum of the data from Figure 78

- it is a simple task to find local maxims higher than a given threshold value and to feed their positions as initial estimates into the fitting procedure.
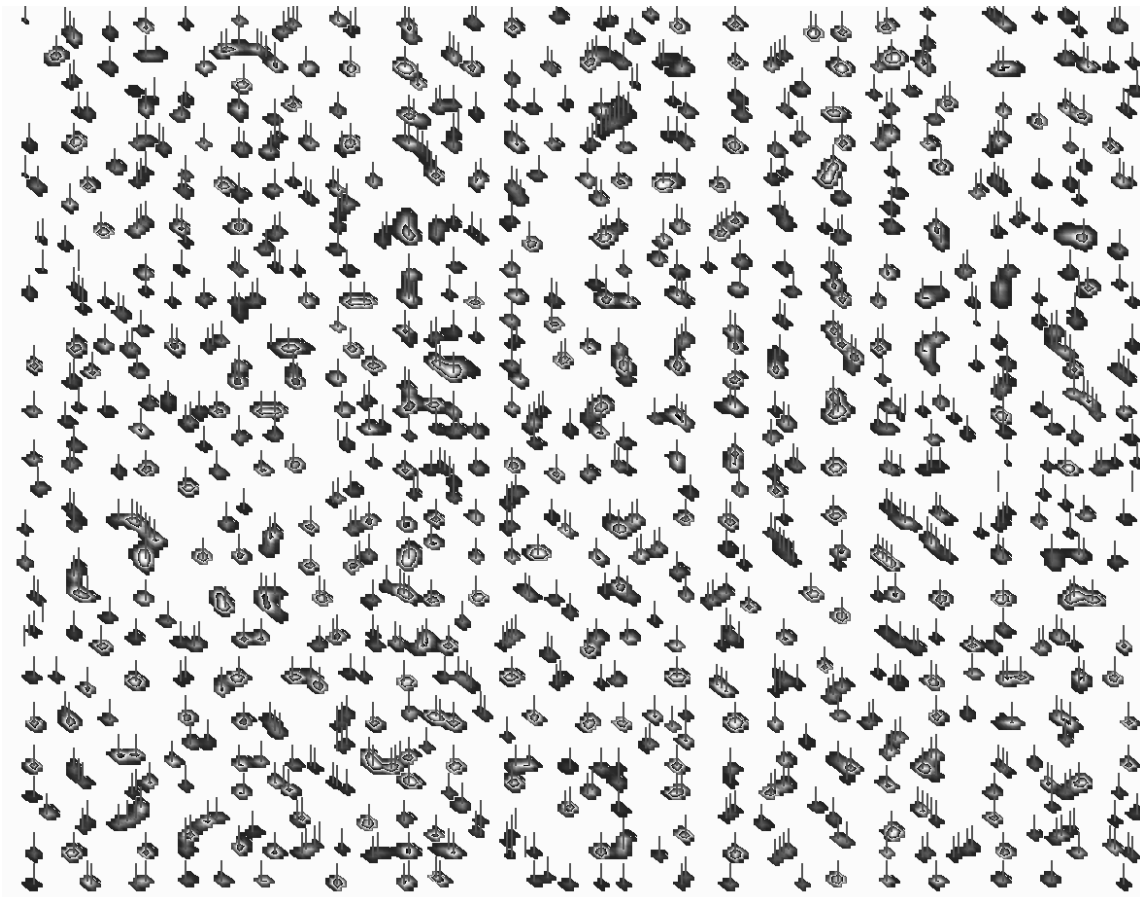
Figure 80 Rectangular view of deconvolved spectrum with identified peaks denoted by markers

- each peak is represented by 7 parameters and together with σ_x , σ_y and background it represents 1108 x 7+3=7759 estimated parameters. Thanks to fast algorithms

without matrix inversion it can be carried out in a reasonable time.
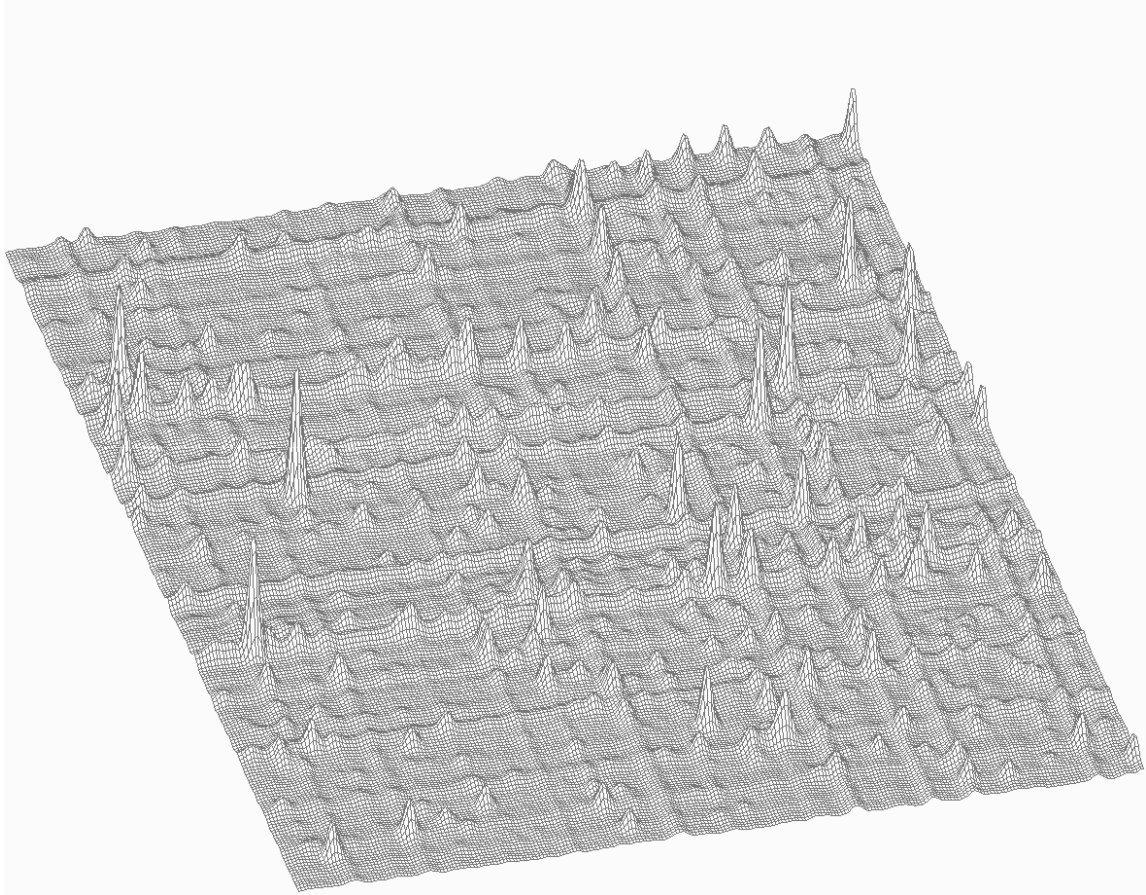
Figure 81 Two-dimensional fitted spectrum of the data from Figure 77

Movies

Visualization

Direct visualization techniques

- the principles and basic results of visualization using direct techniques of one-, two-, three-, and four-parameter nuclear spectra are presented in

Reference:
Morháč M., Kliman J., Matoušek V., Turzo I., Sophisticated visualization algorithms for analysis of multidimensional experimental nuclear data, Acta Physica Slovaca 54 (2004) 385.

- throughout the work we have presented a great number of examples illustrating the visualization capabilities of DaqProVis system.

- there exist a considerable number of display modes and parameters that allow creating various display configurations. Here we show some other examples of the visualization of nuclear spectra not mentioned before.

a. Two-dimensional spectra
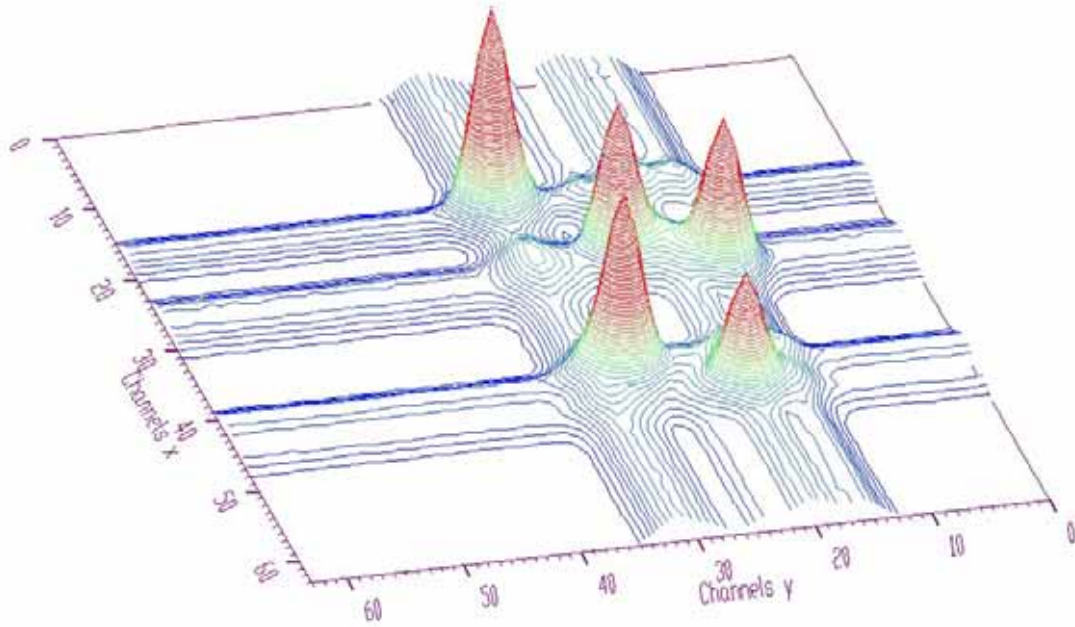
Figure 82 Two-dimensional spectrum shown in contours display mode
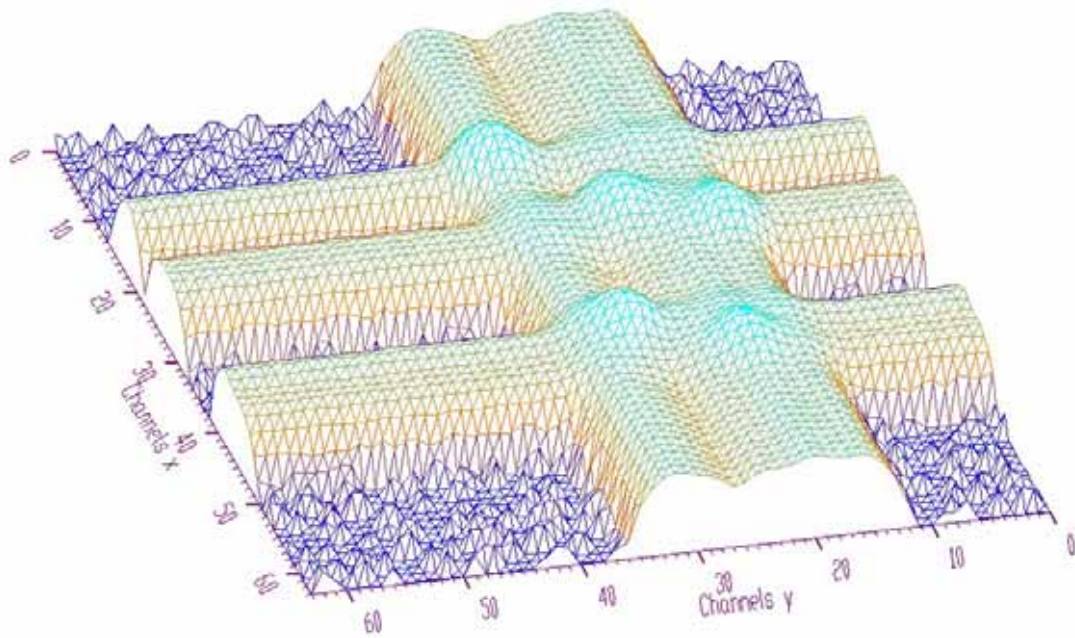
Figure 83 Two-dimensional spectrum shown in triangle display mode (log scale)
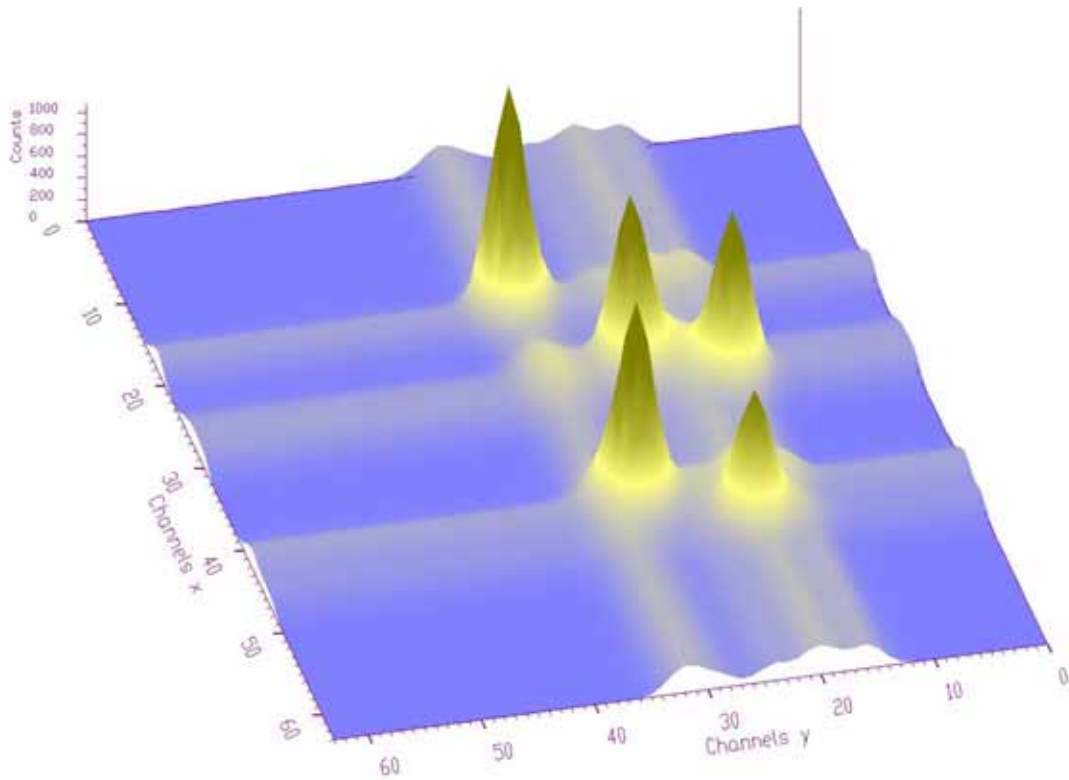
Figure 84 An example of surface display mode with shading according to heights
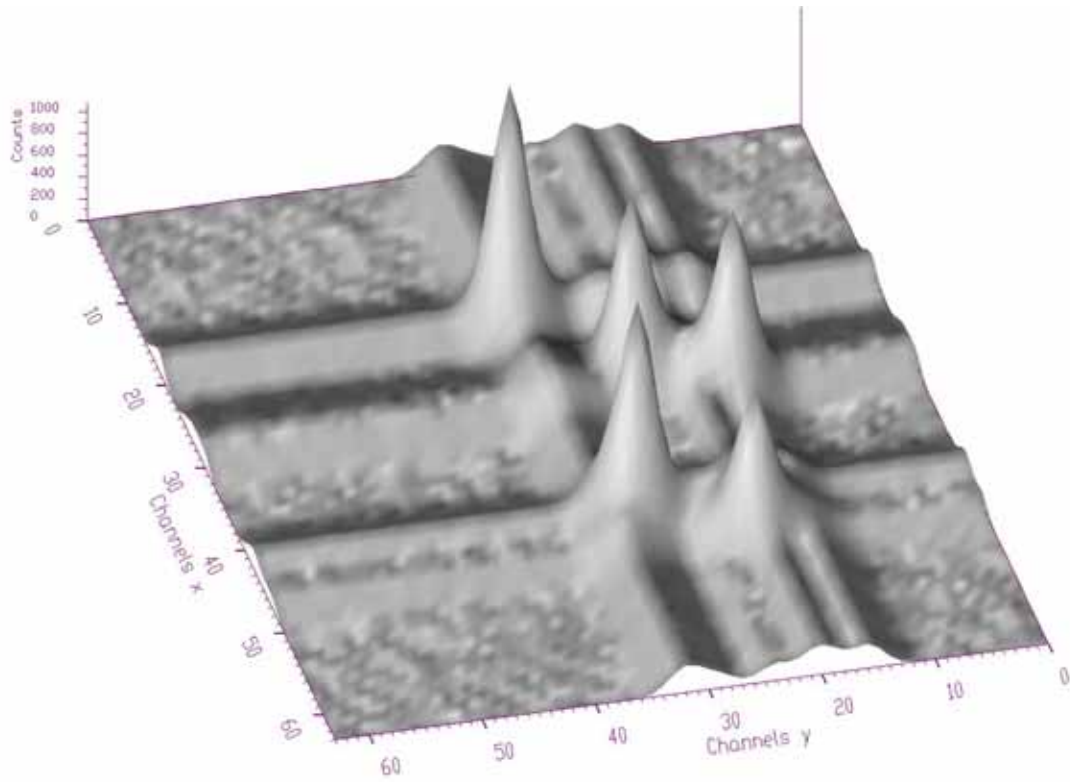
Figure 85 An example of surface display mode with shading according to fictive light source
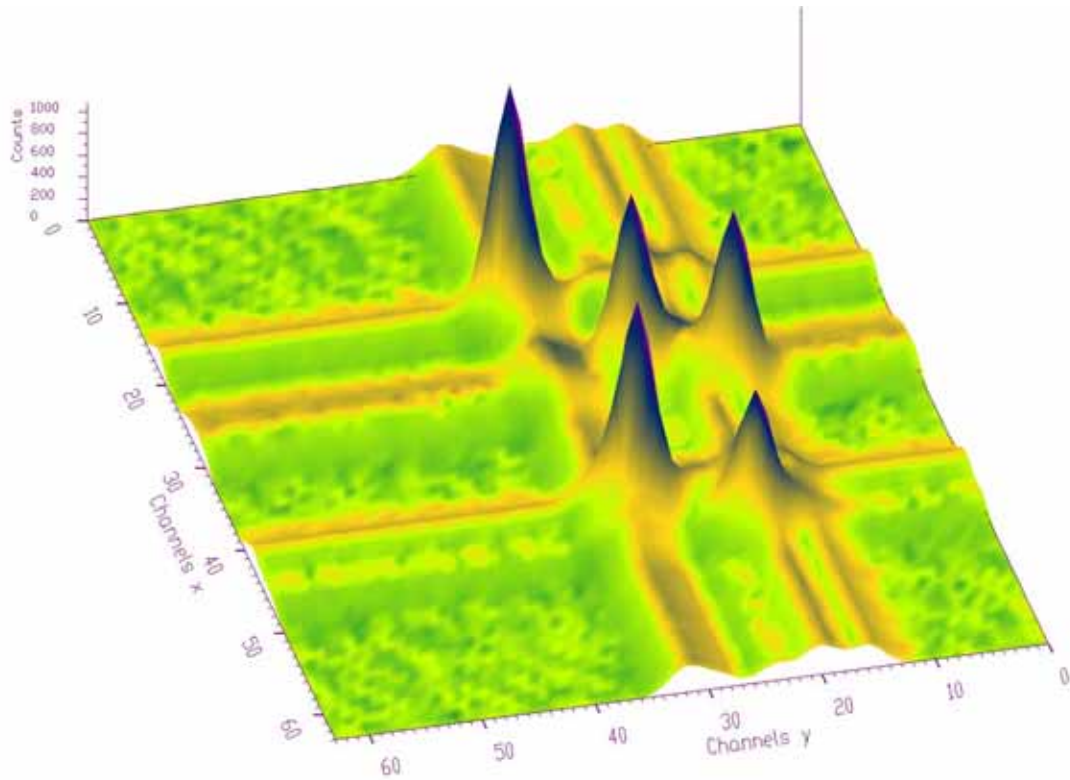
Figure 86 An example of surface display mode with combined shading algorithms (given in Figure 94 and Figure 95)
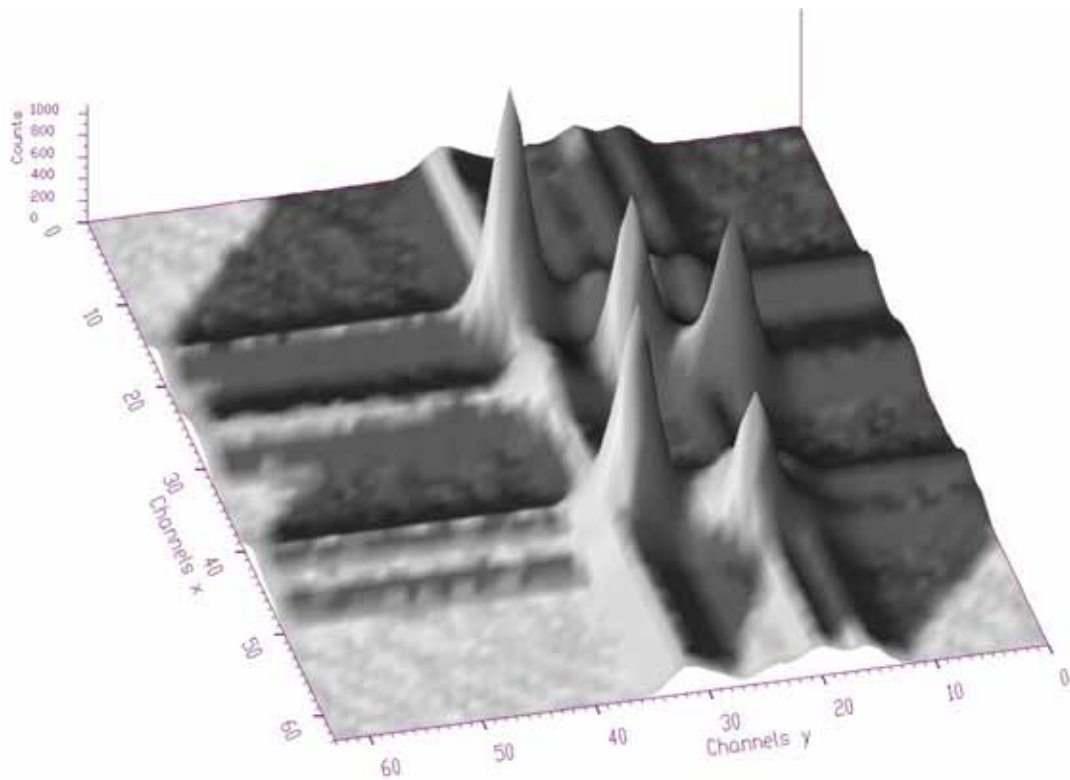
Figure 87 Surface display mode (like in Figure 85) with shadows
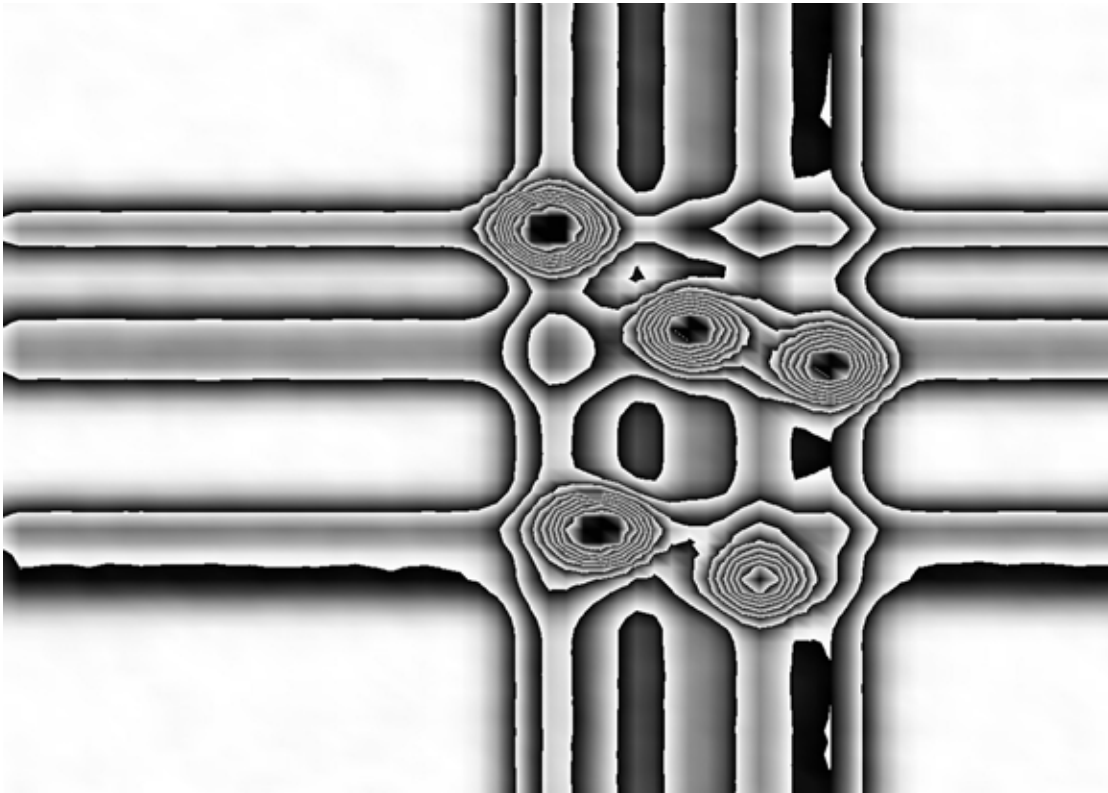
Figure 88 Rectangular view of the data shaded according to heights (10 levels of contours)
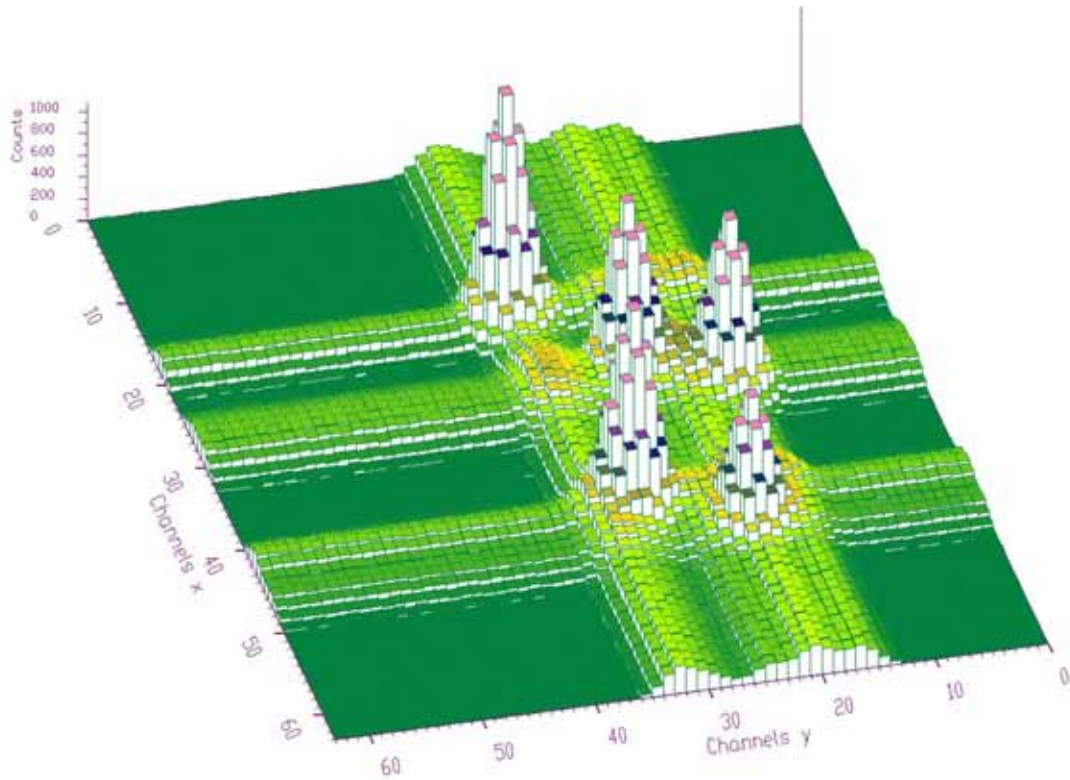
Figure 89 Bars display mode with shading according to heights
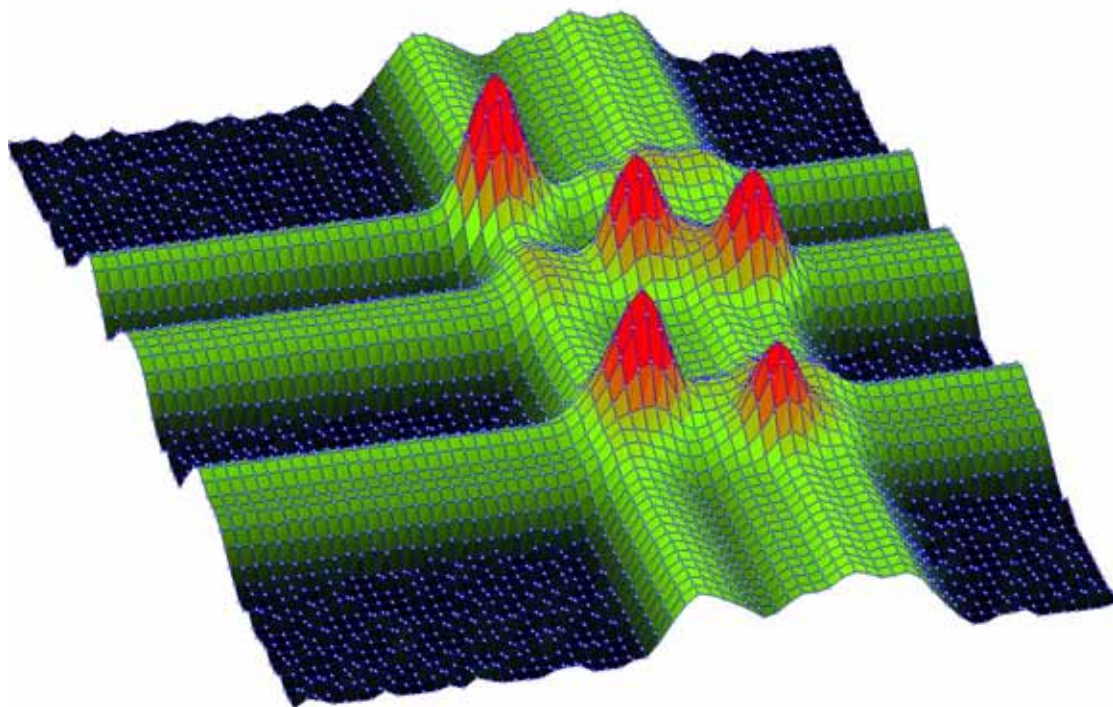
Figure 90 Surface display mode with shading according to heights (sqrt scale, channel marks and grid lines)
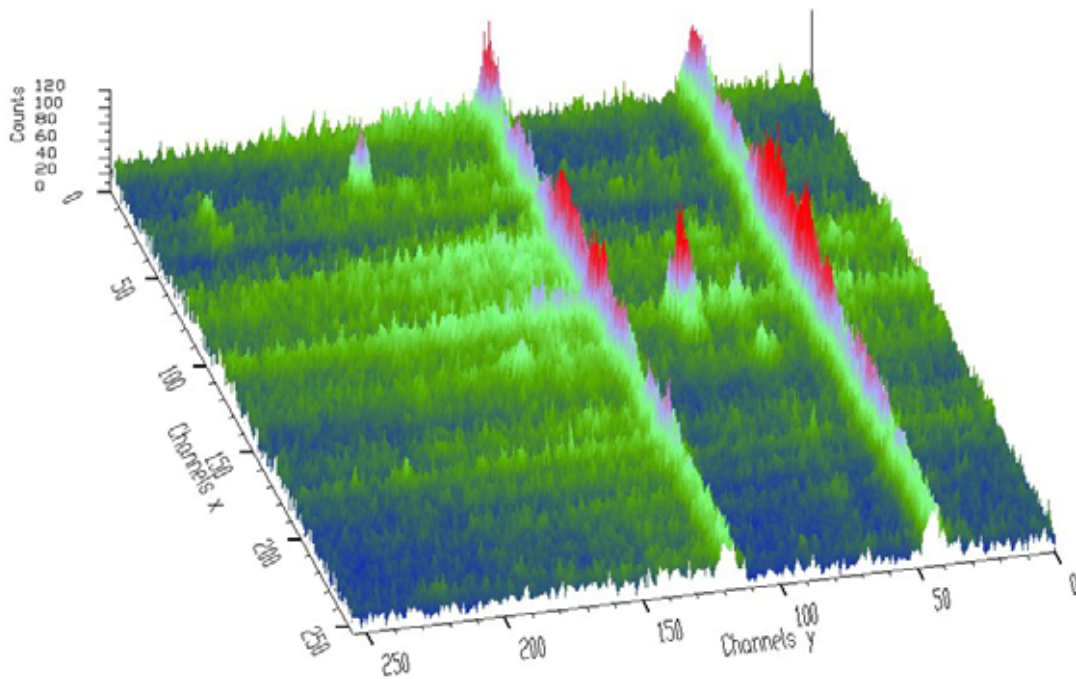
Figure 91 Two-dimensional noisy low statistics $\gamma - \gamma$ -ray coincidence spectrum with shading according to heights.
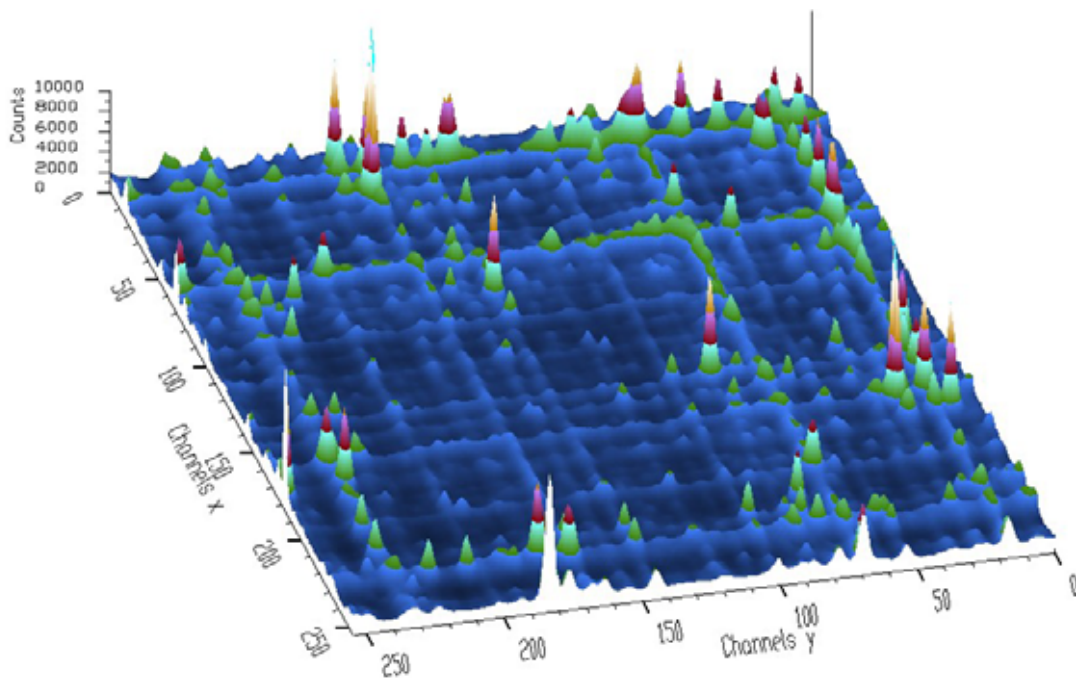
Figure 92 Two-dimensional $\gamma - \gamma$ -ray coincidence spectrum with contours shading
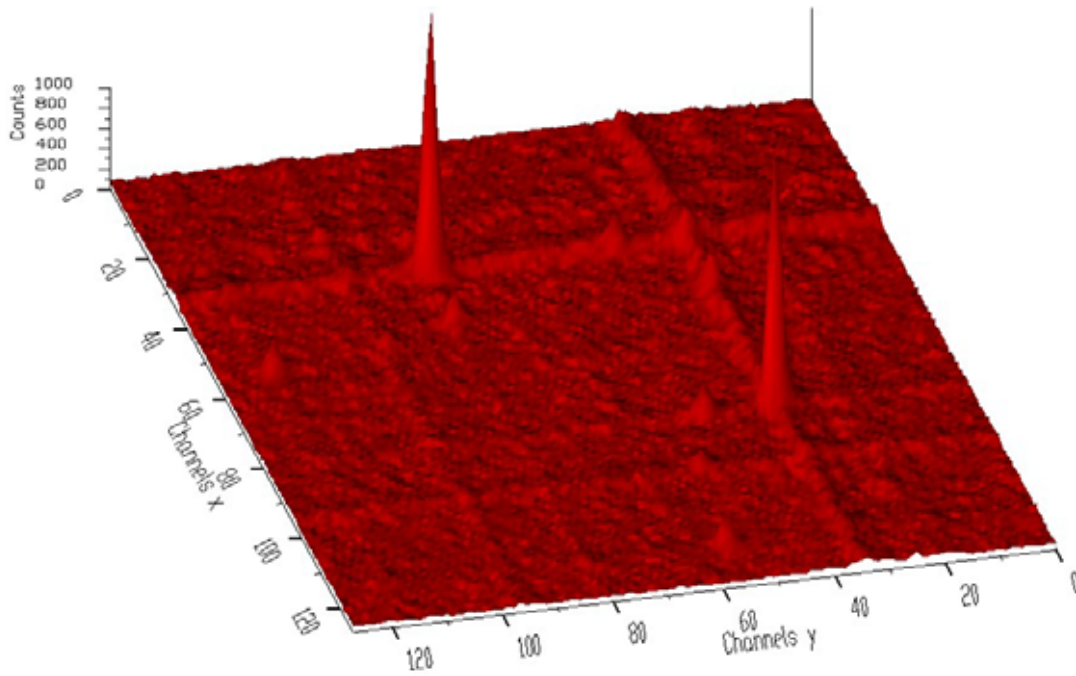
Figure 93 Two-dimensional $\gamma - \gamma$ **-ray spectrum with shading according to the fictive light position in color mode**
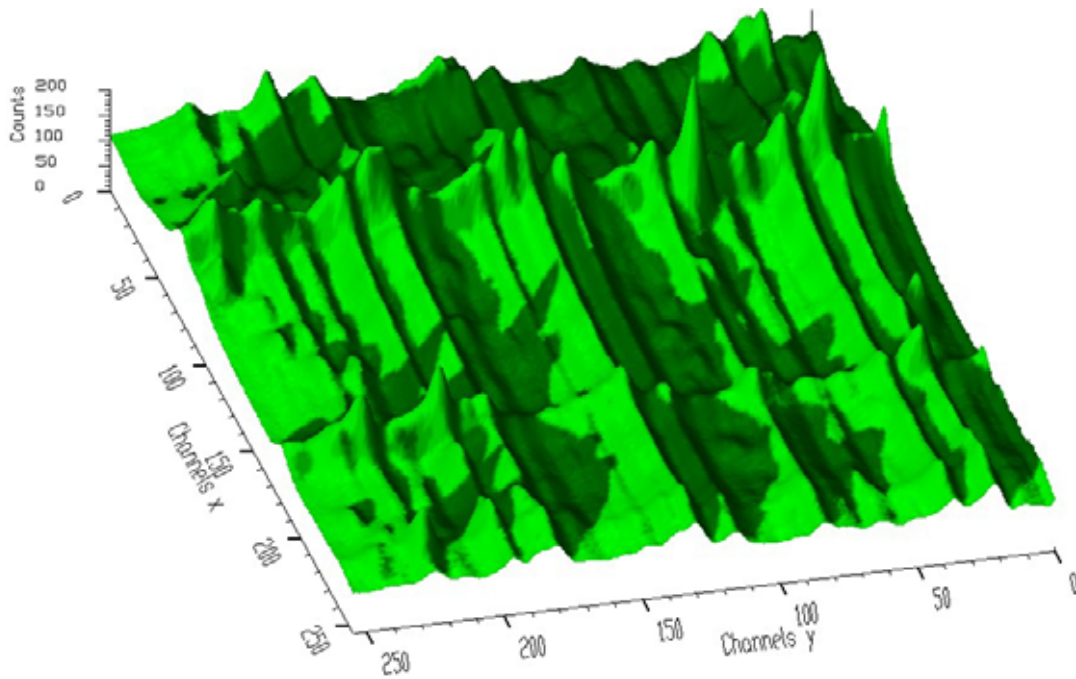
Figure 94 Two-dimensional $\gamma - X$ **-ray spectrum with shading according to the fictive light position in color mode shown with shadows**
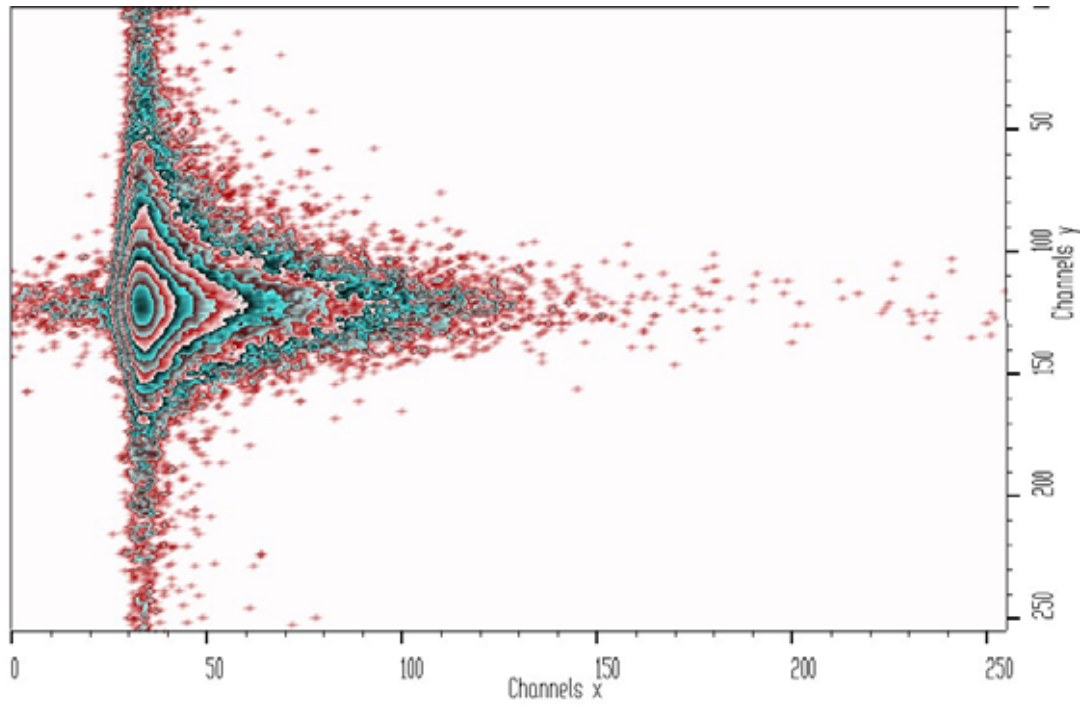
Figure 95 Rectangular view of positron annihilation spectrum with contour shading
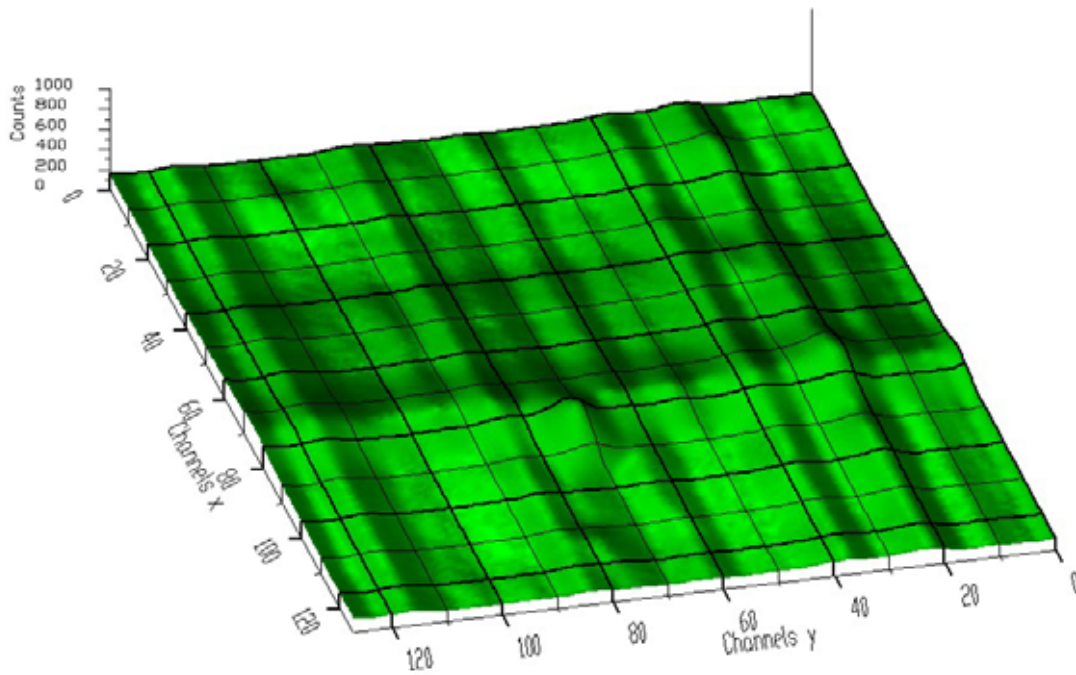
Figure 96 Two-dimensional $\gamma - X$ -ray spectrum shown with raster
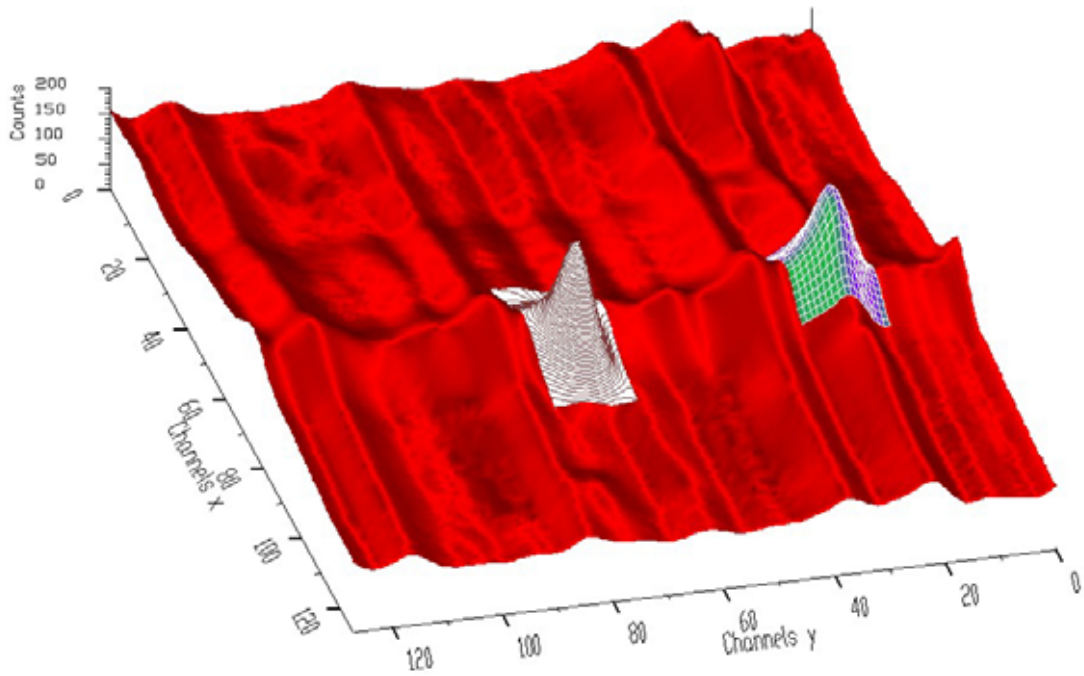
Figure 97 Two-dimensional $\gamma - X$ -ray spectrum with two ROIs
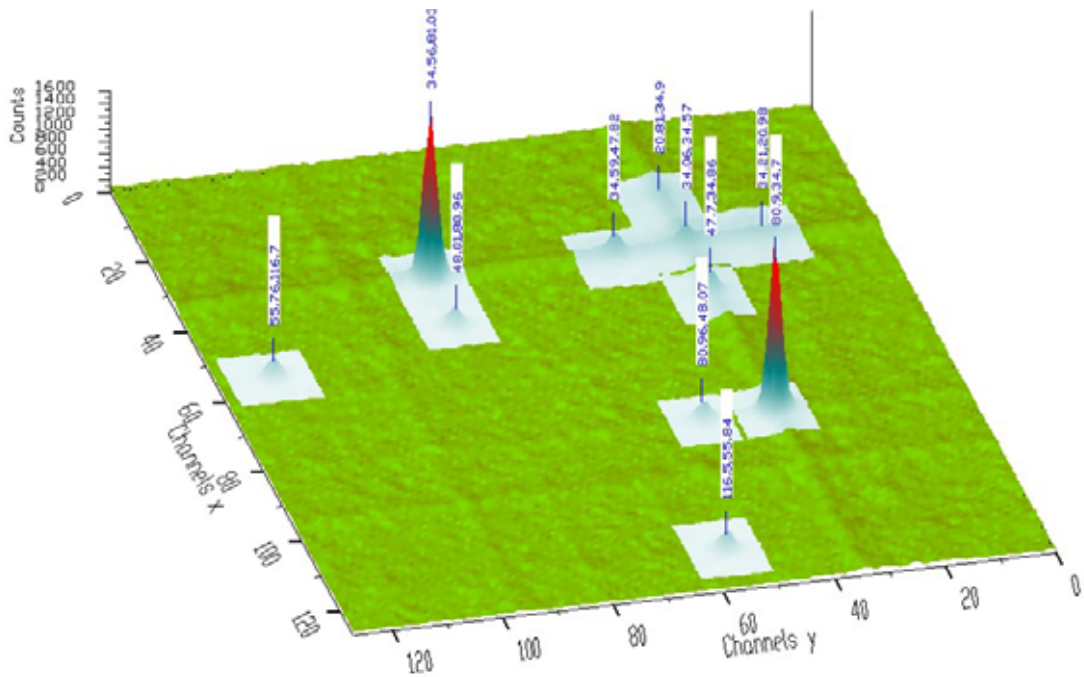
Figure 98 Two-dimensional $\gamma - \gamma$ -coincidence spectrum with displayed peaks markers and areas

b. Three-dimensional spectra
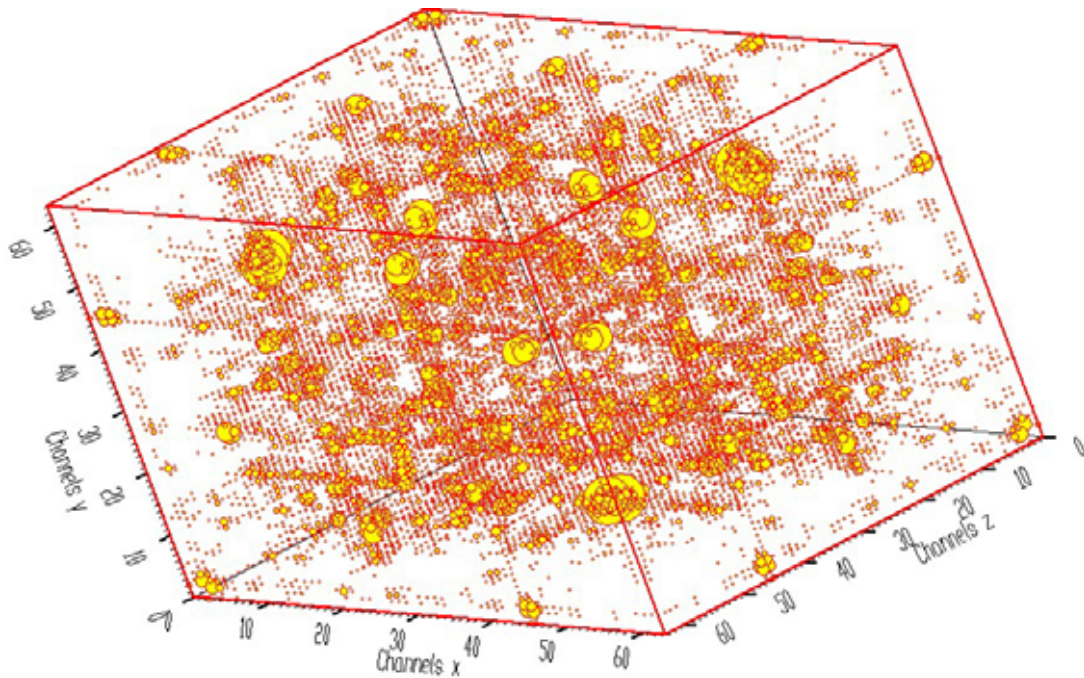
Figure 99 Three-dimensional $\gamma - \gamma - \gamma$ -coincidence spectrum with channels shown as spheres with diameters proportional to counts
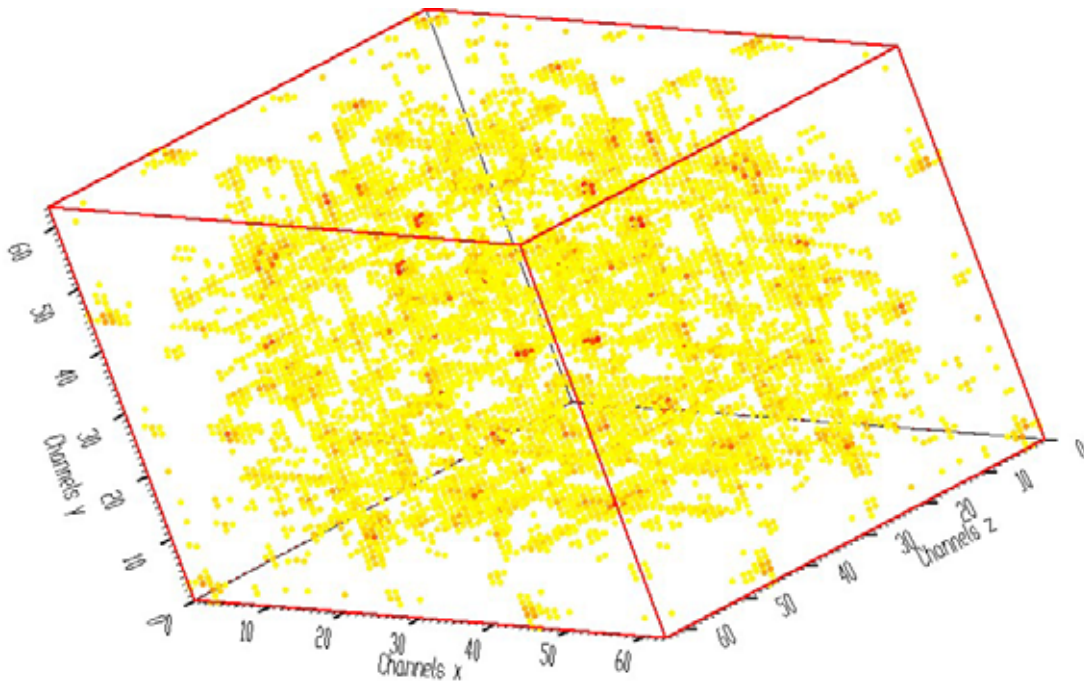
Figure 100 Three-dimensional $\gamma - \gamma - \gamma$ -coincidence spectrum with channels shown as spheres with colors proportional to counts
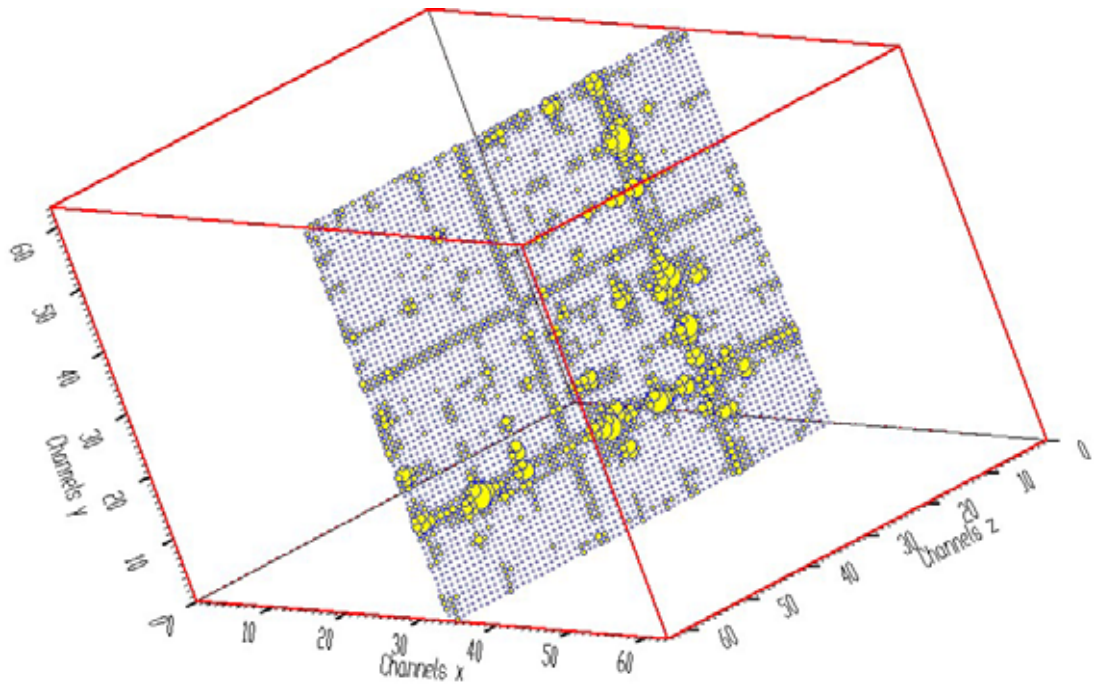
Figure 101 Two-dimensional slice in three-dimensional spectrum
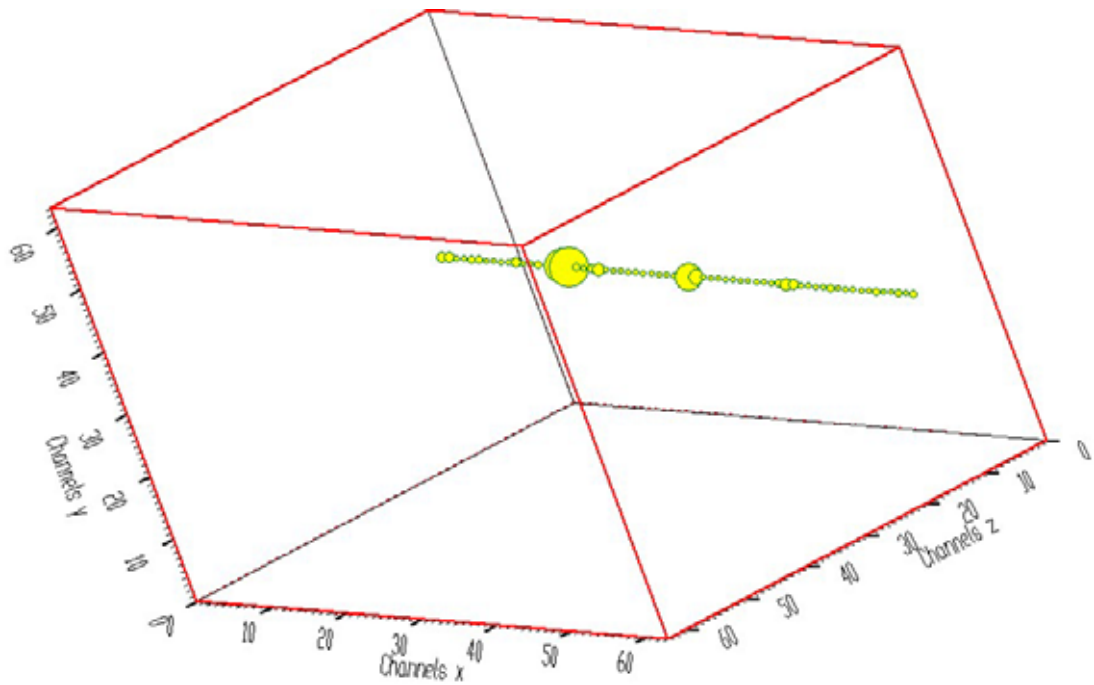
Figure 102 One-dimensional slice in three-dimensional spectrum
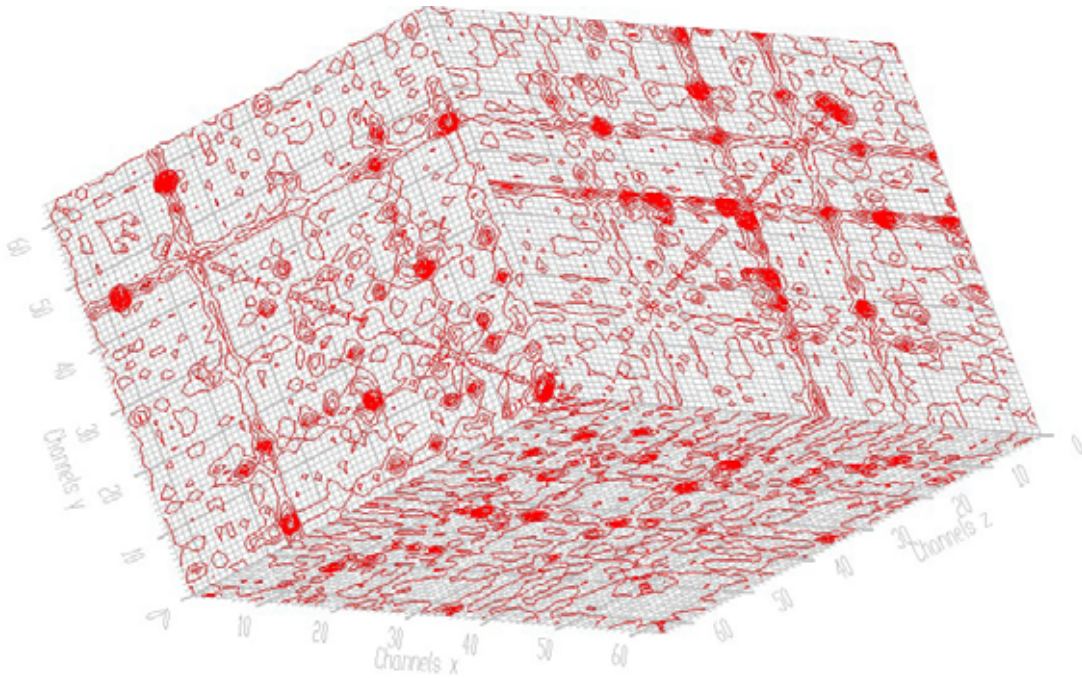
Figure 103 Projections of contour images to the planes of the coordinate system
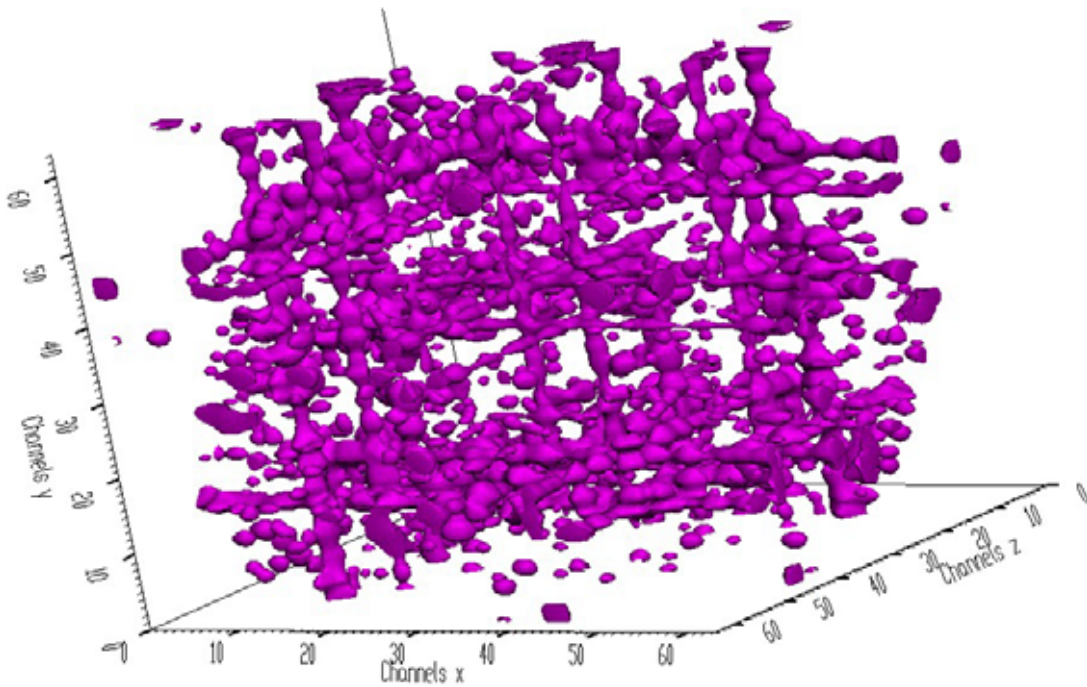
Figure 104 Three-dimensional $\gamma - \gamma - \gamma$ -ray coincidence spectrum shown in smoothed surface display mode
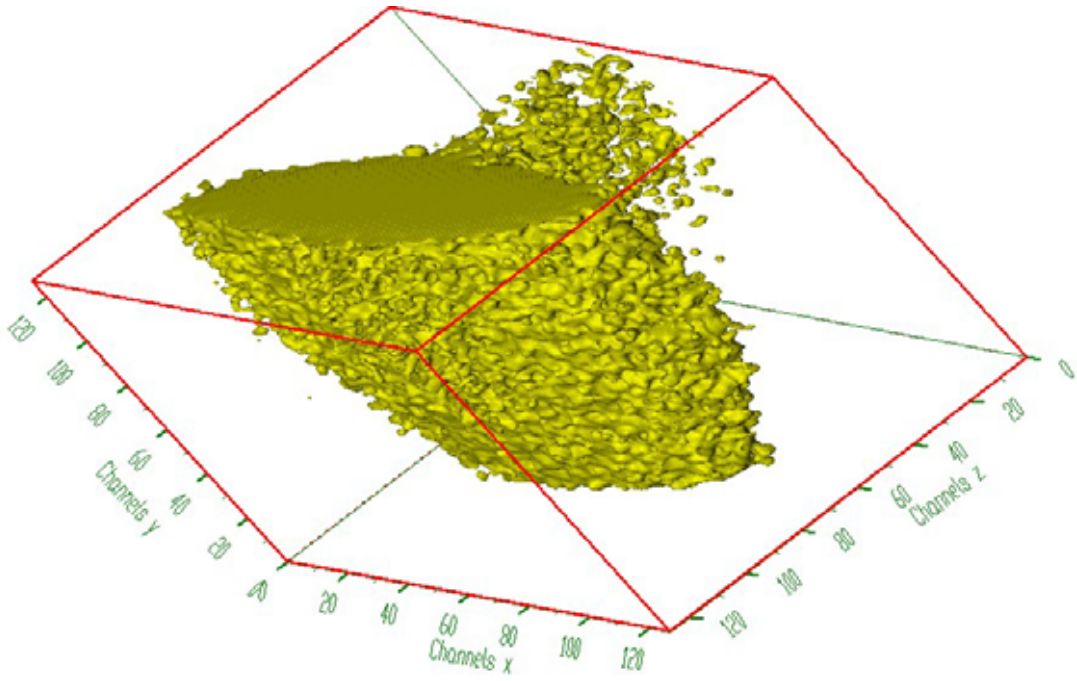
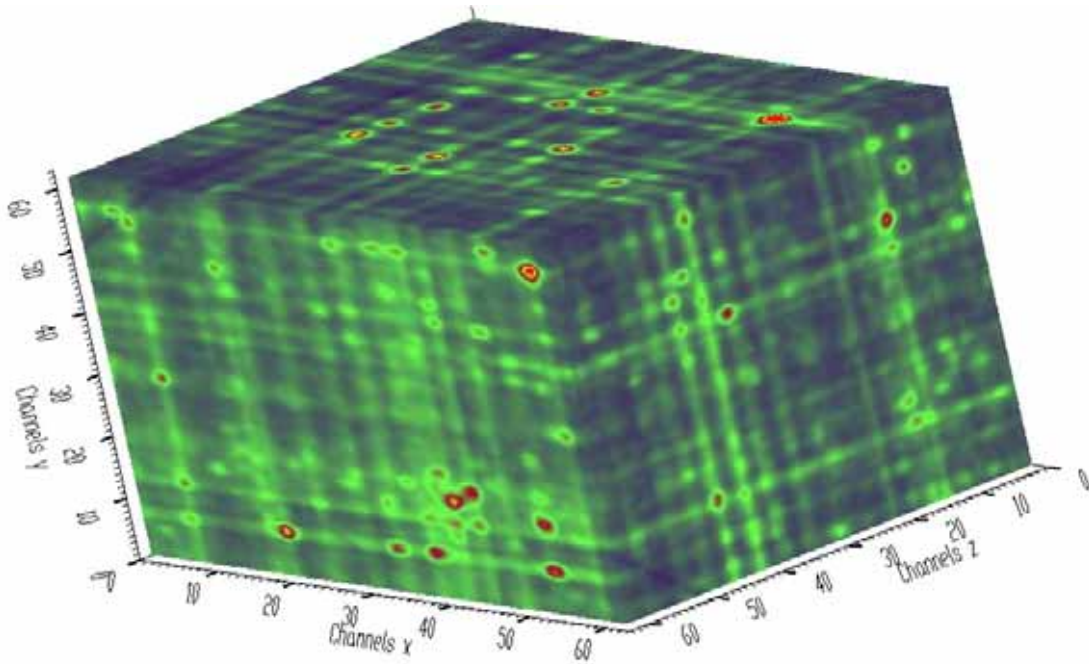**Figure 105 Three-dimensional positron annihilation spectrum shown in smoothed surface display mode**

Figure 106 Three-dimensional $\gamma - \gamma - \gamma$ -ray coincidence spectrum shown in volume rendering mode
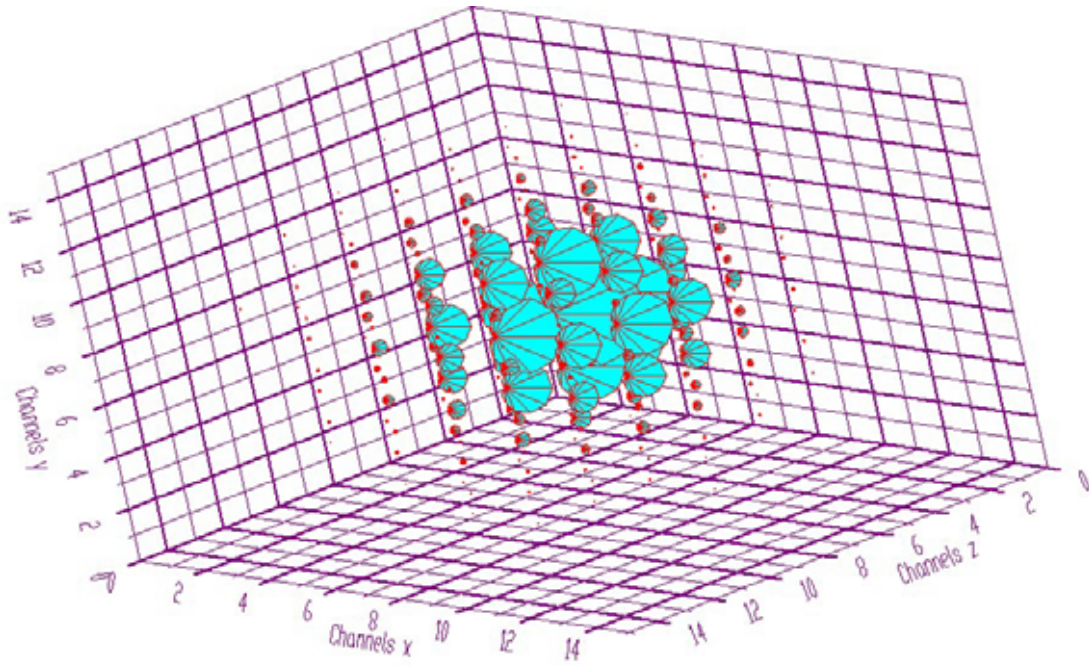
c. Four-dimensional spectra

76

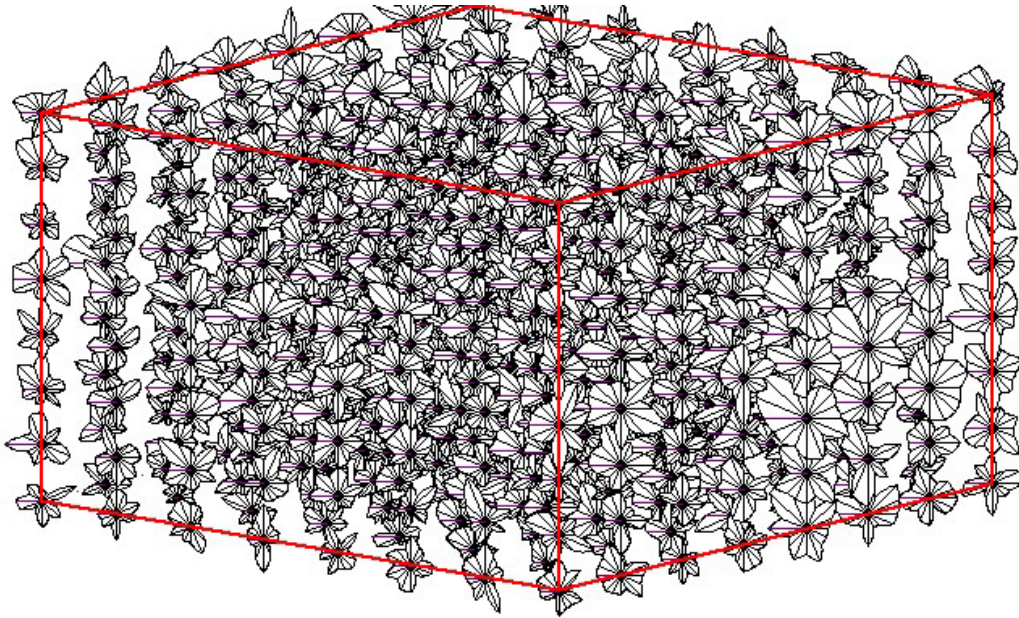**Figure 107 Display of four-dimensional synthetic Gaussian**

Figure 108 Original noisy four-dimensional $\gamma - \gamma - \gamma - \gamma$ -ray coincidence spectrum
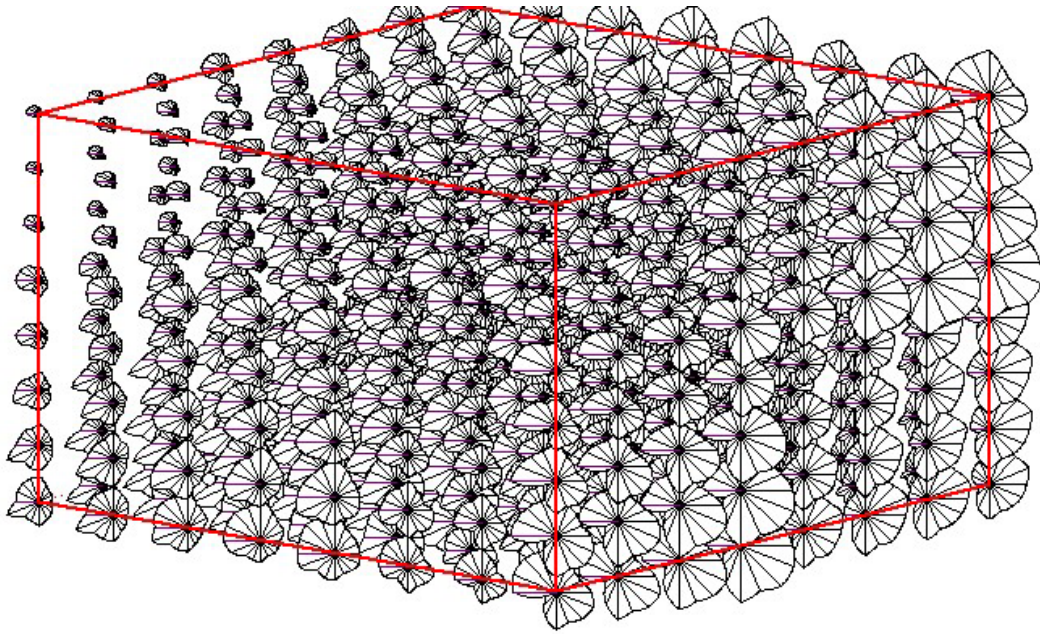
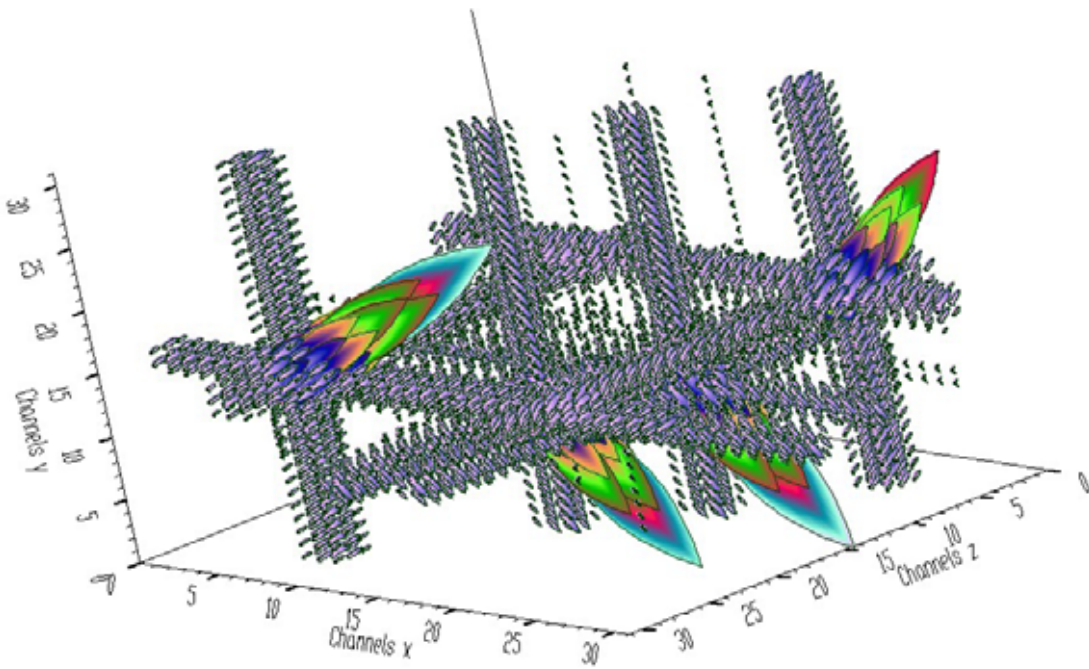**Figure 109 Decompressed spectrum of the data from Figure 108**

Figure 110 Synthetic four-dimensional spectrum before background elimination
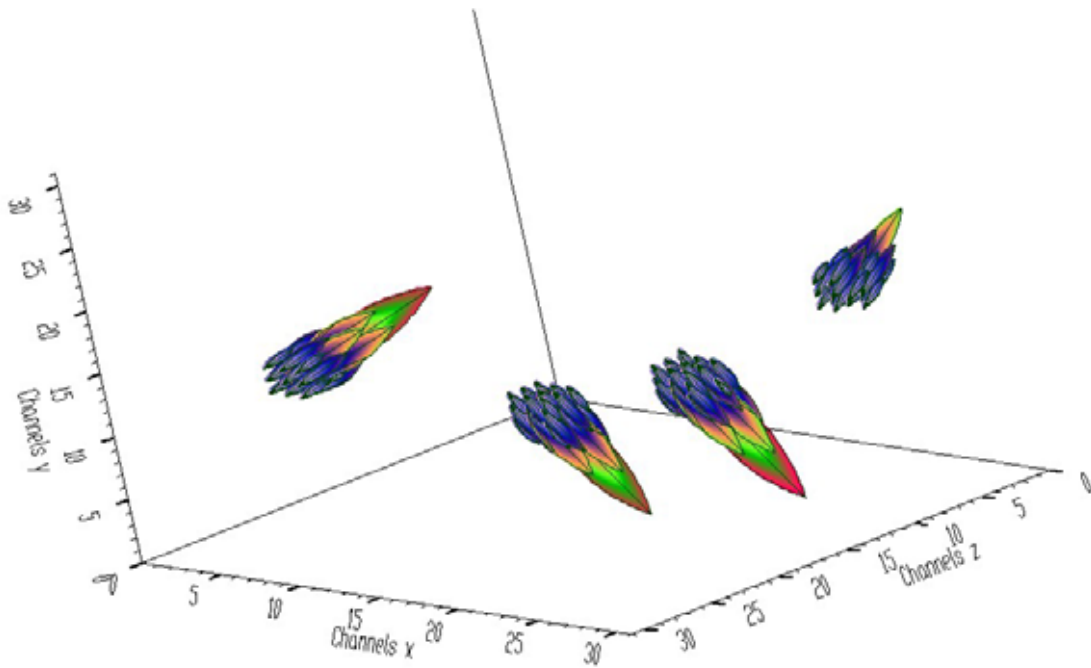
Figure 111 Four-dimensional peaks after background elimination from the data from Figure 120
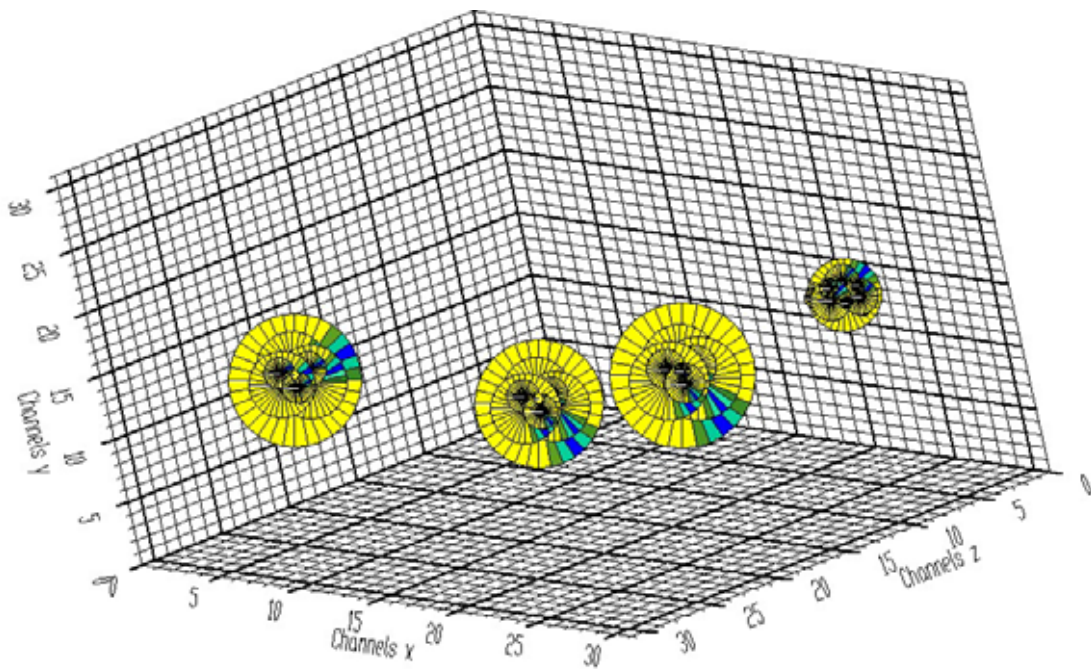

Figure 112 Four-dimensional peaks from Figure 111 displayed in pies display mode
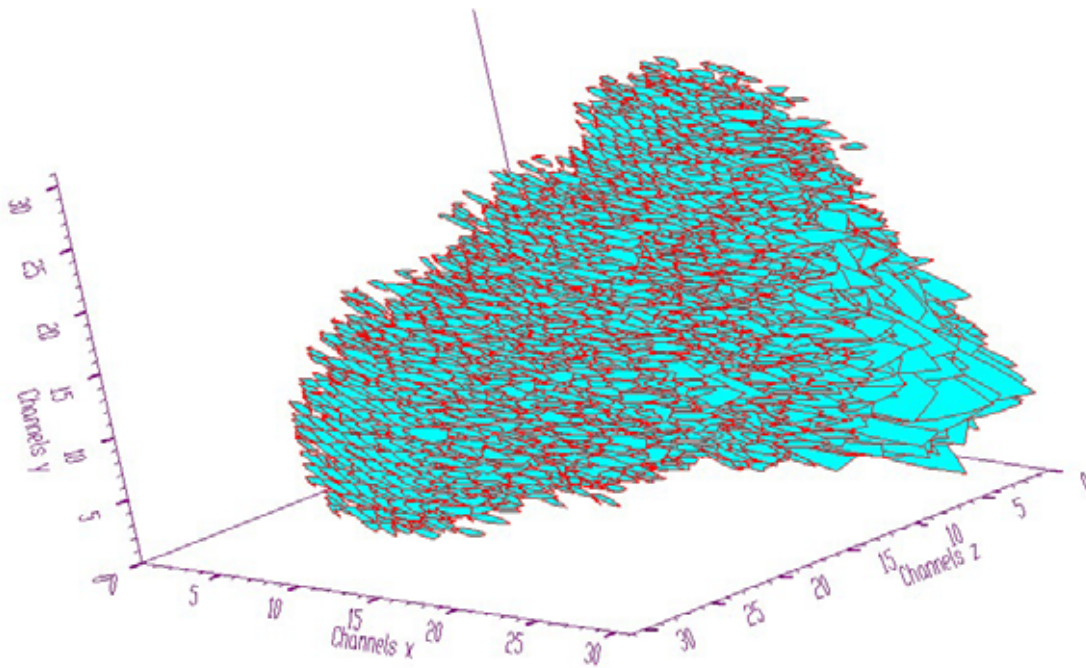
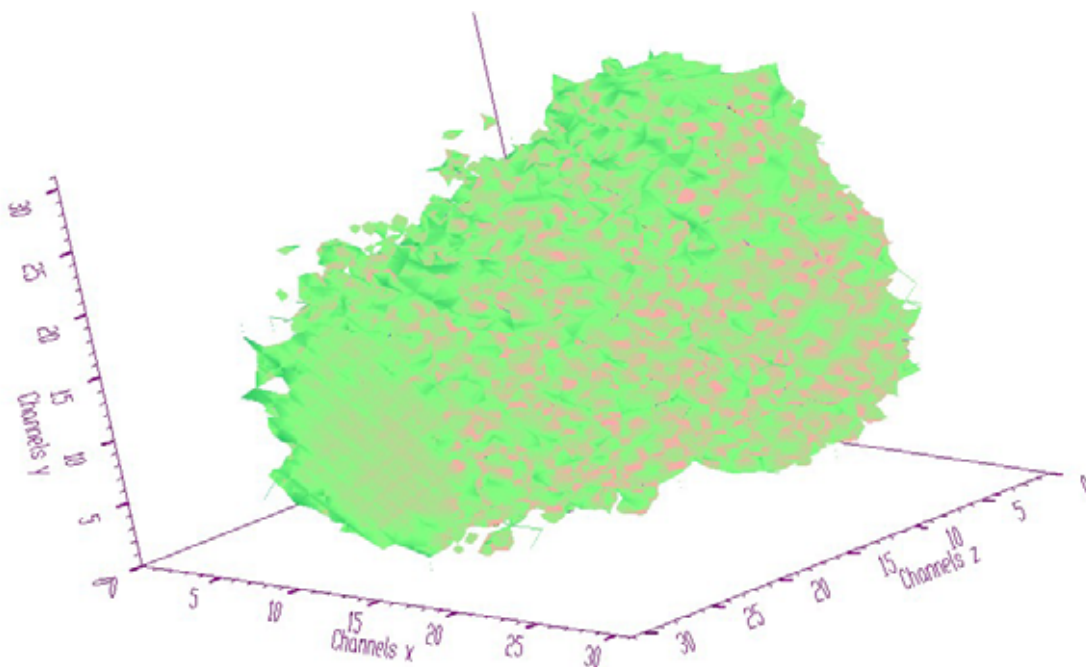**Figure 113 Four-fold coincidence positron annihilation spectrum**

Figure 114 Four-dimensional spectrum shown in isosurface display mode

Techniques of inserted subspaces and successive projections

- the dimensionality of above presented visualization techniques is limited to four.
- we proposed visualization algorithms that allow localizing peaks and scanning nuclear spectra of even higher dimensionality.

a. Three-dimensional spectra
- using this technique we can divide three-dimensional space to outer two-dimensional space and inner one-dimensional subspaces (slices in the third variable). An example of the projection of synthetic three-dimensional Gaussian and two ridges to two-dimensional outer subspace is given in next Figure
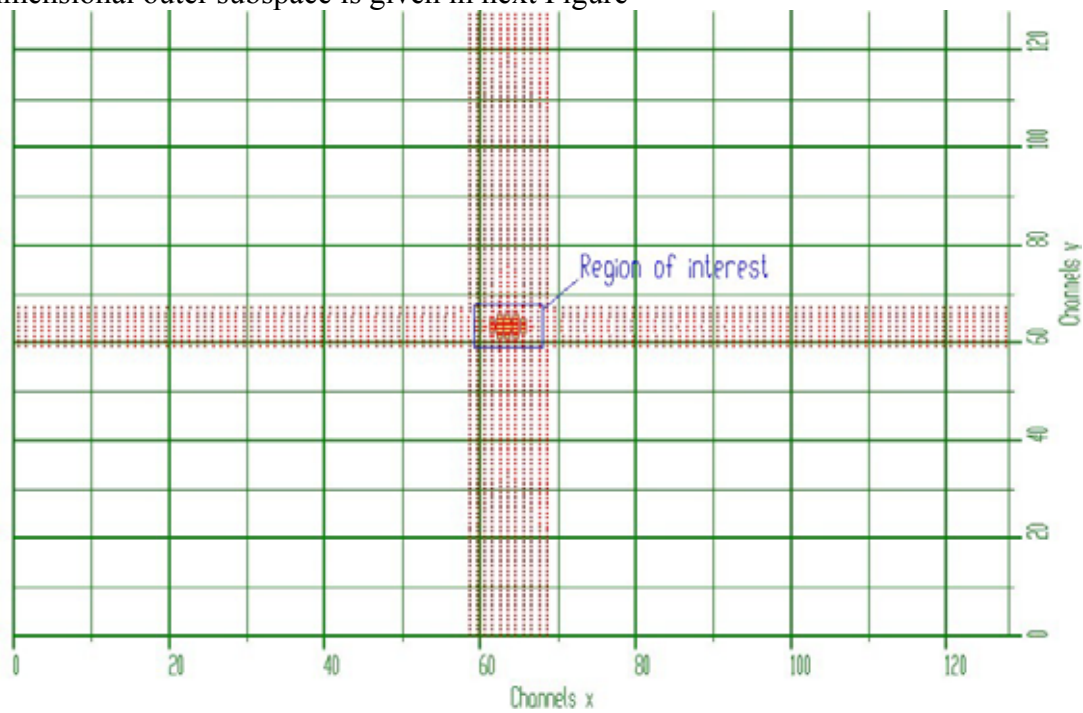

Figure 115 Projection of three-dimensional synthetic spectrum to two-dimensional outer subspace

- the sizes of rectangles are proportional to the contents inside of the slice in the appropriate channel of outer space.
- the display inside of rectangles is senseless because of poor resolution.
- let us imagine that we are interested in the peak region denoted as Region of interest. Let us focus the display to the ROI and enable the display inside rectangles
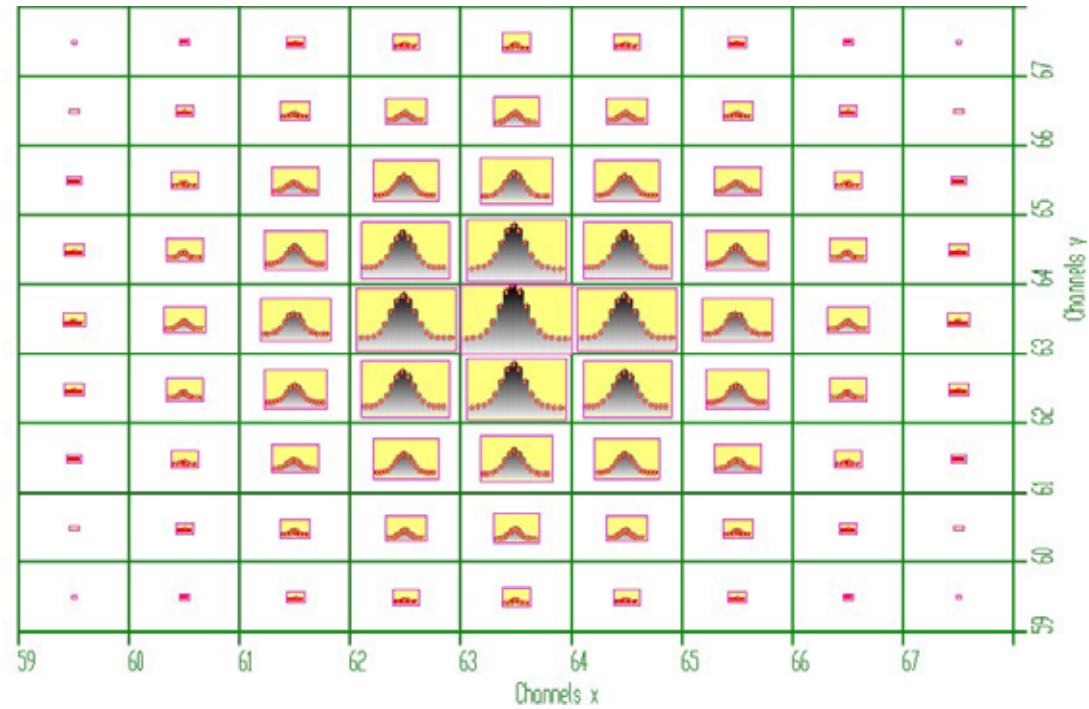
Figure 116 Displayed one-dimensional inner subspaces of the ROI

- one can see simultaneously the distribution of the two-dimensional projection (yellow squares) together with one-dimensional slices.
- one can observe correlations among neighboring points inside of rectangles as well as correlation of corresponding points in rectangles in both x and y directions.
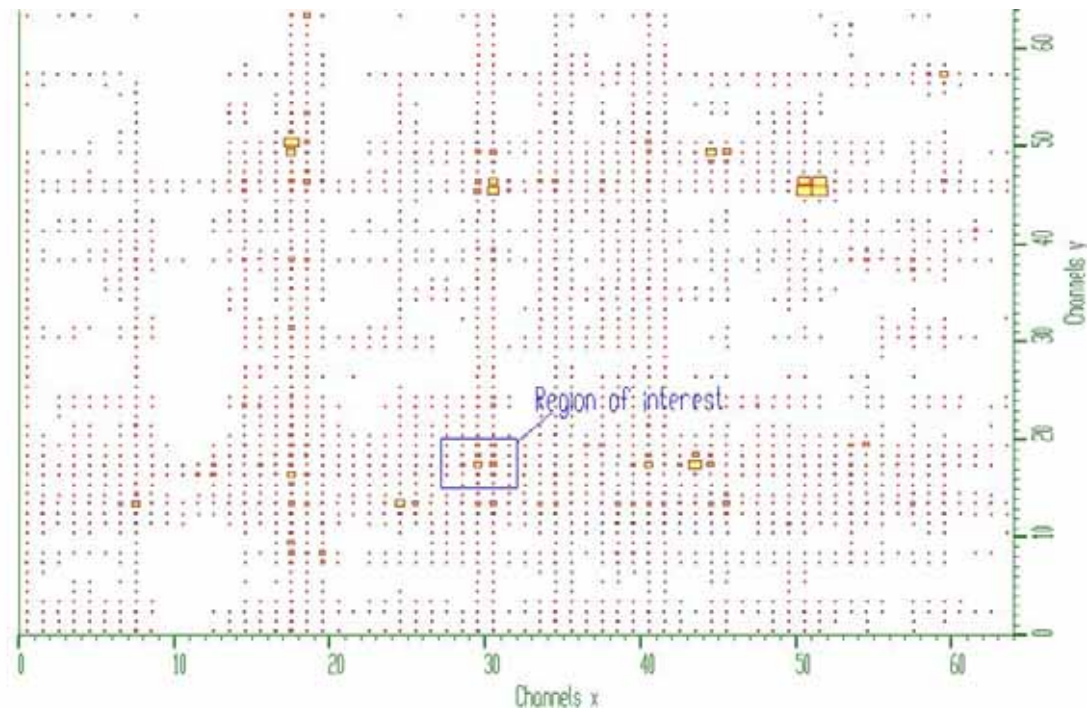

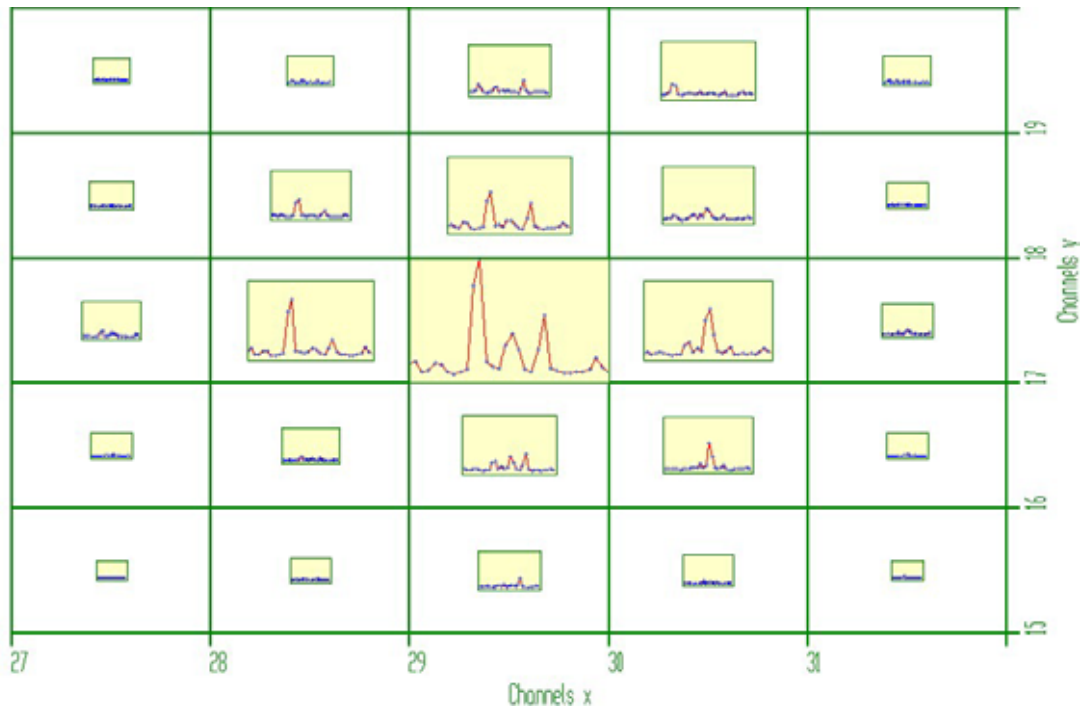**Figure 117 Experimental three-dimensional spectrum - outer subspace**

Figure 118 Zoomed ROI of the data from Figure 117

b. Four-dimensional spectra

- now the dimensionality of both outer and inner subspaces will be two. An example of a view focused on four-dimensional synthetic Gaussian is illustrated in next Figure.
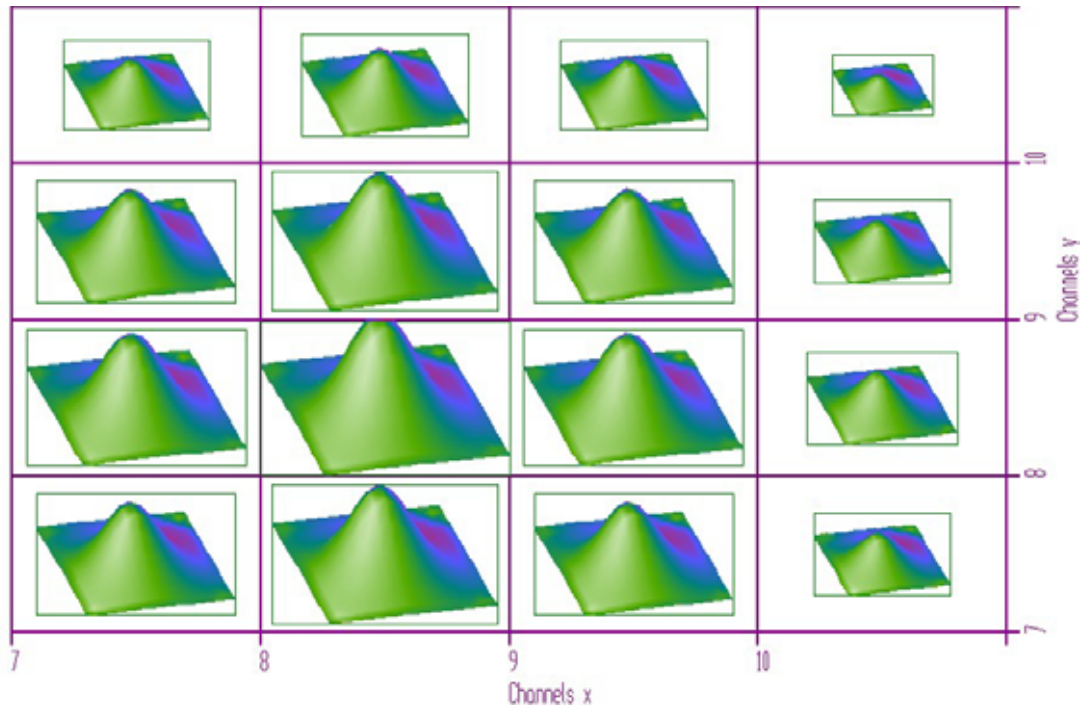
Figure 119 Four-dimensional synthetic Gaussian (shown both, outer and inner subspaces)

- now one can watch correlations in four dimensions, i.e., in two-dimensional subspace in each rectangle and among corresponding points in neighboring rectangles in both directions in outer subspace.
- let us proceed to experimental four-dimensional spectrum. In Figure 120, one can see a projection of the four-dimensional rather noisy spectrum to outer subspace and in Figure 121 zoomed ROI of it.
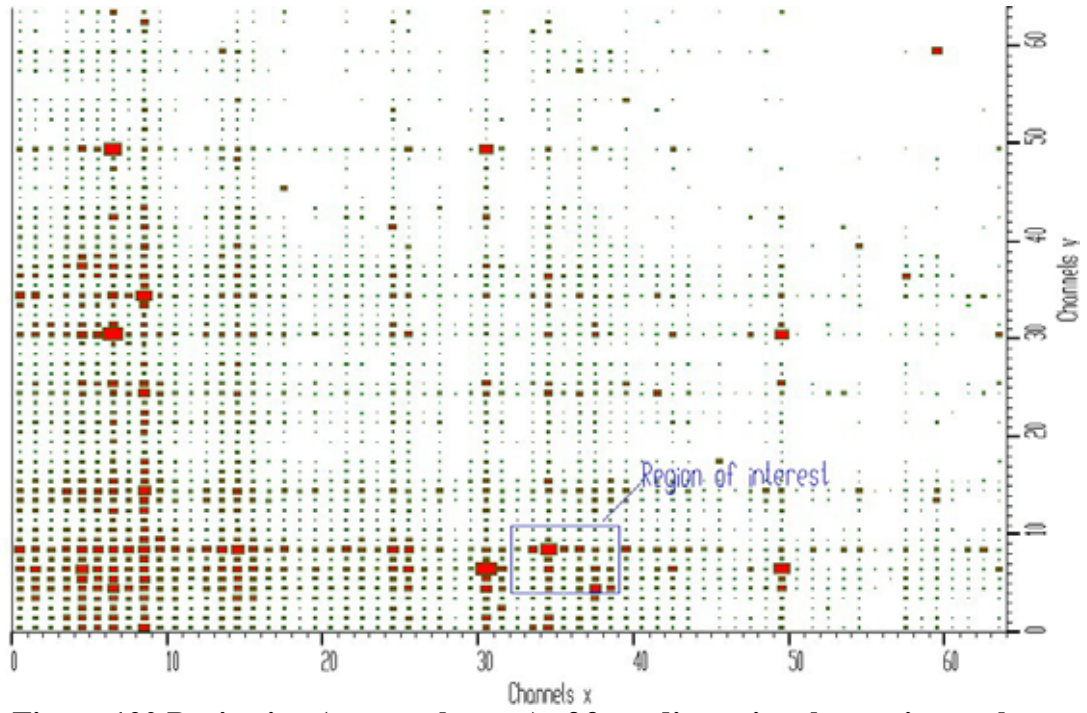
Figure 120 Projection (outer subspace) of four-dimensional experimental
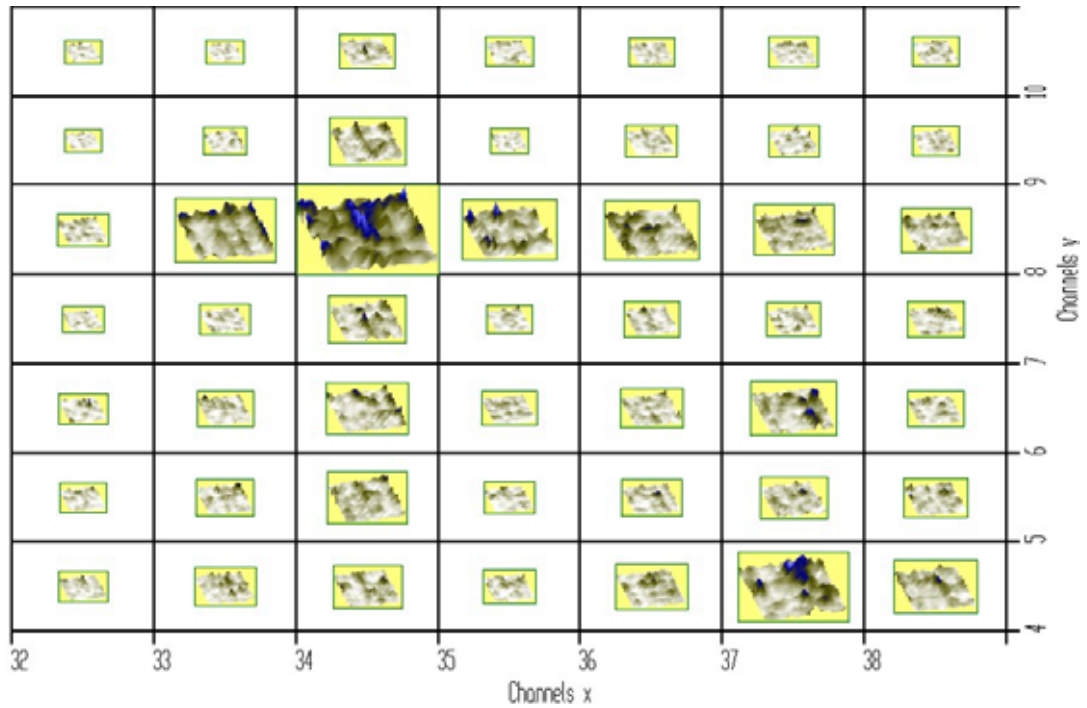$\gamma - \gamma - \gamma - \gamma$ **-ray coincidence spectrum**

Figure 121 Zoomed ROI of the data from Figure 120

- if desired to see better the details one can expand rectangles to equal size (Figure 122).
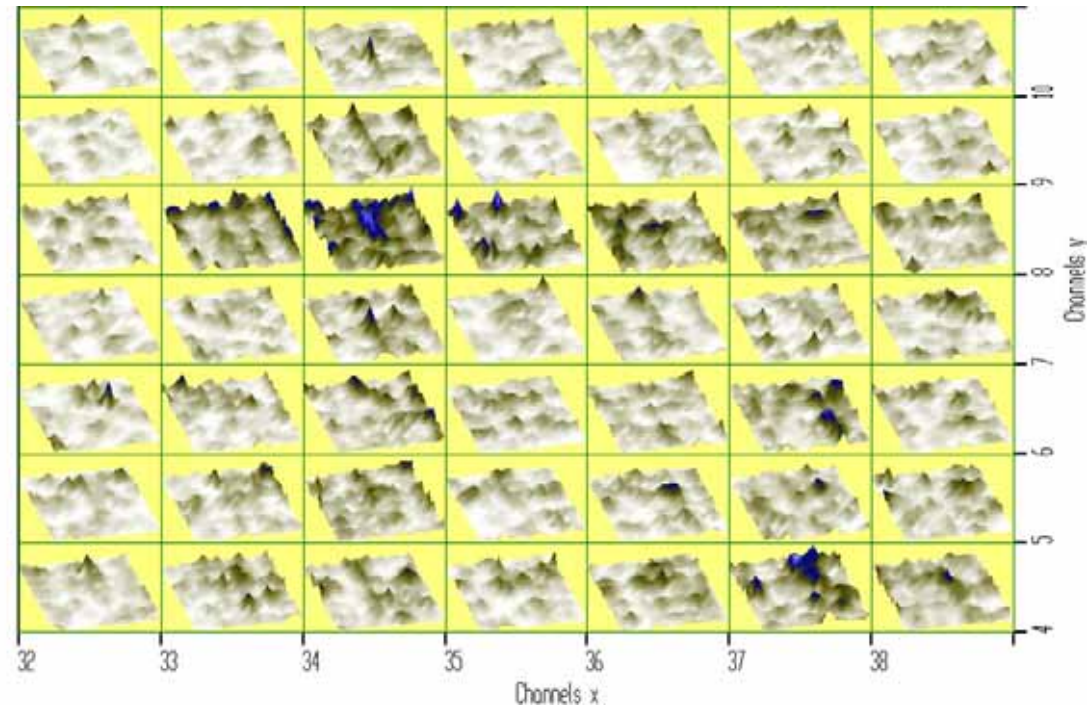
85

Figure 122 Zoomed ROI of the data from Figure 120 with equal sizes of rectangles

c. Five-dimensional spectra
- five-dimensional space can be divided in two ways, i.e., either two- plus three-dimensional subspaces or two- plus two- plus one-dimensional subspaces. Let us start with the first case.
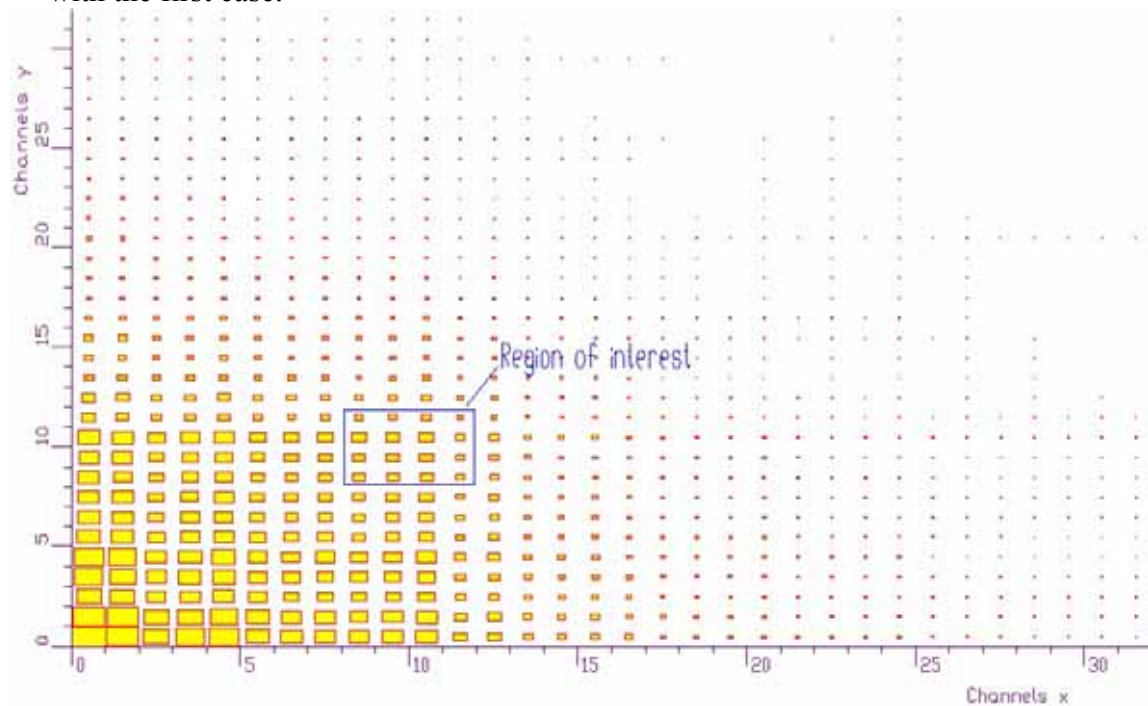

Figure 123 Outer subspace of five-fold γ – ray spectrum

- one can observe high level of background due to relatively low statistics in the spectrum. Let us assume we are interested in the drawn ROI.
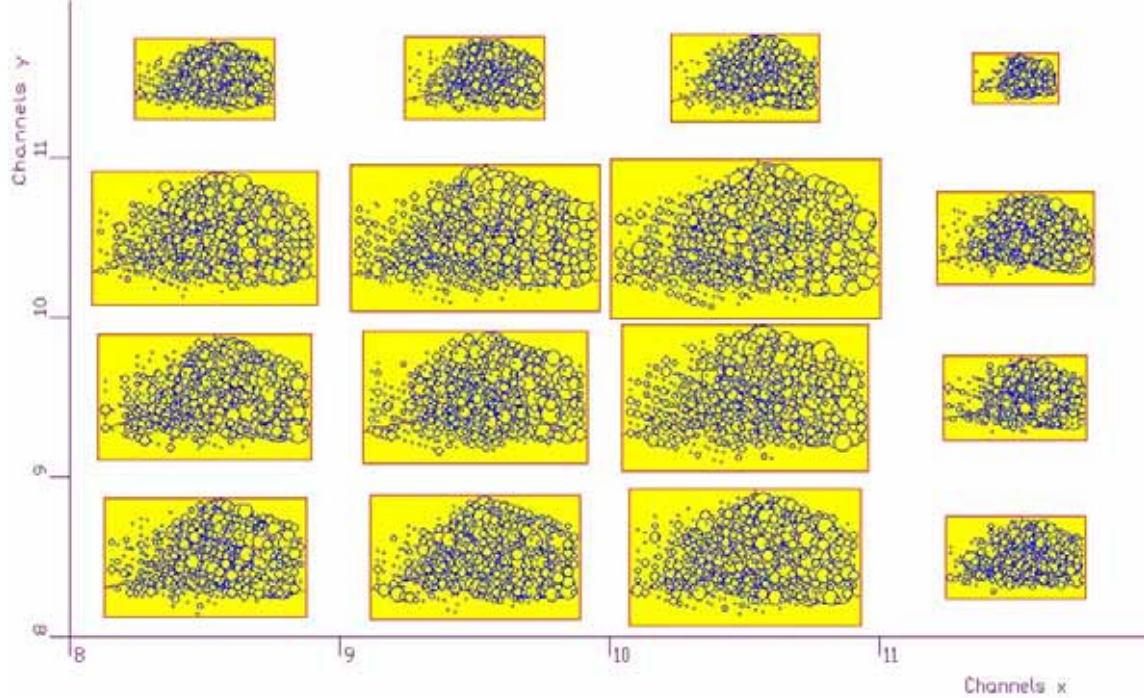

Figure 124 Zoomed ROI of the data from Figure 123 with displayed three-dimensional inner subspaces

- from the presented chunk of the five-dimensional space, mainly from the shown inner three-dimensional subspaces it is difficult to discover tendencies in the spectrum. It can be improved, to some extent, by smoothing the data using B-splines and employing isosurface display technique shown in Figure 125.
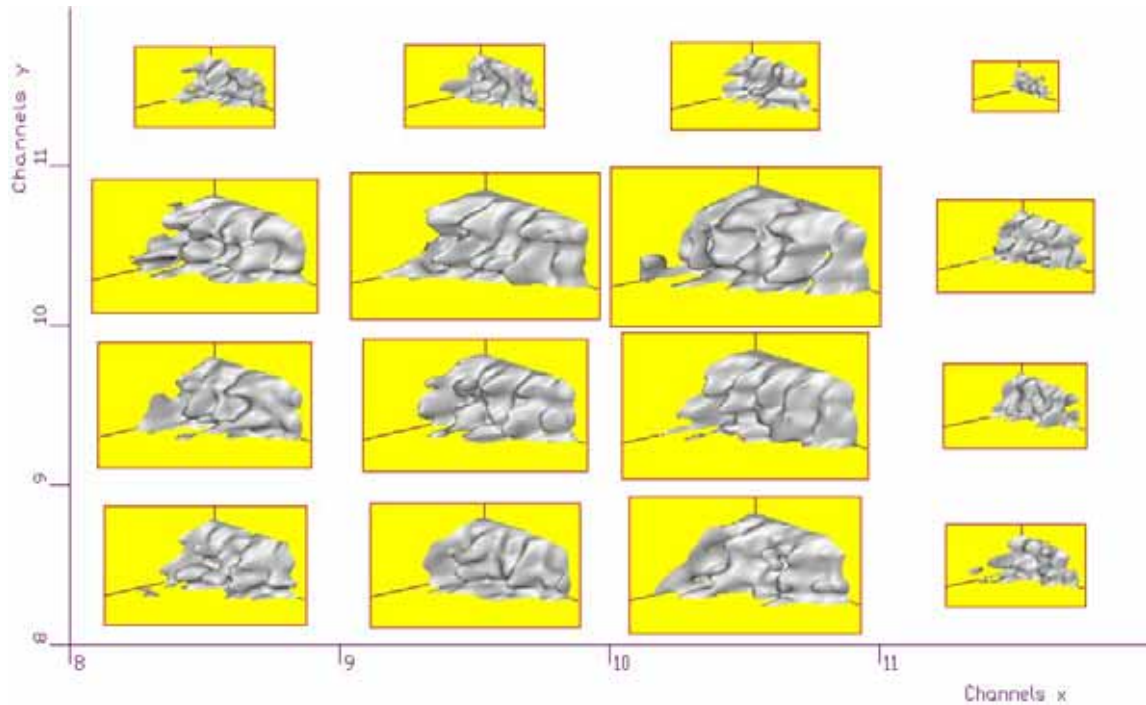
Figure 125 Zoomed ROI of the data from Figure 123 with inner subspaces displayed in isosurface display mode with B-spline smoothing

- the alternative way is to proceed in the projections and to divide inner three-dimensional subspaces to two- plus one-dimensional ones.
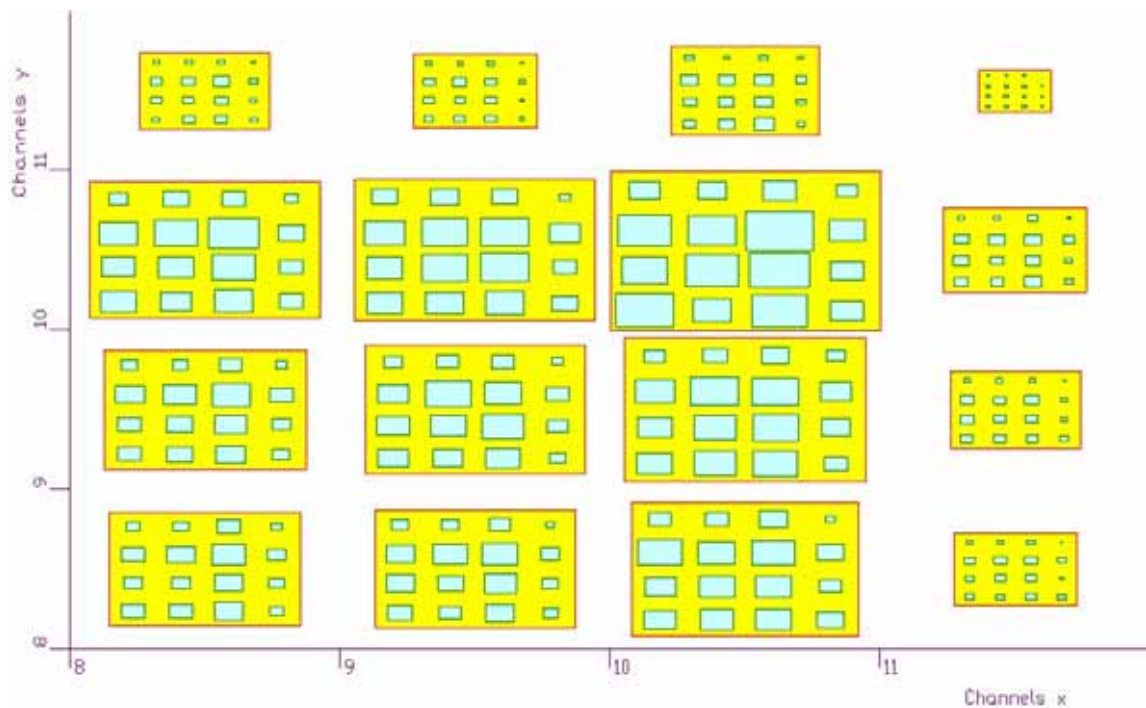

Figure 126 Zoomed ROI with shown outer and the first level inner subspaces

- while yellow rectangles represent outer subspace, the light blue ones represent the first level inner subspaces. If we enable the display of the second level subspaces, we can see all three levels simultaneously (Figure 127).
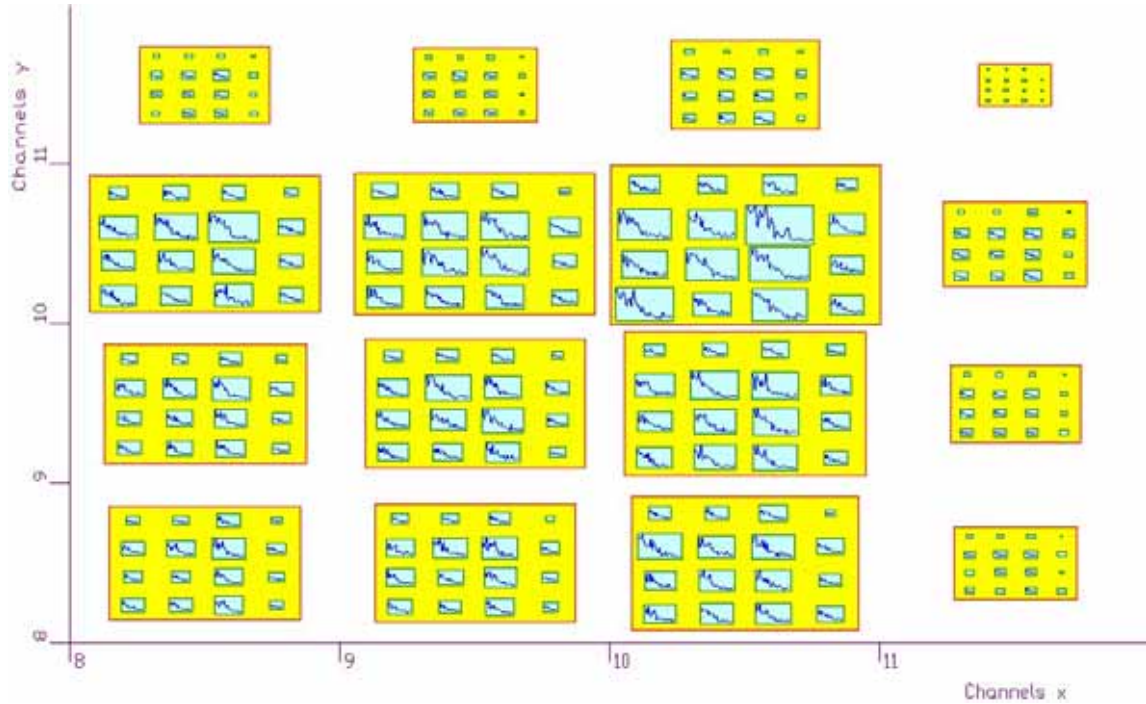

Figure 127 Zoomed ROI with shown outer, the first level and the second level inner subspaces

- one may focus attention to the channel x=10, y=10, where the volume of data is the biggest (yellow rectangle here is the largest, Figure 128).
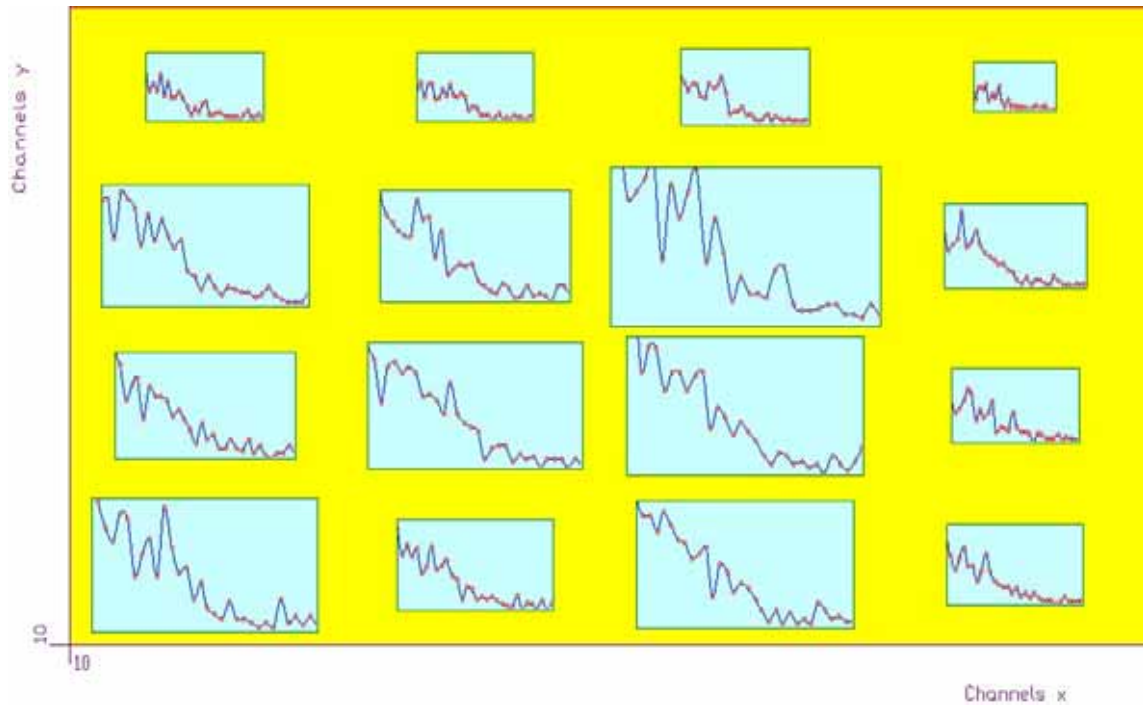
Figure 128 Zoomed one channel of the outer subspace

- supported formats (e.g. jpg, bmp, pcx, ps). It allows exporting and importing pictures.
- the system has built-in graphical editor that allows supplementing pictures with additional drawings.
- all motion and intermediate results during processing can be stored as a sequence of frames in avi files. This proved to be very instructive mainly in the correction and developing of the data processing algorithms and in tuning of the parameters during the analysis of the experimental data.

Conclusions

- modular structure of the DaqProVis system provides a great flexibility for both experimental and post-experimental configurations
- to write the software we have employed the object oriented approach
- objects such as detection line, event, gate/condition, filter, analyzer, sampler, compressor spectrum, picture etc. are internally represented by structures.
- the experimental, processing and visualization configurations are completely stored in the networks of structures

Additional information:

http://www.fu.sav.sk/nph/projects/DaqProvis
http://www.fu.sav.sk/nph/projects/ProcFunc